

FEASIBILITY STUDY OF CLOSED-LOOP GEOTHERMAL
HEAT EXTRACTION CONCEPTS USING
RESERVOIR SIMULATION

by
Santiago Rocha

© Copyright by Santiago Rocha, 2021

All Rights Reserved

A thesis submitted to the Faculty and the Board of Trustees of the Colorado School of Mines in partial fulfillment of the requirements for the degree of Master of Science (Petroleum Engineering).

Golden, Colorado

Date _____

Signed: _____
Santiago Rocha

Signed: _____
Dr. Luis Zerpa
Thesis Advisor

Golden, Colorado

Date _____

Signed: _____
Dr. Jennifer Miskimins
Professor and Head
Department of Petroleum Engineering

ABSTRACT

This work evaluates the feasibility of closed-loop geothermal heat extraction concepts using reservoir simulation and proposes ideal conditions to guide the development of future field-ready technologies for electricity generation. Additionally, this thesis presents alternative uses of this technology for direct use in remote communities based on abandoned petroleum wells with high reservoir temperatures. Technical analysis is presented focusing on the possible applicability of closed-loop geothermal heat extraction with available technology, identifying the parameters required to develop technologies for electricity generation.

First, a base case is verified against results from published modeling studies for two closed-loop geothermal concepts including a pipe-in-pipe model and a U-shaped model. These models are developed using reservoir simulator software (CMG-STARs). Then different properties, such as, depth of the reservoir, number of laterals, reservoir temperature, type of fluid, and total production flow rate, are modified to analyze different scenarios that can benefit from Closed-Loop Geothermal (CLG) technologies. Ultimately, technical analysis is performed on all of the cases to assess the feasibility of these concepts.

Results show that residence time, flow rates, reservoir temperatures, and properties of working fluids are the parameters impacting thermal outputs. Higher flow rates lead to lower surface production temperatures; however, higher mass flow rates have higher thermal energy production. On the other hand, water and supercritical carbon dioxide show fair results that are enhanced with a fluid combining water with copper nanoparticles. Direct use application may be feasible in abandoned petroleum wells that are already completed as capital investment is reduced. Electricity generation may be feasible with current technology when multiple wells feed the power plant.

This thesis demonstrates that CLG is a concept that may be used for direct use application with abandoned oil and gas wells, and with further technological developments, it could also be applied for electricity generation from geothermal reservoirs without having to enhance the reservoir permeability. Additionally, it is demonstrated that reservoir simulation software can be applied to related disciplines, such as geothermal heat extraction, and that knowledge from petroleum engineering can be applied to develop alternative solutions for energy generation.

TABLE OF CONTENTS

ABSTRACT iii

LIST OF FIGURES vi

LIST OF TABLES viii

NOMENCLATURE x

LIST OF ABBREVIATIONS xii

ACKNOWLEDGMENTS xiii

CHAPTER 1 INTRODUCTION 1

 1.1 Previous Results 2

 1.1.1 Slender Body Theory – U-Shape 2

 1.1.2 Green Fire Energy – Pipe-in-Pipe 3

 1.2 Why CLG concept? 5

 1.3 Objectives 6

 1.4 Thesis Organization 7

CHAPTER 2 OVERVIEW 8

 2.1 Geothermal Heat Extraction 8

 2.2 Closed-Loop Geothermal Heat Extraction 8

 2.2.1 Pipe-in-Pipe 9

 2.2.2 U-Shaped Configuration 12

 2.2.3 Working Fluids 13

 2.3 Numerical Modeling for Geothermal Energy 15

 2.3.1 CMG-STARS 15

 2.4 Direct Use Application 17

2.5	Geothermal for Electricity Generation	19
CHAPTER 3 MODELING CLOSED-LOOP GEOTHERMAL SYSTEMS		22
3.1	Base Case Scenarios	22
3.1.1	Pipe-in-Pipe Model	22
3.1.2	U-Shaped Model	33
3.2	Experimental Matrix	41
3.2.1	Pipe-in-Pipe	41
3.2.2	U-Shaped	49
3.3	Working Fluids	57
3.3.1	Supercritical Carbon Dioxide (sCO ₂)	58
3.3.2	Water with Nanoparticles of Copper	60
3.4	Haynesville Shale Real Application	61
CHAPTER 4 TECHNICAL EVALUATION		67
CHAPTER 5 SUMMARY AND CONCLUSIONS		72
CHAPTER 6 FUTURE WORK		75
REFERENCES CITED		76
APPENDIX A TECHNICAL ANALYSIS MATRIX		79
APPENDIX B PIPE-IN-PIPE CASE .DAT CODE		81
APPENDIX C U-SHAPE CASE .DAT CODE		111
APPENDIX D LIST OF SUPPLEMENTAL FILES FOR COPYRIGHT PERMISSIONS . .		126

LIST OF FIGURES

Figure 1.1	Heat exchanger’s geometry for the base case., reprinted by permission of Koenraad Beckers.	3
Figure 1.2	Down-Borehole Heat Exchanger (DBHX) schematic. , ©2020 by Green Fire Energy Inc., reprinted by permission of Green Fire Energy Inc.	5
Figure 2.1	Wellbore Heat Exchanger (WBHX) configuration. Reuse with permission provided by Elsevier and Copyright Clearance Center	10
Figure 2.2	U-shaped configurations. , reprinted by permission of Koenraad Beckers.	13
Figure 2.3	Two stage ORC diagram with an air cooled condenser.	20
Figure 2.4	Kalina Cycle diagram.	21
Figure 3.1	Temperature distribution for the pipe-in-pipe base case model.	24
Figure 3.2	Well configuration for FlexWell.	29
Figure 3.3	Surface fluid temperature output for 20 years of simulation for Nalla et al. (2005) and CMG-STARS.	31
Figure 3.4	Temperature distribution for the working fluid through the pipe network and the rock in the same grid cell after 5 and 20 years of simulation.	31
Figure 3.5	Temperature distribution along the surrounding regions of the well for the pipe-in-pipe base case for 5, 10, 15, and 20 years of simulation.	32
Figure 3.6	Temperature distribution for the U-shape base case model.	34
Figure 3.7	Surface fluid temperature output for 20 years of simulation for the SBT analytical model and CMG-STARS.	38
Figure 3.8	Working fluid temperature profile along the well after 5 and 20 years of simulation for CMG-STARS model.	39
Figure 3.9	Temperature distribution along the surrounding regions of the well for the U-shaped base case at 5, 10, 15, and 20 years of simulation.	40
Figure 3.10	Surface fluid temperature output for 20 years of simulation for different flow rates in a pipe-in-pipe configuration.	43
Figure 3.11	Surface fluid temperature output for 20 years of simulation for different lateral lengths in a pipe-in-pipe configuration.	45

Figure 3.12	Surface fluid temperature output for 20 years of simulation for different reservoir temperatures in a pipe-in-pipe configuration.	46
Figure 3.13	Surface fluid temperature output for 20 years of simulation for the ideal pipe-in-pipe case.	48
Figure 3.14	IK 2D view temperature distribution for a pipe-in-pipe ideal case.	49
Figure 3.15	Surface fluid temperature output for 20 years of simulation for different flow rates in a U-shape configuration.	50
Figure 3.16	Surface fluid temperature output for 20 years of simulation for different flow rates in a U-shape configuration.	51
Figure 3.17	Surface fluid temperature output for 20 years of simulation for different lateral lengths.	52
Figure 3.18	Temperature profile for the fluid and the rock through the well path.	53
Figure 3.19	Surface fluid temperature output for 20 years of simulation for different reservoir temperatures.	55
Figure 3.20	IK 2D view temperature distribution for an U-shape ideal case.	57
Figure 3.21	Surface fluid temperature output for 20 years of simulation for different mass rates using sCO ₂ as working fluid.	59
Figure 3.22	Surface fluid temperature output for 20 years of simulation for different mass rates using water with nanoparticles of copper as working fluid compared to normal water at the same flow rates.	61
Figure 3.23	Haynesville well trajectory to be used in the real case.	62
Figure 3.24	Surface fluid temperature output for 20 years of simulation for different flow rates for the Haynesville Shale real model.	65
Figure 3.25	IK 2D view temperature distribution for Haynesville Shale case.	66
Figure 4.1	Utilization efficiency for different power plant types as a function of wellhead temperature and dry-bulb ambient temperature.	70
Figure A.1	Technical analysis matrix displaying all the parameters calculated and analyzed for all the cases run in the research.	80

LIST OF TABLES

Table 2.1	Best case scenario for vertical pipe-in-pipe. Modified from Nalla et al. (2005) . . .	12
Table 3.1	Input parameters for the reservoir and grid section	23
Table 3.2	Input parameters for the components section	25
Table 3.3	Input values for relative permeability tables	25
Table 3.4	Input parameters for the initial conditions section	26
Table 3.5	Input parameters for the initial 'Annulus' well	27
Table 3.6	Input parameters for the initial 'Tubing' injector well	28
Table 3.7	Input parameters for the initial 'Concentric Tubing' producer well	28
Table 3.8	Input parameters for the injected fluid	28
Table 3.9	Input parameters for the well radius under the perforations definition	29
Table 3.10	Input parameters for the insulated pipe	30
Table 3.11	Input parameters for wall diameters	30
Table 3.12	Input parameters to verify with the SBT analytical model. Modified from Beckers (2020)	33
Table 3.13	Input parameters for the components section	35
Table 3.14	Input values for relative permeability tables	35
Table 3.15	Input parameters for the initial conditions section	35
Table 3.16	Input parameters for the initial "Injector" well	36
Table 3.17	Input parameters for the initial "Producer" well	37
Table 3.18	Input parameters for the injected fluid	37
Table 3.19	Input parameters for wall diameters	37
Table 3.20	Parameter values for the cases evaluated in the pipe-in-pipe configuration	42

Table 3.21	Temperature gain and potential thermal output for different flow rates using a pipe-in-pipe configuration	43
Table 3.22	Temperature gain for different lateral lengths using a pipe-in-pipe configuration	45
Table 3.23	Temperature gain for different reservoir temperatures and depths in a pipe-in-pipe configuration	47
Table 3.24	Pipe-in-pipe ideal case input parameters	47
Table 3.25	Temperature gain and potential thermal output for an ideal pipe-in-pipe case . .	48
Table 3.26	Temperature gain and potential thermal output for different flow rates using a U-shape configuration	50
Table 3.27	Temperature gain and potential thermal output for flow rates varying from 8 to 19 L/s	52
Table 3.28	Temperature gain and potential thermal output for different lateral lengths . . .	53
Table 3.29	Reservoir temperature and depth for the experimental matrix	54
Table 3.30	Temperature gain for different reservoir temperatures and depths	55
Table 3.31	U-shape ideal case input parameters	56
Table 3.32	Temperature gain and potential thermal output for an ideal U-shape case	56
Table 3.33	Cases proposed for sCO ₂ as working fluid	58
Table 3.34	Temperature gain and potential thermal output for different flow rates using sCO ₂ as working fluid	59
Table 3.35	Temperature gain and potential thermal output comparison after 20 years of simulation for different flow rates of water and water with copper nanoparticles as working fluids	61
Table 3.36	Direct use scenario for vertical using parameters from an already drilled well in Haynesville Shale using a pipe-in-pipe configuration	63
Table 3.37	Temperature gain for different flow rates after 20 years of simulation for a case in Haynesville Shale	64

NOMENCLATURE

Ad_i		adsorbed component i
C_f		fluid heat capacity [J/(kg °C)]
D_{wi}		component dispersibilities
H_w		water enthalpy
S_w		water saturation
T_2		temperature outlet (°C)
T_1		temperature inlet (°C)
U_i		internal energy for i phase
U_r		energy per rock volume
V		total volume of the grid block
\dot{m}		mass rate (kg/s)
q_w		water source/sink flow rate
q_{wk}		water well phase rate
w_i		concentration of component i

Greek Letters

ϕ_f		fluid porosity
ϕ_v		void porosity
ρ_w		water density
Δw_i		change in concentration of component i in aqueous phase
ϕ		absolute porosity
ΔT		temperature gradient
K		thermal conductivity

η Carnot's efficiency (fraction)

LIST OF ABBREVIATIONS

BHP Bottom Hole Pressure

CLG Closed-Loop Geothermal

DBHX Down-Borehole Heat Exchanger

DFN Discrete Fracture Network

EGS Enhanced Geothermal Systems

EPB Electro Pulse Boring

GEOPHIRES Geothermal energy for Production of Heat and electricity Economically Simulated

HHTP High Temperature High Pressure

ID Inner Diameter

KCP Kalina Cycle Power Plant

NCG Non-Condensable Gas

NP Nanoparticles

OD Outer Diameter

O&G Oil and Gas

ORC Organic Rankine Cycle

PSS Pseudo Steady State

SBT Slender Body Theory

SCO₂ Supercritical Carbon Dioxide

STW Surface Water Rate

UBA User Block Address

WBHX Wellbore Heat Exchanger

ACKNOWLEDGMENTS

Without the help of many people during my research, studies, and daily life, this research could not have been possible. I would like to acknowledge them.

I thank first, Dr. Tutuncu for opening CSM's doors to me. Her legacy will always be present at CSM and in my future research and work, being kind, lovely, and sincere all the time, just as she was.

I would like to thank Dr. Zerpa for helping me through all this process, for his trust in my work, for being always there to answer my questions, for his wiseness, and for giving me the chance to finish my studies at Mines. I want to acknowledge Bud for all his guide and knowledge on this research, he gave me the base and fundamentals of CLG and reservoir simulation. I want also to thank Koenraad and Kate for their collaboration in the early stages of this research, which gave me the confidence to complete this thesis.

I feel honored to had the opportunity of gaining knowledge from CSM's professors and staff. Dr. Wu, Dr. Miskimins, Dr. Kazemi, Dr. Ozkan, and Dr. Battalora, thank you for your classes and expertise.

Thanks to the Petroleum Engineering Department members for their support, particularly Denise, for all your help during these two years, I feel blessed knowing someone like you.

Sincere thanks to Manosur, Esad, Joaquin, Deep, Tugce, Gizem, Val, Musab, and Roy for this great time at CSM, I was never bored during my studies and know I have a broader view of life because of you guys.

Thank you, Karen, for your company, love, and patience in this process, you make my life calm and better, allowing me to focus on my studies. Thank you for always being there for me.

Finally, I thank my parents, Carlos and Silvia, all my achievements are because and for you two. I appreciate every single effort and support you have done for me.

CHAPTER 1

INTRODUCTION

Geothermal energy is considered a promising energy resource to supplement fossil energy. Nowadays, this alternative form of energy is not completely developed, and the industry needs to design and develop efficient technologies beyond current geothermal energy extraction methodologies. Geothermal energy technologies need a geologic formation with high temperature (i.e., high heat flow) and, in the same way, to have the ability to transfer heat in the media. Most geothermal reservoirs are in impermeable rock formations, and to access the heat retained in the rock, fractures need to be created in the matrix of the rock.

The main problem for geothermal energy to be accepted as a global energy source is not the lack of reservoirs that can be used to develop the technique, as at sufficient depth, geothermal energy is available everywhere. The challenge for this alternative energy source is to overcome the experimental phase of technology development. While the techniques show reliable results, the implementation has not shown the desired results, or the required investment to implement the technology is prohibitively high.

These are the currently available technologies:

- Shallow, low enthalpy aquifers: shallow groundwater reservoirs (below 100 m) with temperatures averaging 20°C that are used for direct use at surface above the aquifer (Winsloe et al. 2020).
- Water production from oil and gas operations: oil production is usually accompanied by water and in some cases, the production temperature of the water can be used for direct use in the communities surrounding the oil fields (Winsloe et al. 2020).
- Enhanced Geothermal Systems (EGS) are geothermal resources that “were considered unrecoverable due to lack of water, location, or rock type” (National Renewable Energy Laboratory 2020). With hydraulic fracturing and new drilling technology, these types of reservoirs are estimated to have 500,000 megawatts (National Renewable Energy Laboratory 2020) of potential energy production. However, the initial investment for this type of project is high.

- Closed-loop (or conduction based) geothermal (CLG): systems where a fluid is injected in a closed well, without direct contact with the rock. The fluid temperature increases during flow through the system and it is produced through the same well that is drilled to certain depths with high temperatures. This concept may be used for electricity generation or direct use near well locations.

The first two technologies just mentioned (shallow, low enthalpy aquifers and water production from oil and gas operations) are already under development and are ready for expansion scale. On the other hand, both technologies (shallow, low enthalpy aquifers and water production from oil and gas operations) need to stimulate the reservoir by hydraulic fracturing, which is a very unpopular technique due to the potential of induced seismicity. Therefore, the CLG concept is a technology that does not require creating fractures in the rock, but it has shown low temperature output potential in previous models (Nalla et al. 2005). However, as new projects and techniques develop in the oil and gas industry, this technology is becoming a promising alternative (Winsloe et al. 2020).

1.1 Previous Results

This section presents the background reported in the technical literature related to CLG concepts. An analytical model is studied to compare results obtained using a numerical reservoir model for a U-shaped configuration. Also, an ideal case previously studied with an analytical model will be used to verify a pipe-in-pipe configuration using numerical reservoir simulation. The following are paramount remarks from each of the models to be used to create the base case models.

1.1.1 Slender Body Theory – U-Shape

Beckers et al. (2015) developed a transient heat conduction model based on the Slender Body Theory (SBT). The base case proposed consists of two wells drilled directionally, to 3 km depth and 2 km apart down-hole, as shown in Figure 1.1.

The SBT reduces the discretization of a three-dimensional domain into a one-dimensional analysis for complex geometries for heat transfer solutions (Beckers et al. 2015). The computational time is reduced as the method uses an analytical solution for inner heat transfer, combined with Green’s functions that can solve the outer heat transfer problem. This method is effective when analyzing “bodies that are much larger than their radius” (Beckers et al. 2015), where heat transfer

happens between the body and its surroundings.

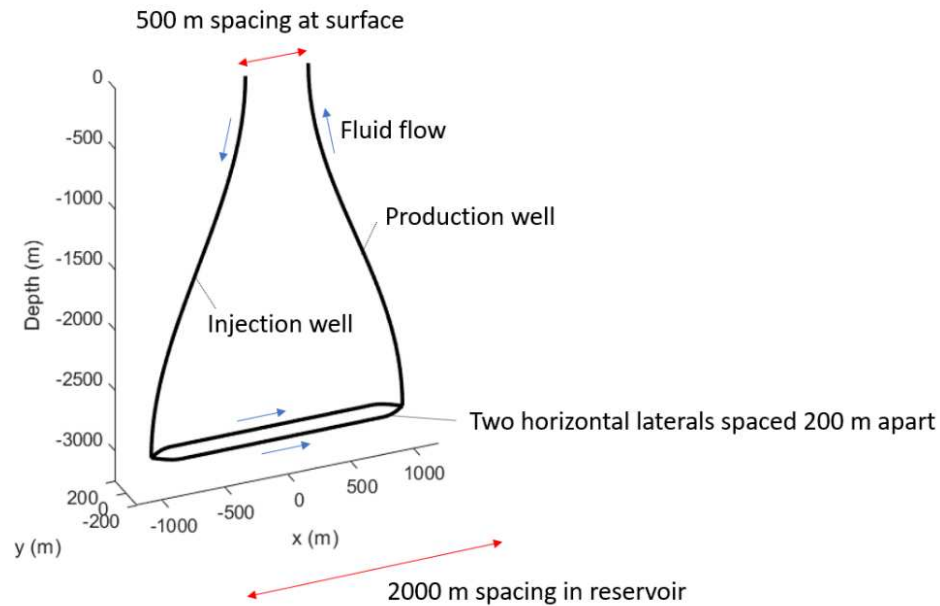


Figure 1.1: Heat exchanger’s geometry for the base case.(Beckers 2020), reprinted by permission of Koenraad Beckers.

This theory was applied and used by Beckers et al. (2015) to demonstrate its application on reservoir heat transfer for oil, gas, and geothermal wells. They used two heat transfer case studies: one using two parallel cylinders and the other with a slinky-coil design. For this research, the results are compared with results obtained using a thermal numerical reservoir simulator (CMG-STARS). It verifies the ability of CMG-STARS to model CLG concepts, and it will also serve as the base case for the models to be analyzed in this research. From the given properties of the reservoir, the simulation will be developed in CMG-STARS and compared with the SBT results.

1.1.2 Green Fire Energy – Pipe-in-Pipe

In the Coso Geothermal Field, GreenFire Energy has developed different demonstrations to prove the feasibility of CLG technology (Amaya et al. 2020a). In the different demonstrations done by this company, they have tested water and supercritical carbon dioxide (sCO₂) as working fluids in a tube-in-tube heat exchanger at 330 meters down the well. By using a down-borehole heat exchanger (DBHX), shown in Figure 1.2, GreenFire Energy has proved the potential of CLG technologies. The following are the results summaries under these demonstrations.

- *Water*: The main achievement of this demonstration is to verify the models created by Green Fire Energy as well as to prove that old and abandoned wells can be used to generate energy. The primary results using water show nearly 1 MW of electrical power without producing non-condensable gas (NCG) (Amaya et al. 2020b). In this case, low production rates were associated with higher temperature output in the surface and were verified by predicted results. For this case, with water as the working fluid, further work is required to consider the thermal energy depletion of the reservoir while enthalpy is being extracted, as most of these demonstrations only showed the initial output temperature. To make feasible the CLG concept, models and practical results need to show the sustainability of high temperatures and energy outputs during a long period of time.
- *sCO₂*: As a complimentary demonstration, sCO₂ was used as working fluid. Initially, this fluid increased the output temperature. One of the reasons to use sCO₂ as a working fluid is that it can achieve a strong thermosiphon effect to circulate the fluid in the loop without the need for a pump to sustain the fluid flow process, which was achieved in the demonstration. For this demonstration case, no supercritical expander with a generator was used to directly generate power. Different flow rates were tested, and as expected from the modeling results, lower flow rates led to higher output temperatures. The test results confirmed the models created by Green Fire Energy, and showed a smaller power generation for sCO₂ when compared to water as working fluid, but demonstrated that for this type of cycle no pumps are necessary to flow the gas into the loop.

The authors concluded that sCO₂ could be used as working fluid and increase the power output when the injected fluid can travel sufficient depth in order to build up pressure and maintain the thermosiphon. Additionally, a pump could be installed at surface to increase power production, so a greater amount of fluid can be injected into the closed-loop. Different well schemes and variables could be modeled in order to achieve better results and confirm the use of the closed-loop systems as well as an appropriate cost-benefit analysis.

The principal objective of this investigation is to determine the viability of the CLG technique and how the technology of the oil and gas industry can be implemented to make feasible this idea. From this, further properties are going to be modified to provide the best-case scenario to be implemented. On the other hand, the proposed model and simulations will be compared to

define sensitivities. Finally, all the results will be presented and discussed in order to propose ideal scenarios to generate geothermal energy.

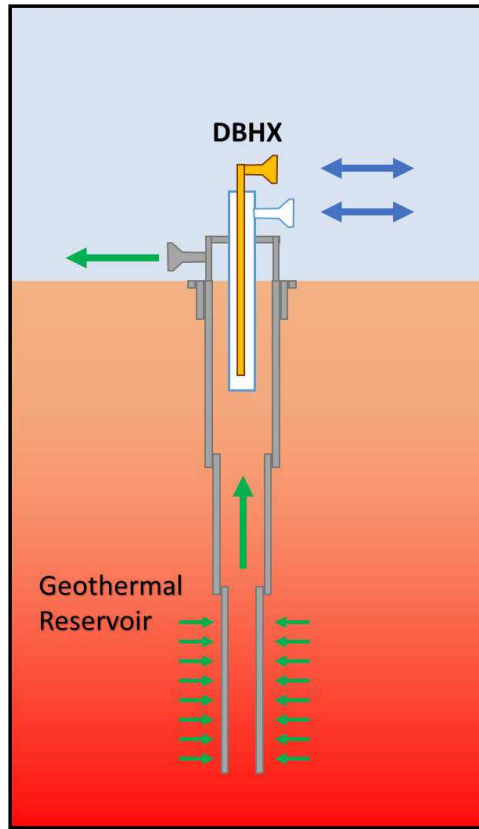


Figure 1.2: Down-Borehole Heat Exchanger (DBHX) schematic. (Amaya et al. 2020a), ©2020 by Green Fire Energy Inc., reprinted by permission of Green Fire Energy Inc.

1.2 Why CLG concept?

The CLG concept gives control of the reservoir geometry where there is no limitation on the direction of the well from the temperature convection side. It also works in tight hard rocks as it has no flow exchange between the reservoir and the injected fluid, controls fluid flow by the designed drilled paths. However, some of the paths proposed to be drilled require drilling techniques not currently available, but some of them are under investigation and development, such as Electro Pulse Boring (EPB), which can drill wells of 5-10 km by applying electro-pulse to the bottom of the well loosening the matrix surface at depth. It can drill well diameters up to 50 cm (Schiegg et al. 2015). Having said that, geothermal loops provide a non-ending energy source that can be used continuously for almost 30 years and can be an alternative use of abandoned petroleum wells

where the bottom hole temperature is suitable for this application.

Different simulations have been performed to estimate the produced temperature and heat over a 20-year lifetime for two different pipe geometries. The numerical model applied is based on the SBT for transient heat conduction (Beckers et al. 2015). SBT is selected to be evaluated in this investigation as it is an alternate solution, combining an asymptotic analysis with a numerical implementation to evaluate the heat transfer from the rock to the working fluid. Hence, the SBT is able to reduce computational times and gives accurate results. However, the SBT does not have the ability to evaluate pipe-in-pipe models, so it will be used to verify the results from the oil and gas software (CMG-STARs) for U-Shaped models, while previous studies will be used to verify pipe-in-pipe models.

1.3 Objectives

The main objective of this research is to evaluate the feasibility of CLG heat extraction technologies and to propose ideal cases that will help to develop this technology in the future for electricity generation. In addition, this research will help to understand the possible uses of this technology, especially for direct use in remote communities near abandoned petroleum wells with high temperatures at depth. Finally, technical analysis will be performed in order to determine the actual applicability of the concept, while also suggesting minimum requirements to completely develop the concept for electricity generation.

The following is the workflow proposed for this investigation, having three different approaches where the technology will be evaluated to determine its feasibility. At first, by using ideal data from a published modeling study, a base case will be created and simulated for each of the previous works in order to verify the applicability of a thermal reservoir simulator, CMG-STARs, for geothermal modeling. From the base case in a CLG configuration, different properties such as depth of the reservoir, reservoir temperature, type of fluid to be circulated in the pipes, and total production flow rate, are going to be modified in order to analyze different scenarios that can be applied to the CLG geothermal technology, following a numerical experimental matrix.

The proposed simulation software to run the cases is the thermal reservoir simulator STARs by Computer Modelling Group Ltd. This program has been applied for advanced modeling of oil recovery processes involving the injection of steam, solvents, air, and chemicals (Computer Modeling Group Ltd 2009). This program will provide reliable results as different models have

been developed by recent investigations at Colorado School of Mines. As a part of the investigation, some of the simulations are going to be compared with software outside of the oil and gas industry and previous work on Geothermal Closed-Loop heat extraction (Beckers et al. 2015).

The project is divided into the following research tasks:

- Task 1: Justify and verify previous results on geothermal heat extraction with petroleum engineering software (CMG-STARS).
- Task 2: Evaluate Closed-Loop geothermal designs using a numerical experimental matrix for the following configurations and working fluids:

U-Shape

Pipe-in-pipe

sCO₂ model

Water with nanoparticles of copper

- Task 3: Evaluate the feasibility of CLG application in Haynesville Shale abandoned oil and gas wells.
- Task 4: Technical analysis to assess the feasibility of the different CLG concepts evaluated in this research.

1.4 Thesis Organization

This thesis consists of six chapters. The summary of each chapter is presented as follows:

- Chapter 1 introduces the theoretical background and previous studies, explains the objectives of this research, and shows the thesis organization.
- Chapter 2 describes early studies done using a CLG concept and summarizes the main concepts used in the research.
- Chapter 3 presents the base case models and experimental matrix procedure and results.
- Chapter 4 evaluates the feasibility of each of the models studied in this research.
- Chapter 5 concludes the research and states the achievements and contributions of this study.
- Chapter 6 suggest future work as a continuation of this research.

CHAPTER 2

OVERVIEW

The following chapter presents an overview of the main concepts studied in this research. First, geothermal heat extraction and CLG are explained. In the second place, some of the most relevant CLG heat extraction case studies performed are described. Thirdly, the software proposed to model new cases is described, taking into account the basic equations used to model and simulate the heat transfer process in geothermal reservoirs. Finally, the possible applications of the concept are elucidated to give a background on the potential power generated from CLG.

2.1 Geothermal Heat Extraction

Low enthalpy aquifers, water production from oil and gas operations, Enhanced Geothermal Systems, Sedimentary Geothermal Systems, and CLG configurations are the most studied and proven technologies that can make geothermal a scalable source of energy. The latter has been studied with unsuccessful results that were not reliable, or were successful when modeled but not when implemented (Nalla et al. 2005). With modeling and drilling techniques from the O&G industry, most of these concepts are expected to have better modeling and implementation outcomes (Winsloe et al. 2020).

2.2 Closed-Loop Geothermal Heat Extraction

One of the main issues to generate geothermal power nowadays is strictly linked to the production of the heated fluid after the interaction with the rock at depth. Most of these liquids can be contaminated with dissolved chemicals or acid gases from the rock. These type of contaminants will need further treatment at surface and may also provoke corrosion throughout all the production system. Additionally, some geothermal reservoirs do not have enough permeability to recover the injected fluid at sufficient rates (Oldenburg et al. 2016). This problem is also linked to the methods needed to enhance permeability, such as hydraulic fracturing, which is controversial at political and social levels, as well as there are challenges associated with the effective stimulation of those reservoirs.

There have been many geothermal wells drilled to generate energy and have been left unused as the energy that was extracted did not meet the expected power to be commercial. By using closed-loop technologies and down-bore hole exchangers (DBHX), these type of wells could be re-adapted to increase their power production potential (Amaya et al. 2020a). The DBHX technology will be further explained as a pipe-in-pipe heat exchanger, where only one well needs to be drilled with fluid flow through a tubular and annular spaces.

Moreover, other CLG technologies have been proposed and are expected to be reliable for heat extraction. The U-shape well is conceptually the connection at the toe between an injection and a production horizontal wells where there are no open perforations to the geothermal reservoir. This type of concept has proven thermal power outputs of over 3MW to 5MW (Riahi et al. 2017). This heat extraction concept will be explained in the following sections.

The following are the proposed and initial scenarios to be studied in this research. Starting from the pipe-in-pipe and the U-shape configuration, initial models will be developed that serve as a base case for the design of an experimental matrix to determine the ideal parameters that could make the closed-loop concept feasible for electricity generation using water as the working fluid. Then, models for sCO₂ and water with nanoparticles of copper will be developed to understand and compare the potential efficiency of CLG with these working fluids. Finally, a realistic case will be modeled to determine the impact that this concept may have with potential abandoned petroleum wells, which can be used as pilots for this concept for possible direct use or electricity generation applications.

2.2.1 Pipe-in-Pipe

The pipe-in-pipe configuration is also known as coaxial heat extraction or Well Bore Heat Exchanger (WBHX), it consists of two concentric pipes. The fluid could be injected from the annular or the tubular section, circulated to the bottom of the well, and then produced from the section that is not injecting as it is shown in Figure 2.1. This configuration prevents direct fluid contact with the rock and has the advantage of producing from the same location where the fluid is injected. Also, it provides a simpler well path that can be easily drilled and could be found within abandoned O&G wells.

Since the 1980s, different studies have been conducted to prove and analyze the performance of a coaxial heat exchanger to extract heat from the subsurface. Initial studies considered conductive

heat transfer into a well, showing that for this type of configuration to be feasible, injection flow must be maintained at the same Reynolds number in the upward and downward flows (Horne 1980). Additionally, the reverse flow configuration (i.e., injection through the annular and production from the tubular) shows slightly better results. Some other considerations such as the outer diameter of the well seemed to be of major importance to achieve higher temperature outputs.

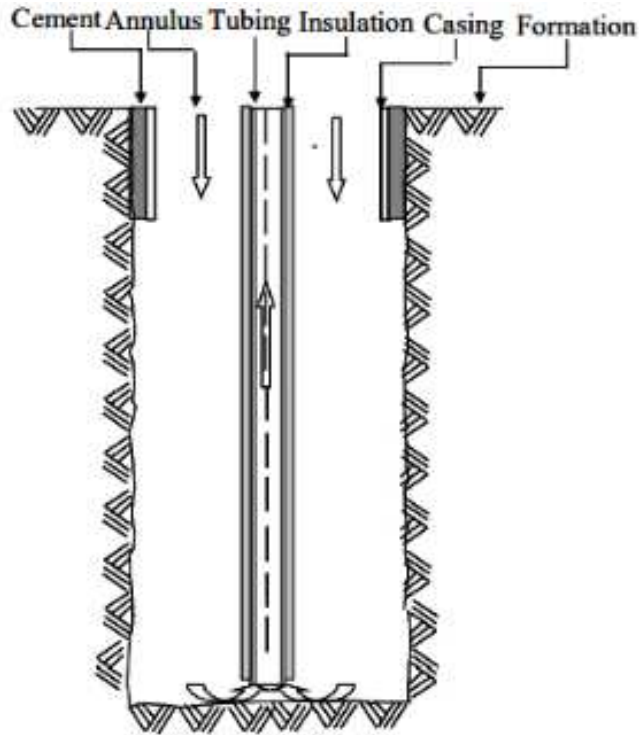


Figure 2.1: Wellbore Heat Exchanger (WBHX) configuration. Reuse with permission provided by Elsevier and Copyright Clearance Center (Nalla et al. 2005).

Recent studies started using numerical simulation and new technologies available to depict a better demonstration of this type of configuration. Starting from the basic explanation of the WBHX with a vacuum insulated pipe that will provide ideal insulation from the injected to the produced fluid, Nalla et al. (2005) developed different models using TETRAD software. All the models, in this case, were created for a vertical well. After different models were created and simulated, an ideal and “Best Case” was obtained, representing the best results considering the following parameters after a sensitivity analysis:

- *Circulation rates:* After analyzing different flow rates, it is clear that residence time is a key factor to achieve higher temperatures at surface when the fluid is circulated through the loop. Parallel to the produced temperature, the mass rate needs to be correlated to the ideal work rate to produce enough energy. From the results, 100 gpm of circulation was chosen to be the ideal flow rate for the case studied.
- *Wellbore diameter:* While residence time proves to have a major influence on ideal work rates, a bigger well diameter is associated with higher drilling costs. After different runs, the increase in well diameter will give better results but will not be feasible after comparing the increase in drilling costs.
- *Tubing properties:* Nalla et al. (2005) finds that tubing properties were of secondary importance to the efficiency of energy extraction.
- *Working fluid:* Based on water as working fluid, the main properties that affect the fluid thermal exchange were modified (i.e., fluid density, specific heat, volumetric heat capacity). After different runs, the best case showed that a fluid with higher volumetric heat capacity will give better results. On the other hand, regular water showed promising results after reaching Pseudo Steady State (PSS), where there is no temperature decrease in the produced fluid.
- *Basal Heat Flux:* Authors compared different basal heat fluxes with known geological data from specific formation types. This varies the depth to where 350 °C can be found.
- *Formation Types:* Thermal conductivity and thermal diffusivity are the main properties that would lead to a higher and stable temperature diffusion from the formation to the working fluid. Shale and limestone showed better results once PSS is reached.

The following were the parameters taken into account for the Best-Case scenario:

In this work, this case will be modeled using CMG-STARs to review the results and to verify the consistency between the numerical results with the results displayed in Nalla et al. (2005). Starting from this model and using some of the data from the Coso Geothermal Field, different ideal scenarios will be taken into account to create an experimental matrix. These models will be simulated with horizontal wells to study the possible energy output increase by modifying the parameters mentioned earlier.

Table 2.1: Best case scenario for vertical pipe-in-pipe. Modified from Nalla et al. (2005)

Parameter	Value
Tubing Inner Diameter	3 in.
Tubing Outer Diameter	3.5 in.
Insulation Outer Diameter	4 in.
Casing Inner Diameter	9 in.
Casing Outer Diameter	9.625 in.
Well Depth	5,593 m
Basal Heat Flux	0.1 W/m ²
Formation Thermal Conductivity	1.89 W/m °C
Formation Volume Capacity	1875.7 kJ/m ³ °C
Working Fluid Volume Capacity	4186.8 kJ/m ³ °C
Insulation Thermal Conductivity	0.07 W/m °C
Circulation Rate	100 gpm (6.3 L/s)
Surface Temperature	26.7 °C
Bottom Hole Temperature	350 °C

2.2.2 U-Shaped Configuration

Most recent studies have developed new and novel ideas where the CLG configuration may obtain the desired results to generate power. This type of configuration has shown an expected thermal power of 8 MW after 20 years (Beckers et al. 2015). Most of these designs are feasible from the modeling side but have big challenges from the practical side.

Initially, all of these designs come from the theoretical idea of a producer and an injector well that connect at the toe of their horizontal section. Both wells should be completed in order to not interchange fluids with the formation, creating a closed-loop environment. From one well, the fluid will be injected, then circulated through the loop where the fluid gets heated up, and finally, produced at surface in the producer well.

From the beginning, connecting both wells will need a clinical, exhaustive, and costly directional drilling procedure to connect at specific coordinates, as well as some completion challenges. The problem of connecting a couple of wells will be challenging, connecting two or more will increase the complexity and consequently, the drilling cost. The challenge will be magnified if multiple laterals are drilled as sidetracks from the parent well (Figure 2.2(a)).

The spiral design, as shown in Figure 2.2(b), will need not only the challenge of connecting the “producer” and the “injector” well. The well trajectory is challenging as to reach these spirals,

the build angle will be high as nearly as impossible, as well as the measurement of the process. Surveys will be nearly ineffective as the measurement point will be a spiral behind on where the bit is located and without an exact location on where the bit is located, the complete process is impossible even with today's technology.

As the modeling side has been proven to be feasible, the results of these simulations could be replicated using petroleum engineering software. From this point, the trajectories shown in Figure 2.2, can be modeled and can be used as a starting point to simulate models that are feasible from the theoretical, and practical point of view.

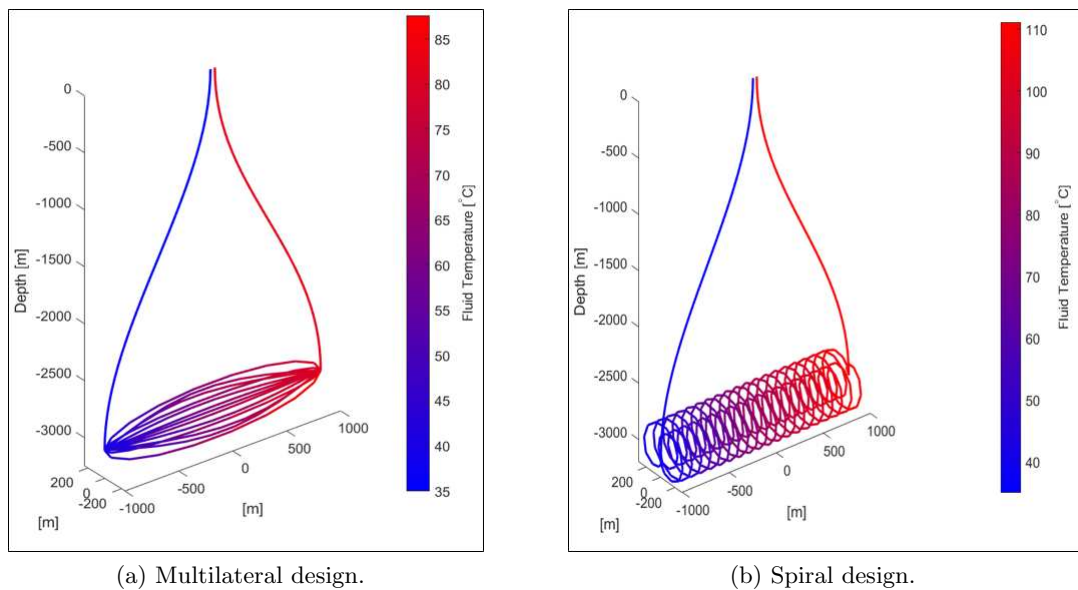


Figure 2.2: U-shaped configurations. (Beckers 2018), reprinted by permission of Koenraad Beckers.

2.2.3 Working Fluids

As well as residence time and mass rate injected in the process, the type of fluid has a big impact on the output temperature and energy potential of the process. In this study, different types of fluids will be evaluated in terms of the CLG system performance, considering output temperature, efficiency, and costs. The initial fluids to be studied (water and $s\text{CO}_2$) have been already evaluated in this type of concept. However, an additional working fluid is studied in this work as its theoretical application could enhance the heat extraction from high temperature sources at depth. The proposed fluids are:

- *Water:* As the most common fluid at any operation, water has proven reliability in almost every scenario for geothermal technologies. However, most of these applications required low flow rates that result in high temperature outputs but with low energy generation. Desirable CLG systems should produce high temperatures and energy outputs during a long period of time with high injection rates. Nonetheless, water is a valuable resource, that is sparse in many regions in the world, as well as it is corrosive and may induce problems in the pipes of the system (Phuoc et al. 2017) where it might not be feasible to be used for this type of technologies.
- *sCO₂:* As an alternative to water, carbon dioxide shows closer energy outputs than water in early investigations. sCO₂ can develop a thermosiphon to circulate the fluid in the loop, so no pump would be needed in the process, reducing investment and energy input during the operation of the CLG system. sCO₂ could be used as working fluid and increase the power output when the injected fluid can travel to sufficient depths in order to build up pressure and maintain the thermosiphon. Different well schemes and variables could be modeled in order to achieve better results; nonetheless, there are convergence obstacles that need to be taken into account when creating CO₂ models. On the other hand, the flow rate needed for CO₂ is about 5 times higher than that of the water in order to achieve the same thermal efficiency, in consequence, the energy output from the process using carbon dioxide could be up to ten times more than water as working fluid (Phuoc et al. 2017).
- *Fluids with nanoparticles of copper:* It is "well known that at room temperature, metals in solid form have orders-of-magnitude larger thermal conductivities than fluids." (Choi and Eastman 1995). As a consequence of the size of a nanoparticle, it is expected to flow in the loop as a molecule of fluid. Furthermore, as a consequence of not having physical contact with the rock, the actual composition of the fluid will not deteriorate the rock properties, which could be an issue when using nanoparticles in an injected fluid. Previous studies have shown a large improvement in effective conductivity with fluids that contain copper nanoparticles, an advantage that can be used to enhance the heat extraction on a CLG concept (Choi et al. 2001).

2.3 Numerical Modeling for Geothermal Energy

There have been copious geothermal reservoirs simulated around the globe. Numerical simulation from oil and gas could be applied in order to model geothermal processes, where thermal changes are simulated along the rock surrounding the reservoir. CMG-STARS has this capability and previous models can be verified using this software to prove its feasibility in the CLG concept. While different models are created and evaluated, technologies can be developed to make geothermal feasible.

As mentioned by Fanchi (2018), every reservoir simulator includes two different models – a reservoir model and a well model. The reservoir model represents the flow and interaction of the fluids in the rock, while the well model shows the extraction or injection of fluids from and into the reservoir. Reservoir simulators can be used in areas outside oil and gas (Fanchi 2018), for this specific case, thermal and fluid interaction can be used to model a closed-loop geothermal system. The most important interactions and physical phenomena for a geothermal simulation are included in simulation packages such as CMG-STARS, where both fluid flow and thermal equations are included in the reservoir model, accompanied by a complex well model (FlexWell).

2.3.1 CMG-STARS

The following are the conservation equations used by CMG-STARS, describing the changes based on a region of interest, where we have (Computer Modeling Group Ltd 2009):

Rate of change of accumulation =

$$\text{Net rate of inflow from adjacent regions} + \text{Net rate of addition from source and sink} \quad (2.1)$$

For this specific case, STARS will use conservation of mass and energy for water to predict thermal and fluid changes in the reservoir. The mass conservation equation considering only the water phase is,

$$V \frac{\partial}{\partial t} \left[\phi_f(\rho_w S_w w_i) + \phi_v A d_i \right] = \rho_w S_w w_i + \phi \rho_w D_{wi} \Delta w_i + \rho_w q_{wk} w_i \quad (2.2)$$

A general mass conservation equation considering multiple phases that could be present in the reservoir is,

$$\begin{aligned}
V \frac{\partial}{\partial t} \left[\phi_f (\rho_w S_w w_i + \rho_o S_o x_i + \rho_g S_g y_i) + \phi_v A d_i \right] = \\
\rho_w S_w w_i + \rho_o S_o x_i + \rho_g S_g y_i + \\
\phi \rho_w D_{wi} \Delta w_i + \phi \rho_o D_{oi} \Delta x_i + \phi \rho_g D_{gi} \Delta y_i + \\
\rho_w q_{wk} w_i + \rho_o q_{ok} x_i + \rho_g q_{gk} y_i
\end{aligned} \tag{2.3}$$

Where V is total volume of the grid block, ϕ_f is fluid porosity, ϕ_v is void porosity, ρ_w is water density, S_w is water saturation, w_i is concentration of component i in aqueous phase, Δw_i is change in concentration of component i in aqueous phase, $A d_i$ is adsorbed component i , q_w is water source/sink flow rate, q_{wk} water well phase rate, D_{wi} is component dispersibilities, and ϕ is absolute porosity.

The energy conservation equation considering water phase and the reservoir rock is,

$$V \frac{\partial}{\partial t} \left[\phi_f (\rho_w S_w U_w + \phi_v c_s U_s + (1 - \phi_v) U_r) \right] = \rho_w V_w H_w + K \Delta T + \rho_w q_{wk} H_w \tag{2.4}$$

A general energy conservation equation considering multiple fluid phases and solid rock is,

$$\begin{aligned}
V \frac{\partial}{\partial t} \left[\phi_f (\rho_w S_w U_w + \rho_o S_o U_o + \rho_g S_g U_g) + \phi_v c_s U_s + (1 - \phi_v) U_r \right] = \\
\rho_w V_w H_w + \rho_o V_o H_o + \rho_g V_g H_g + K \Delta T + \rho_w q_{wk} H_w + \rho_o q_{ok} H_o + \rho_g q_{gk} H_g
\end{aligned} \tag{2.5}$$

Where U_i is internal energy for $i = w, o, g, \text{ and } s$; U_r is energy per rock volume; c_s is total solid concentration; H_w is water enthalpy, ΔT is temperature gradient, and K is thermal conductivity.

CMG-STARS is able to convert the initial data for a Black Oil fluid model into a STARS compositional model. To achieve this, density, viscosity, and phase equilibrium are converted to achieve temperature dependence. With this, CMG-STARS is able to model fluid properties taking into account the effect of energy and temperature for a thermal process in the reservoir.

CMG's most recent versions have introduced a complex flexible wellbore modeling tool, which is capable of simulating special well geometries. This subsection of CMG-STARS is able to simulate advanced well completion and geometries as well as it can model complex interaction between the well and the reservoir that are related to heat transfer and fluid flow that cannot be modeled by a sink/source well. This optional section can evaluate well configurations of an annulus and up to three tubing strings where one of them could be a concentric tubing (Computer Modeling Group Ltd. 2015).

For this specific research, FlexWell allows modeling the complexities needed in a CLG system. It is able to model "temperature and pressure interaction between each element of the wellbore and the reservoir" (Computer Modeling Group Ltd. 2015), which is one of the main aspects to be evaluated in a pipe-in-pipe configuration. CMG-STAR3 is the adequate model for this study as FlexWell is able to simulate the heat transfer in the well, while the traditional mass and energy conservation equations are used for the changes in the reservoir.

2.4 Direct Use Application

Some of the preliminary results and early studies show that the CLG concept can be used as an alternative for direct use applications. When having low rates but high temperatures, the energy output may not be feasible for power generation; however, the high temperatures show an opportunity to be used for heat pumps, space heating, greenhouse, open-ground heating, and industrial heating processes (Lund et al. 2005). Iceland's infrastructure is an ideal example of direct use applications, where its implementation supplies up to 62% of the country's energy demand and almost 90% of the heating demand (Tester et al. 2015).

Direct-use application can save 30 to 50% of conventional heating methods, but its application requires a detailed and excellent engineering design. Transmission pipelines and distribution networks need to be selected and designed in the most efficient way in order to achieve a successful process. Additionally, these applications have different temperature ranges to be used so the fluid needs to be efficiently used, for each of the temperatures so many processes can be developed from the heated fluid in underground resources (United States Department of Energy 2016).

Low temperature direct use systems need at least the following elements (United States Department of Energy 2016):

- Production facility.
- Mechanical system.
- Peaking or back-up plants.
- Disposal system.

The main goal of a CLG system is to obtain high differences between the temperature of the injected fluid and the produced fluid at the end of the process. The higher the difference, the

smaller the investment, as well as less equipment would be needed to develop direct-use applications. Additionally, a two-way distribution network would be feasible for a CLG process, as the working fluid is needed to be recycled in the process (United States Department of Energy 2016).

One of the biggest factors that has made CLG not feasible in the past is the cost of the drilling operation. As the residence time of the injected fluid plays a major role in outlet temperature, longer wells are most effective for this technology. Additionally, as deeper wells might be costly because of high pressures and high temperatures, pre-existing wells where high temperatures have been encountered can be re-adapted for this technology saving initial costs of drilling and completing new wells.

Haynesville Shale play is one of the unconventional reservoirs that has been developed as a consequence of hydraulic fracturing. Since 2008, this play has increased the wells drilled, especially with horizontal technology to be eventually used for hydraulic fracturing. As a Jurassic Period rock formation (Parker et al. 2009), it is located at high depths, with high pressure and high temperature conditions at net pay depths.

There is evidence of temperatures that reach up to 335 °F (168.3 °C) in the Haynesville Shale Formation (Franquet et al. 2019) more specifically at DeSoto Parish, LA. at depth that ranges from 10,300 ft to 14,000 ft (Parker et al. 2009). On the other hand, after the “fracking boom,” copious horizontal wells have been drilled in this play followed by hydraulic fracturing. While this shale play has been increasing its gas production, many wells are starting to deplete or even being abandoned. These wells can be recycled not only to perform studies, but also to prove an energy output for direct geothermal use near the location of the wells.

Direct use application may be achieved by the use of these abandoned or low productive wells. As most of the wells have already been drilled, cemented, and completed, the costs of energy production or initial investment will decrease significantly. On the other hand, most of the wells drilled in this shale play, have sufficient Measured Depth (MD) to increase the time of residence of the injected fluid. When adding the reservoir depth (10,000-14,000 ft) plus the horizontal length (3,000 ft) a total of 13,000 to 17,000 ft can be achieved and used for the application of closed-loop geothermal heat extraction.

For this study, the energy output will be analyzed for both ideal and real scenarios in order to determine the feasibility of power generation or direct use application. Additionally, as this

scenario is taken into account, there will be more opportunities to develop the concept as it can be used in a simpler and economic way. Direct use offers a simpler and more economic investment in surface equipment compared to power generation where the investment needs to be greater. Furthermore, technical analysis will show a proper application of the process taking into account technology developments available in the present to make CLG feasible in Haynesville or any other reservoir with similar temperatures.

2.5 Geothermal for Electricity Generation

Geothermal resources have been used for a long time in the history of mankind, as it takes advantage of Earth's heat and energy; however, most of these applications are only used for direct use applications. To completely make geothermal energy a feasible replacement of fossil fuels, an effective conversion from thermal power into electrical power is needed; nonetheless, this conversion has maximum conversion rates of around 50% (Beckers 2016). This is why the main focus on geothermal needs to find the ideal hydrothermal resource and develop efficient power plants where thermal outputs can be used for electricity generation.

While there has been a long development of geothermal resources for direct use applications, geothermal for electricity has been studied for many decades. Many high temperature resources have been used to generate electricity by condensing turbines, which have the same principle as conventional coal and oil-fired power plants, these types of power plants need temperatures above 200 °C to work efficiently (Verkis Consulting Engineers 2014). Temperatures below 200 °C are not feasible for electricity generation using steam condensing power plants. Nonetheless, binary plants can generate electricity from lower thermal inputs as low as 75 °C. Additionally, these plants are developed to generate power as low as 250 kW (Verkis Consulting Engineers 2014) and are a perfect fit for CLG as the fluid can be re-injected in the loop after being used in the power conversion.

The most common and studied binary plants can be divided into two categories:

- Organic Rankine Cycle (ORC)
- Kalina Cycle Power Plant (KCP).

ORC is a common application for low enthalpy applications where the geothermal fluid is passed through the plant and it is able to heat up a working fluid with a lower flashpoint that is able to vaporize and expand into a turbine to generate electricity. Then the fluids in both sides of the

interchanging unit return to their respective loop. These cycles have thermal efficiencies between 7-15% when using one stage. When the process is improved to a two-stage cycle, the efficiency can be enhanced (Verkis Consulting Engineers 2014). A diagram of a two-stage ORC can be seen in Figure 2.3.

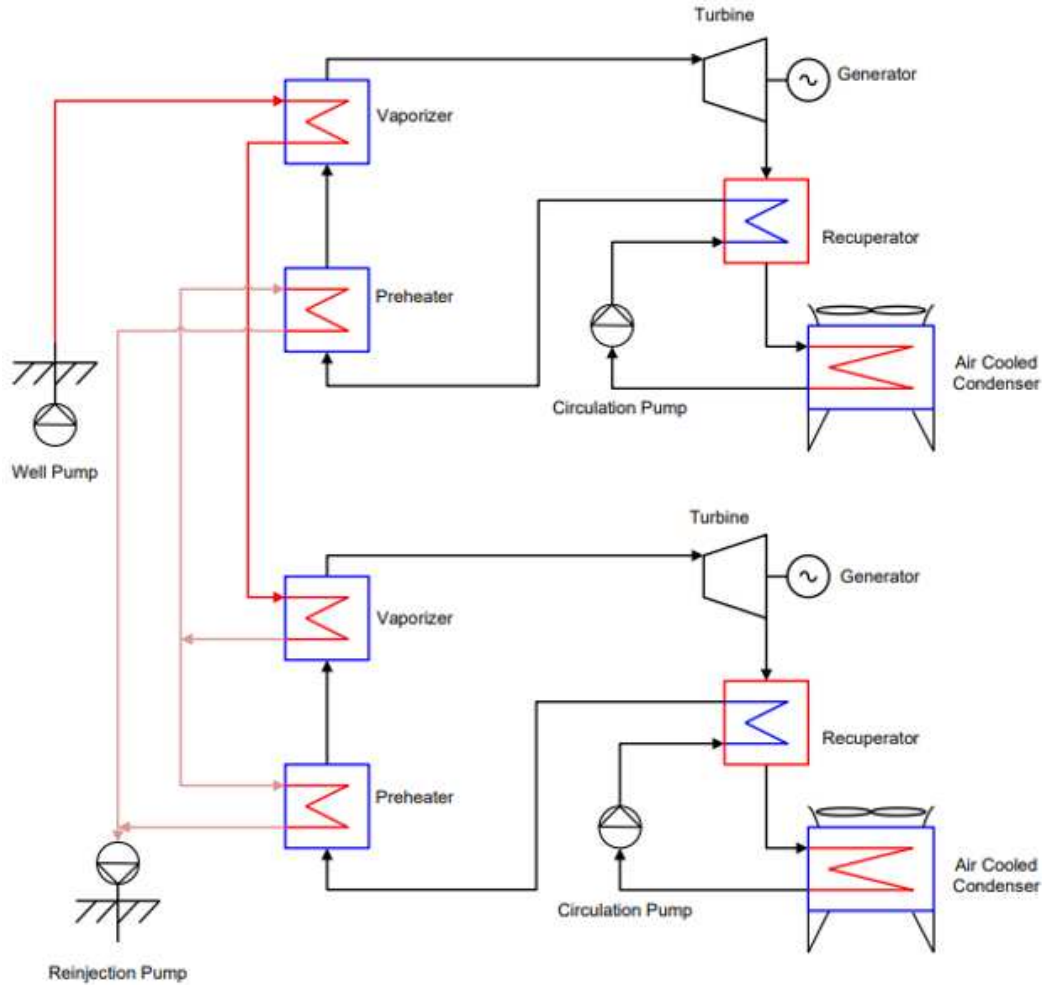


Figure 2.3: Two stage ORC diagram with an air cooled condenser. (Verkis Consulting Engineers 2014), © 2014 by Verkis Consulting Engineers, reprinted by permission of Verkis Consulting Engineers.

Despite their thermodynamic efficiency, KCP is less developed than ORC plants. KCP uses ammonia and water as working fluids where the concentration of ammonia is changed during the process. An increase of 10-30% in efficiencies can be expected from Kalina Cycle as the exhaust pressure is above the atmospheric conditions (Dincer and Demir 2018). However, there are not many applications referenced for these types of plants (Verkis Consulting Engineers 2014), but for

CHAPTER 3

MODELING CLOSED-LOOP GEOTHERMAL SYSTEMS

To assess the feasibility of Closed-Loop Geothermal Systems, different modeling scenarios and working fluids are considered in this simulation study, which will be analyzed later to recommend conditions for feasible application. Two different modeling scenarios will be evaluated in an experimental matrix; a U-shape and pipe-in-pipe configuration. Three working fluids are analyzed as well; freshwater, sCO₂, and water with nanoparticles of copper. Additionally, ideal cases will be created that enhance results, to identify required conditions for electricity generation. Then, a real case will be modeled in order to land CLG to an existing reservoir and well path. Finally, a technical evaluation of direct use will be performed, in order to expand the concept into a new and more realistic application.

3.1 Base Case Scenarios

At first, two base case scenarios will be created to evaluate ideal parameters in the previously described concepts. A pipe-in-pipe model that will be verified against the model presented by Nalla et al. (2005). This model will be used to begin the experimental matrix for the concept evaluation. Followed by the pipe-in-pipe base case model, a U-Shaped model will be verified against the SBT model described by Beckers et al. (2015) and following the same process, it will be used to evaluate different parameters in an experimental matrix. It is to be mentioned that these models are based on hypothetical cases, so the reservoir parameters are to be treated as shown in natural circumstances, calculating pressure and temperatures along the wellbore with standard gradients, respectively. Furthermore, the model is created assuming heterogeneity in the rock surrounding the well. The following are the procedure and results for the base case scenarios.

3.1.1 Pipe-in-Pipe Model

As mentioned earlier in Chapter 1, previous studies show that some pipe-in-pipe configurations have promising results. Here, a pipe-in-pipe model presented by Nalla et al. (2005) is reproduced, where they studied the feasibility of the pipe-in-pipe configuration on a vertical well. The input parameters used for this model are shown in Table 2.1. CMG-STARs is used to create this model

and the results are compared for verification.

The following is the procedure for the creation of the model:

Reservoir grid and properties:

At first, a Cartesian grid is created for the I, J, and K direction having 65, 59, and 86 blocks, respectively. Each block is addressed by a User Block Address (UBA). As mentioned in Nalla et al. (2005), the well depth used in this study was 5,593 m (18,350 ft). These parameters allow a correct geometry generation. In order to achieve better convergence, the grid size was not the same for all the grid blocks - along with the wellbore location, the grid size has been refined. Refining the grid along the wellbore also allows a better representation of temperature changes in the rock surrounding the well.

Secondly, the reservoir parameters need to be defined. For this specific type of configuration, there is no interaction between the injected fluid and the rock, so porosity and permeability were set up as constants with values of 5% and 0.001 md, respectively. A water saturation of 100% was defined. Pressure also needs to be defined, even if the model has no open perforations. To determine the pressure distribution within the reservoir, a normal hydrostatic gradient is used assuming 10 kPa/m. Rock compressibility is also assumed as $4.35 \text{ E}^{-7} \text{ kPa}^{-1}$. The previous properties do not affect the simulation output; nevertheless, they are needed to initialize the numerical simulation.

Table 3.1: Input parameters for the reservoir and grid section

Parameter	Value
Constant Porosity	5%
Constant Permeability	0.001 md
Water Saturation	100%
Hydrostatic Gradient	10 kPa/m
Rock Compressibility	$4.35 \text{ E}^{-7} \text{ kPa}^{-1}$
Formation Thermal Conductivity	1.89 W/m °C
Formation Volume Capacity	1,875.7 kJ/m ³ °C
Working Fluid Volume Capacity	4,186.8 kJ/m ³ °C
Temperature Gradient	0.062578 °C/m

The thermal properties of the rock and the fluids need to be precisely defined as they indeed, affect the simulation output. From Nalla et al. (2005), the volumetric heat capacity used for the best case described was 1,875.7 kJ/m³°C, with a formation thermal conductivity of 1.89 W/m°C and a working fluid volumetric heat capacity of 4,186.8 kJ/m³°C. Since the bottom hole temperature

is 350 °C, a temperature gradient was calculated using this temperature in order to determine the temperature distribution within the reservoir, noticing that this may not be a normal temperature gradient.

The reservoir parameters used in the CMG-STARs model are presented in Table 3.1. Figure 3.1 depicts the 3D view of the base case model along with the temperature distribution calculated with the temperature gradient.

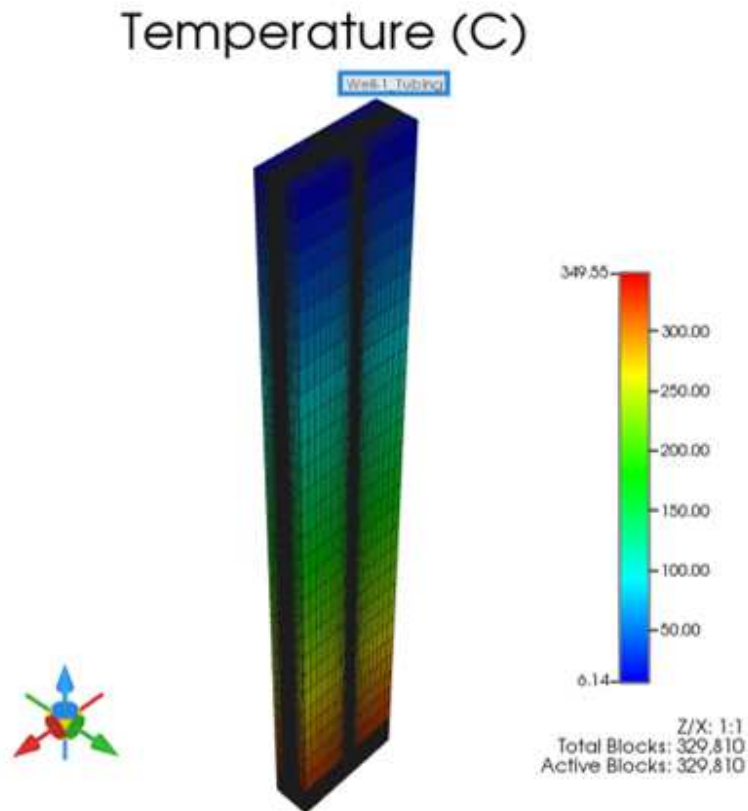


Figure 3.1: Temperature distribution for the pipe-in-pipe base case model.

Components:

In Nalla et al. (2005), freshwater is being used as the working fluid for the model. For CMG, we simply add H₂O and use its default values. Under liquid phase properties/densities, 0 should be the input for CMG to calculate the values, the same procedure should be followed for the H₂O values under the enthalpies tab. For the liquid phase viscosities, AVISC and BVISC values should be 0.0047352 cp and 1515.7 °C, respectively, as it is recommended in the STARs manual for the given temperature (Computer Modeling Group Ltd 2009). Also, the reference pressure

and temperature need to be specified under the general tab, as well as the surface pressure and temperature. Atmospheric pressure and the reference pressure at 5593 m from the geothermal gradient (126,797 kPa) are used. Surface temperature is established in the paper as 26.7 °C and temperature at depth of 350 °C.

Table 3.2 shows the list of properties used in this section.

Table 3.2: Input parameters for the components section

Parameter	Value
AVISC	0.0047352 cp
BVISC	1515.7 °C
Reference Pressure	126797 kPa
Reference Temperature	350 °C
Surface Pressure	101 kPa
Surface Temperature	26.7 °C

Rock-Fluid:

As in this concept there is no interaction of the injected fluid with the rock, the input parameters related to rock-fluid interactions do not play a major role; nevertheless, the software needs to have defined relative permeability tables to initialize the simulation. A simple table of two rows can be inputted under the relative permeability tables tab exactly as shown in Table 3.3.

Table 3.3: Input values for relative permeability tables

S_w	k_{rw}	k_{row}
0	0	1
1	1	0

Initial Conditions:

In this section, while needed to generate equilibrium between the phases in a porous media, these inputs do not play a major role in this specific case. The reservoir is fully saturated by water; we are not modeling rock-fluid interaction. Nonetheless, at least a reference pressure and a reference depth need to be entered into the software so it can initialize the simulation. In this case, we will use 5,592 m and 55,920 kPa as the reference depth and reference pressure, respectively, parameters that comply with what could be found at the proposed model. Table 3.4 shows the required data for this section.

Table 3.4: Input parameters for the initial conditions section

Parameter	Value
Reference Pressure	126,797 kPa
Reference Depth	5,592 m

Numerical:

As it is explained in the CMG-STARs users guide (Computer Modeling Group Ltd 2009), the numerical section is not being modified and the model will run with the default values. If there is any problem during the simulation related to the convergence of the numerical solution, these values can also be modified to improve the stability of the simulation.

Geomechanics:

As it is an optional section mainly developed for geomechanical interactions in the reservoir, there is no modification for this section as this model has no flow interaction with the rock.

Wells and recurrent:

This section is the main focus of this model, as the fluid will always be flowing through the well. The wells and recurrent section will be divided into two subsections that are the well creation and the FlexWell definition that is needed for this model.

Well creation:

Three wells need to be created; two wells for the actual configuration needed and an extra well that will play a role as an extra layer in the model that will be connected to the reservoir allowing fluid to enhance the thermal convection throughout the system, the latter will have an open perforation. The “Tubing” injector well will have no open perforations while the “Concentric Tubing” will have an open perforation at depth (UBA: 33, 30, 56). The procedure of the well creation is explained below, starting from the outer section of the well configuration as it will be done during drilling and completion of the wells.

The first well is named “Annulus” as it will be the annular section of the pipe-in-pipe configuration for FlexWell. Its trajectory needs to be attached to the refined grid blocks that have been created in the reservoir and grid properties section, more specifically from the UBA (33, 30, 1) (surface) to the UBA (33, 30, 57) (bottom hole depth). This also helps with future cases, as the well trajectory will be attached not to a specific location, but to a grid block that is already created.

Also, its perforations need to be created with the “quick perf” tool from the software, using the same procedure as the well trajectory where the perforations will be attached to the UBA location.

Followed by the creation of the well trajectory and perforations, the well type needs to be specified. For this case, the “Annulus” section is specified as a producer well under the “ID & Type” tab with an operate constraint of a maximum surface water rate (STW) of 0 m³/day, and an operate constraint, with a minimum bottom hole pressure (BHP) of 5,000 kPa (as shown in Table 3.5), even if in the end, the well is shut-in. Under the well completion, general tab, the radius of the well is specified as 0.115 m.

Table 3.5: Input parameters for the initial 'Annulus' well

Constraint	Parameter	Limit/Mode	Value
OPERATE	STW surface water rate	MAX	0 m ³ /day
OPERATE	BHP bottom hole pressure	MIN	5,000 kPa

As this is a pipe-in-pipe configuration, the initial well is copied to create the same well that will be named “Tubing”. In this case, an injector well will be specified (injector mobweight implicit) with an operate constraint of a maximum surface water rate (STW) of 545 m³/day, and an operate constraint, with a maximum bottom hole pressure (BHP) of 100,000 kPa (as shown in Table 3.6). The water rate is the one indicated in the ideal case by Nalla et al. (2005), the BHP is the one that enables the model to have flow. As there will be no physical connection between the wells and the rock, there is no need to set up completions for this well (it is important to mention that CMG-STARS will show a warning as there are no completions; however, this will not affect the simulation run). Finally, the injected fluid is defined as water that should be available from the previous component definition. As it is the only component in the fluid mixture, 1.0 mole fraction is typed. Other input parameters needed are an injection temperature of 25 °C, steam quality of 0, and pressure of 20,000 kPa, as it is shown in Table 3.8. Under the well completion, general tab, the radius of the well is specified as 0.11 m.

As in the previous step, the same process is repeated to create a well named “Concentric Tubing”. Later on, in the FlexWell option, those wells will be assigned as their name is being implied. The 'Concentric Tubing' well needs to be defined as a producer with an operate constraint of a minimum BHP of 5,000 kPa (as shown in Table 3.7). Under the well completion, general tab,

the radius of the well is specified as 0.0505 m.

Table 3.6: Input parameters for the initial 'Tubing' injector well

Constraint	Parameter	Limit/Mode	Value
OPERATE	STW surface water rate	MAX	545 m ³ /day
OPERATE	BHP bottom hole pressure	MAX	100,000 kPa

Table 3.7: Input parameters for the initial 'Concentric Tubing' producer well

Constraint	Parameter	Limit/Mode	Value
OPERATE	BHP bottom hole pressure	MIN	5,000 kPa

Table 3.8: Input parameters for the injected fluid

Parameter	Value
Temperature	25 °C
Steam quality	0
Pressure	20,000 kPa

FlexWells:

This section allows to model the pipe-in-pipe configuration for this model. But before creating the configuration, the open perforations need to be created for the already created wells. The wells are located from the UBA (33,30,1) to (33,30,57). The “Annulus” well will have all the perforation intervals closed and the last interval will have an open perforation corresponding to $K = 57$. The “Tubing” well will have its last operation interval in $I = 56$ and this perforation should be closed. Finally, the “Concentric Tubing” last perforation interval is located at $I = 55$ and it will be the only open perforation. This allows the model to understand that there is space in between the configuration, and the fluid can move in the desired path as it is shown in Figure 3.2, where the “Annulus” and the “Tubing” act as the real outer volume of the conceptual annular section, while the concentric tubing acts as the conceptual tubular section.

Once the perforations are defined, the FlexWell option is used. Firstly, a new FlexWell is created and the “Filter Wells” option should be selected to select the already created wells. “Annulus” well is selected, leaving the casing properties as default and choosing constant diameter.

Table 3.9: Input parameters for the well radius under the perforations definition

Well	Radius
'Annulus'	0.115 m
'Tubular'	0.11 m
'Concentric Tubular'	0.0505 m

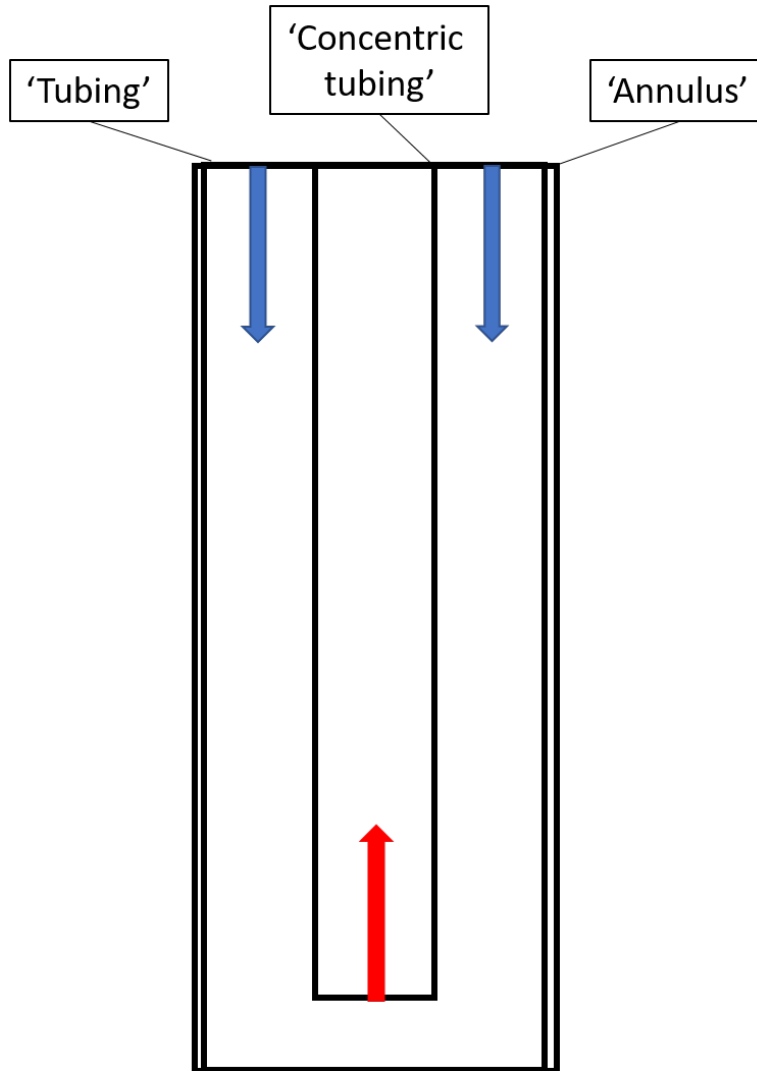


Figure 3.2: Well configuration for FlexWell.

Then the “Tubing” well is added from the option “Add Tubing”, and the insulation heat capacity and insulation heat conductivity need to be corrected to the same default values from the wall properties. Finally, the “Concentric Tubing” is added from the option “Add Concentric Tubing”, and an isolation material needs to be defined by inputting the values given in Table 3.10

Table 3.10: Input parameters for the insulated pipe

Property	Value
Wall Heat Capacity	1.63e+06 J/(m ³ °C)
Wall Heat Conductivity	4,320 J/(m day °C)
Insulation Heat Capacity	3283 J/(m ³ °C)
Insulation Heat Conductivity	168 J/(m day °C)

The last property to be defined is the well diameter. The radius is already defined; nonetheless, it is needed to define the diameter again in the FlexWell option. Simply, as previously the radius was defined and now the input parameter is the diameter, the values of the radius will be multiplied by two for the inner diameter plus the pipe thickness. Table 3.11 shows the input values for these properties. The information needed to run the model is complete once all the input parameters of the FlexWell model are defined.

Table 3.11: Input parameters for wall diameters

Well	Wall ID	Wall OD
'Annulus'	0.24 m	0.244 m
'Tubing'	0.226 m	0.23 m
'Concentric Tubing'	0.101 m	0.114 m

Model Verification:

This model is ran for 20 years of water circulation. Figure 3.3 shows the results for the base case compared with the results reported by Nalla et al. (2005). The difference between Nalla et al. (2005) results and the ones obtained using CMG-STARS is 4.8%, with the results from CMG-STARS displaying a lower output temperature. Early times on the simulation differ from the ones obtained in Nalla et al. (2005). Additionally, the final output temperature from Nalla et al. (2005) neglects transport properties of the fluid, such as, viscosity and flow regime, so there are no friction losses in the system. For CMG-STARS simulation, there are frictional losses of 2,000 kPa at the

outlet of the system, leading to the difference in the results for both models.

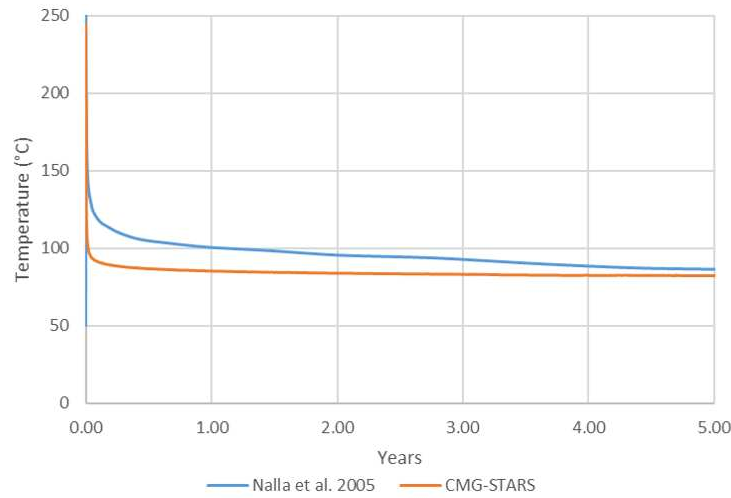


Figure 3.3: Surface fluid temperature output for 20 years of simulation for Nalla et al. (2005) and CMG-STARS.

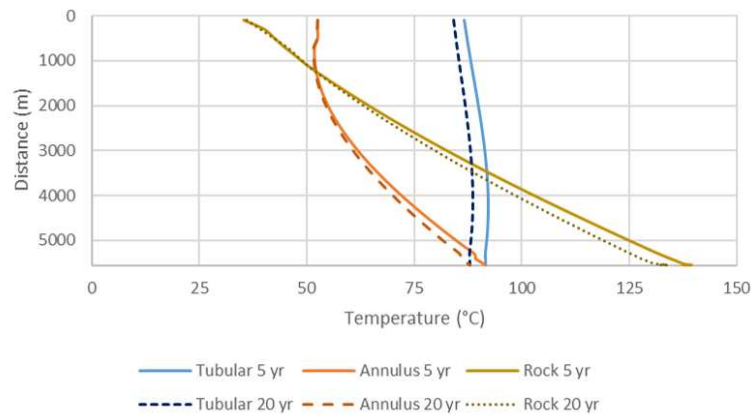
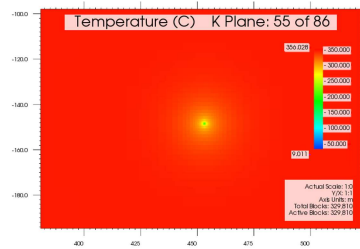


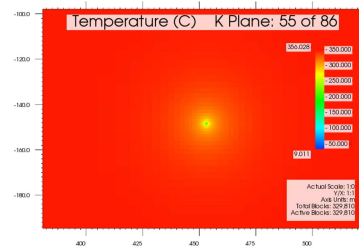
Figure 3.4: Temperature distribution for the working fluid through the pipe network and the rock in the same grid cell after 5 and 20 years of simulation.

CMG-STARS can be used as a thermal numerical simulator for geothermal purposes. FlexWell also proves its capability to model thermal changes between the reservoir and the fluid flowing in the well. Figure 3.5 displays how the reservoir region surrounding the wells cool down as the fluid in the well is flowing at lower temperatures. The model considers heat transfer between the reservoir, cement, well, and working fluid. Results for 5 and 20 years of simulation are presented in Figure 3.4 where it can be seen how the reservoir is transferring energy to the working fluid as the

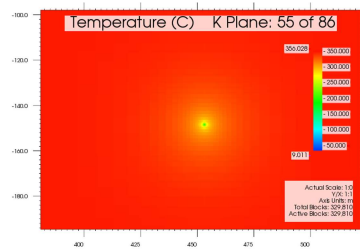
rock loses temperature, while the working fluid gains temperature along time. Also, it is clear that the insulated pipe accomplishes its purpose, as there is a temperature differential between the fluid flowing in the annular and the fluid flowing in the insulated tubular. The refined grid is key in these types of models, as it can show a better view of the heat transfer through the rock surrounding the well. The results capture how the reservoir temperature along the well path is being cooled down, due to heat conduction between the rock and the working fluid in the system.



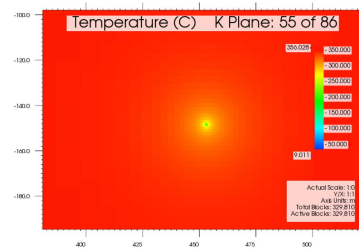
(a) Temperature distribution along the reservoir from an aerial view after 5 years of simulation.



(b) Temperature distribution along the reservoir from an aerial view after 10 years of simulation.



(c) Temperature distribution along the reservoir from an aerial view after 15 years of simulation.



(d) Temperature distribution along the reservoir from an aerial view after 20 years of simulation.

Figure 3.5: Temperature distribution along the surrounding regions of the well for the pipe-in-pipe base case for 5, 10, 15, and 20 years of simulation.

While there is a discrepancy between the new results when compared with a previous model, it is considered that CMG-STARS provides a more reliable solution by considering the transport properties of the fluid. This gives different output temperatures; 86 °C from the previously reported solution and a lower temperature of 82 °C from this simulation study. The case modeled with CMG-STARS will serve as a base model for the following cases where different properties will be modified to enhance the temperature output of a pipe-in-pipe configuration.

3.1.2 U-Shaped Model

Following the previous section procedure, the first step for the U-shaped model is to validate the model with alternate analytical models. As mentioned earlier, the model used for comparison in this case will be the one described by Beckers (2020) using the SBT analytical model. The input parameters are shown in Table 3.12. The following is the description for the creation of the U-shaped base case:

Table 3.12: Input parameters to verify with the SBT analytical model. Modified from Beckers (2020)

Parameter	Value
Vertical Depth	3,000 m
Surface Temperature	15 °C
Reservoir Temperature	250 °C
Geothermal Gradient	80 °C/km
Number of Laterals	1
Surface Spacing Between Injection and Production Wells	2,000 m
Downhole Spacing Between Injection and Production Wells	2,000 m
Reservoir Thermal Conductivity	3 W/(m °C)
Reservoir Heat Capacity	950 J/(kg °C)
Reservoir Density	2,800 kg/ m ³
Well diameter	6 in
Total Production Flow Rate	30 L/sec
Injection Temperature	50 °C
Lifetime	20 years

Reservoir grid and properties:

The grid size for this case is bigger than the one used in the previous model, as it uses two theoretical wells separated horizontally. At first, a Cartesian grid is created for the I, J, and K direction having 141, 59, and 86 blocks, respectively. For this case, the well depth proposed is 3,000 m (9,843 ft) with a horizontal section of 2,000 m. These parameters allow us to generate the model geometry. To achieve better convergence, the grid size is refined following the same principle as the previous model.

Then, the reservoir parameters need to be defined. For this concept, there is no interaction between the injected fluid and the rock, so porosity and permeability are set up as constants with values of 5% and 0.001 md respectively. The reservoir is fully saturated with water. The reservoir pressure needs to be defined, even if the model has no open perforations. To determine the pressure

distribution within the reservoir a normal hydrostatic gradient is used assuming 10 kPa/m. Rock compressibility is also assumed as $4.35 \times 10^{-7} \text{ kPa}^{-1}$. The previous properties do not affect the simulation output; however, are needed to initialize the numerical simulation.

The thermal properties of the rock and the fluids need to be precisely defined as they indeed affect the output of the simulation. The reservoir heat capacity used for the ideal model was 950 J/(kg °C), with a formation thermal conductivity of 3 W/(m °C) and a working fluid thermal conductivity of 35,300 J/ (m days °C). The bottom hole temperature was determined to be at 250 °C, so a temperature gradient was calculated from this temperature to determine the temperature distribution within the reservoir. Figure 3.6 depicts the 3D view of the base case model along with the temperature distribution calculated with the temperature gradient.

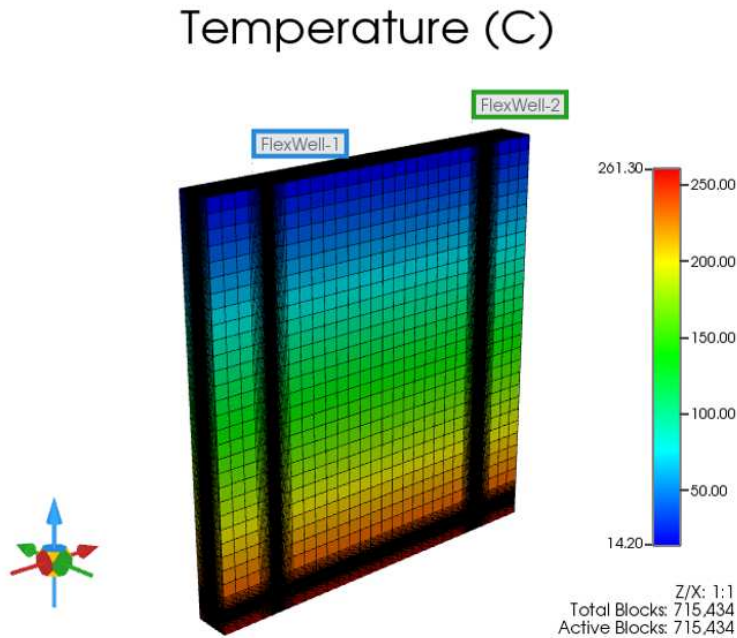


Figure 3.6: Temperature distribution for the U-shape base case model.

Components: Freshwater is the working fluid proposed for this model, using the same parameters and procedures shown in the previous case. The surface temperature is 25 °C and the temperature at a depth of 3,000 m is 250 °C. Table 3.13 shows the list of properties used in this section.

Rock-Fluid:

This section is created in the same way as in the pipe-in-pipe base case model, as it is shown in Table 3.14.

Table 3.13: Input parameters for the components section

Parameter	Value
AVISC	0.0047352 cp
BVISC	1515.7 C
Reference Temperature	250 °C
Surface Pressure	101 kPa
Surface Temperature	25 °C

Table 3.14: Input values for relative permeability tables

S_w	k_{rw}	k_{row}
0	0	1
1	1	0

Initial Conditions:

As in the pipe-in-pipe model, at least a reference pressure and a reference depth need to be entered into the software so it can initialize the simulation. In this case, we will use 3,000 m and 30,000 kPa as the reference depth and reference pressure, respectively. Table 3.15 shows the required data for this section.

Table 3.15: Input parameters for the initial conditions section

Parameter	Value
Reference Pressure	30,000 kPa
Reference Depth	3,000 m

Numerical and *Geomechanics* sections are not modified. Both are left as default in builder, as the former does not need any change unless the simulation has convergence issues, and the latter is an optional section mainly developed for geomechanical interactions in the reservoir, which are not expected in this concept.

Wells & recurrent:

This section is the main focus on this type of concept, as the fluid will always be flowing through the well. The wells and recurrent section will be divided into two subsections that are the well creation and the FlexWell definition that is needed for this model. In the well creation, its location and properties are defined while in the FlexWell section, the well configuration is specified

to accomplish the closed-loop configuration.

Well creation:

Even that this configuration could act as one single well, the schematic is divided into two subsections or wells. The first well will act as the injector well, where the fluid will enter into the system, and the second well will act as the producer and its output is the main focus of this research. Both of the wells are connected at depth (3,000 m of depth and 1,000 m in the horizontal section).

The first well is named “Injector”. Its trajectory needs to be attached to the refined grid blocks that have been created in the reservoir and grid properties section, more specifically from the UBA (33, 30, 1) (surface) to the UBA (33, 30, 57) (surface to the heel of the well), then to the UBA (71, 30, 57) (halfway of the horizontal section). This helps for future cases as the well trajectory will be attached not to a specific location, but to a grid block that is already created. Also, its perforations need to be created with the “quick perf” tool from the software, using the same procedure as the trajectory where the perf will be attached to the UBA location. Perforations can be created along all the well or just in the final section, this will cause no change in the model if we are sure to have all perforations closed.

Followed by the creation of the well trajectory and perforations, the well type needs to be specified. For this case, the ‘Injector’ well is specified as an injector well (injector mobweight implicit) under the “ID & Type” tab with an operate constraint of a maximum surface water rate (STW) of 1635 m³/day (30 L/sec). Under the well completion, general tab, the radius of the well is specified as 0.1524 m as shown in Table 3.16

Table 3.16: Input parameters for the initial “Injector” well

Constraint	Parameter	Limit/Mode	Value
OPERATE	STW surface water rate	MAX	1635 m ³ /day
-	Well Radius	-	0.1524 m

Now, the producer well needs to be created. A new well is created, and following the same procedure as the “Injector” well, the trajectory is attached to the refined grid blocks that have been created in the reservoir and grid properties section, more specifically from the UBA (109, 30, 1) (surface) to the UBA (109, 30, 57) (surface to the heel of the well), and then to the UBA (71,

30, 57) (halfway of the horizontal section). In this case, a producer well will be specified with an operate constraint of a maximum surface water rate (STW) of 1635 m³/day as shown in Table 3.17.

The injected fluid is defined as water that should be available from the previous component definition. As it is the only component in the fluid mixture, 1.0 mole fraction is typed. An injection temperature of 25 °C, steam quality of 0, and pressure of 3,875 kPa are inputted as it is shown in Table 3.18. Under the well completion, general tab, the radius of the well is specified as 0.1524 m.

Table 3.17: Input parameters for the initial “Producer” well

Constraint	Parameter	Limit/Mode	Value
OPERATE	STW surface water rate	MAX	1635 m ³ /day
-	Well Radius	-	0.1524 m

Table 3.18: Input parameters for the injected fluid

Parameter	Value
Temperature	25 °C
Steam quality	0
Pressure	3,875 kPa

FlexWells:

This section allows to model the U-shape configuration, and describes the steps required to capture the temperature change along the reservoir. A new FlexWell is created and the “Filter Wells” option should be selected to select the already created wells. “Injector” well is selected, leaving the casing properties as default, and the well diameter is defined by doubling the size of the already specified radius under the perforations definition. The same process is repeated for the “Producer” well, by creating a second FlexWell. Diameter sizes for both FlexWells are shown in Table 3.19

Table 3.19: Input parameters for wall diameters

Well	Wall ID	Wall OD
'Injector'	0.152 m	0.168 m
'Producer'	0.152 m	0.168 m

The information needed to run the model is complete once all the input parameters of the FlexWell model are defined.

Model verification:

Water circulation is simulated for 20 years. Figure 3.7 shows the results for the base case compared with the results from the SBT analytical approach (Beckers 2020). After 20 years of simulation, it is observed that both of the models have similar results. After 3 years of simulation, both models reach a stable temperature, confirming what has been described in theory where geothermal applications reach a constant temperature output after years of use. The SBT outlet temperature in the proposed simulated time is around 69 °C, while the model created for this research with CMG-STARS, shows an outlet temperature of 65 °C after 20 years of simulation.

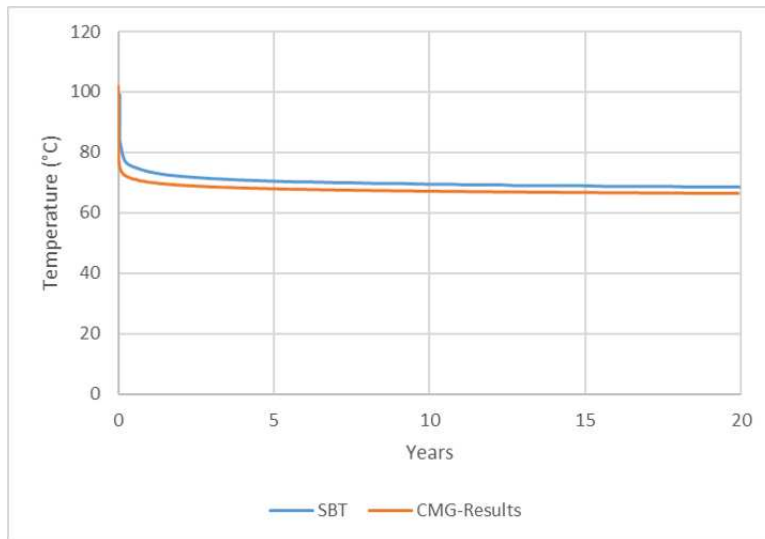


Figure 3.7: Surface fluid temperature output for 20 years of simulation for the SBT analytical model and CMG-STARS.

There is a 3.17% difference between the models where the CMG-STARS model shows lower temperature outputs. This is due to limitations with the SBT approach, which does not take into account the pipe and cement heat transfer barrier that takes place between the reservoir and the working fluid. In other words, the SBT considers direct heat conduction between the rock and the fluid, while CMG-STARS captures this heat transfer resistance between rock and fluid.

These results prove that CMG-STARS can be used as a thermal numerical simulator for geothermal purposes, including CLG concepts. FlexWell is also able to compute the heat transfer from the reservoir, through cement, pipe, and finally working fluid as it is shown in Figure 3.9, where

the temperature decreases in the region surrounding the wells, due to the flow of the colder fluid through the pipe. The refined grid is also an important step in this model, to calculate a precise energy transfer in between the grid blocks, leading to reliable results for this model.

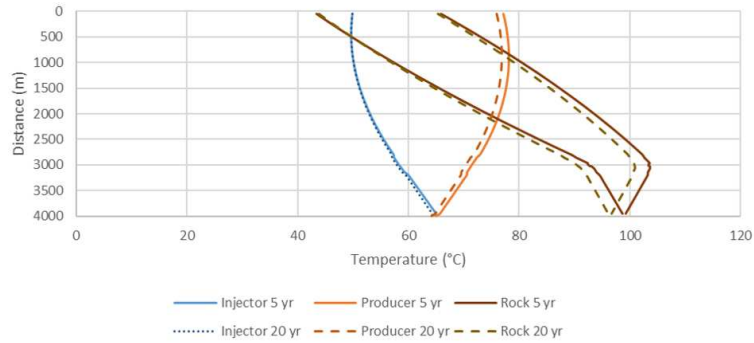
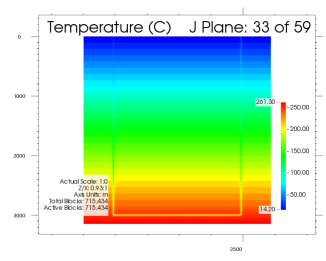
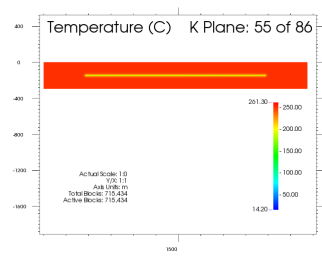


Figure 3.8: Working fluid temperature profile along the well after 5 and 20 years of simulation for CMG-STARS model.

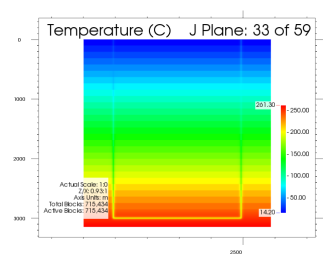
Ultimately, it is important to emphasize the temperature profile of the working fluid as it flows along the well. Figure 3.8 displays how the fluid is being heated up as it travels through the well. The fluid temperature increases during flow down the injection well and through the horizontal sections, due to heat transfer from the rock. Even after reaching the producer’s toe, the well is still heating up, meaning that there is still a potential gain of temperature from the rock. Additionally, it can be seen that the rock temperature decreases with time while the working fluid temperature decreases over time. Figure 3.9 displays the temperature distribution along the well through the rock in different views, showing how the well is being heated up from the rock as the temperature in the rock is losing heat as it gets closer to the well. The rock temperature near the wellbore shows that around 1,000 m, the fluid is being cooled by the rock as the former has a lower temperature than the working fluid. For this specific section, an insulation pipe will enhance the output temperature as the rock is not cooling down the fluid that was already heated up at depth. Taking into account these results and CMG-STARS’ potential, this case will serve as a base for the experimental matrix in the U-shaped model, described in the next section where these results will be enhanced to evaluate the minimum and ideal requirements for the concept to be feasible in future applications where better technology and reservoirs are found and developed, respectively.



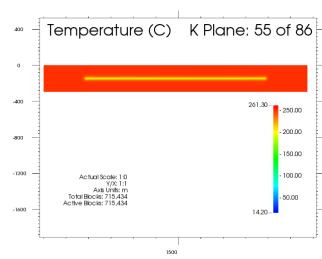
(a) Side view displaying temperature distribution after 5 years of simulation



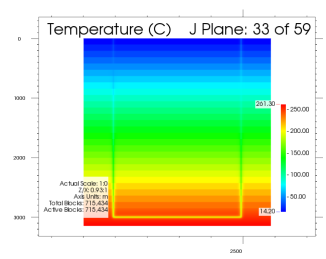
(b) Aerial view displaying temperature distribution after 5 years of simulation



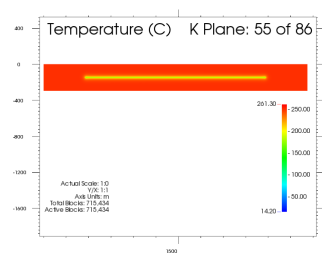
(c) Side view displaying temperature distribution after 10 years of simulation



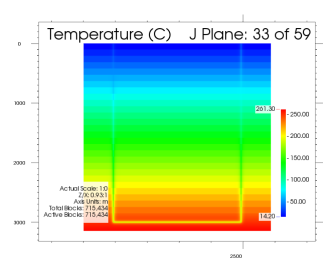
(d) Top view displaying temperature distribution after 10 years of simulation



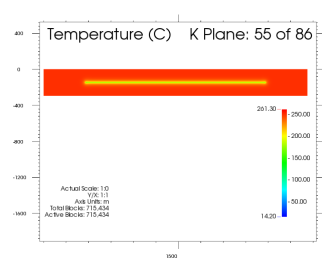
(e) Side view displaying temperature distribution after 15 years of simulation



(f) Top view displaying temperature distribution after 15 years of simulation



(g) Side view displaying temperature distribution after 20 years of simulation



(h) Top view displaying temperature distribution after 20 years of simulation

Figure 3.9: Temperature distribution along the surrounding regions of the well for the U-shaped base case at 5, 10, 15, and 20 years of simulation.

As it can be seen, both of the base case models (pipe-in-pipe and U-shape) do not show promising results, and that is the main reason why in previous studies, the concept has been discarded. Both models show a temperature gain of less than 50 °C, and this also needs to be correlated to the mass rate to be used for electricity or direct use applications. Nevertheless, this research will evaluate how to improve these results by analyzing different parameters that in theory, have a big impact on the outlet thermal energy. The following section will evaluate these parameters and will suggest an ideal case for future applications using CMG-STARS, which has the capability of evaluating geothermal models.

3.2 Experimental Matrix

The main objective of this section is to determine the model parameters that enhance the output temperature and are required to make feasible the CLG concepts. The initial variables that were proposed to be evaluated were: lateral length, injection flow rate, reservoir temperature, injection temperature, and number of laterals; however, the last two will not be evaluated for specific reasons. Injection temperature is a variable that can be easily modified depending on the location of the project, and also does not have a great impact on the project performance, as the initial rock temperature surrounding the system at shallower depths does have a lower or same temperature as surface conditions. The number of laterals does have a big impact on the output temperature as it allows to inject higher flow rates. Nevertheless, the implementation of multiple laterals on real and existing wells becomes unfeasible, but it could be studied and evaluated in future studies. It is important to mention that the working fluid evaluated under this section is water, and other working fluids will be considered in a dedicated section. One experimental matrix is evaluated for each of the configurations proposed: pipe-in-pipe and U-shape. The following are the model modifications and their results for each of the modified parameters.

3.2.1 Pipe-in-Pipe

For the following pipe-in-pipe models, different parameters are proposed to evaluate a configuration closer to today's wells. A J shape or L shape model will be proposed where the well has a vertical section and then it turns 90 degrees to have a long horizontal section. It is to be mention that this is a proposed case, while it is clear that turning 90 degrees in angle for a real well is not feasible. The base case parameters are presented in Table 3.20.

Table 3.20: Parameter values for the cases evaluated in the pipe-in-pipe configuration

Parameter	Value)
Reservoir depth	3,658 m (12,000 ft)
Surface temperature	15 °C (59 °F)
Number of horizontal laterals	1
Reservoir thermal conductivity	3.0 W/(m·K)
Reservoir heat capacity	950 J/(kg·K)
Reservoir density	2800 kg/m ³
Production tubing inner diameter	0.1 m (4 in)
Production casing inner diameter	0.2 m (8.7 in)
Reservoir matrix permeability	0.01 mD
Reservoir matrix porosity	10%
Injection temperature	50 °C (122 °F)
Heat transfer fluid	Water
Flow rate	10 L/s
Lateral length	1,829 m (6,000 ft)
Reservoir Temperature	187 °C (369 °F)

Injection flow rate

The injection flow rate is an operational parameter that could be changed during the life cycle of the project. By evaluating different flow rate values, it is expected to determine a condition that enhances the thermal power of the cycle, while achieving a better residence time with higher output temperature at surface. For the pipe-in-pipe model five flow rates will be evaluated: 1.5 L/s (855 bbl/day), 8.7 L/s (4,717 bbl/day), 10 L/s (5,434 bbl/day), 15 L/s (8,579 bbl/day), and 20 L/s (10,869 bbl/day), to determine a range of flow rates that are feasible for this configuration.

After 20 years of simulation, results are as expected from the literature - the higher the flow rates, the lower the output temperature. 1.5 L/s achieves an output fluid temperature of 100 °C, while at 20 L/s, the system allows producing at 76 °C. All five flow rates temperature output are shown in Figure 3.10, where it can be seen that before two years of simulation, all cases reach a stable temperature showing that the rock is not able to transfer enough heat to the working fluid; nonetheless, the process does not deplete the surrounding temperature of the well.

Taking into account the potential thermal energy output calculations from (Beckers 2016), fluid injection rates of around 10 L/s to 20 L/s are more suitable for power generation. Table 3.21 displays the potential thermal power, where 20 L/s shows to have the biggest potential, while the highest flow rates show higher thermal power potential. However, 8.7 L/s and 15 L/s show similar

potential. Eq. 3.1 displays the equation used for potential thermal power where η is assumed as 1, as the electrical conversion is not being evaluated in this section. This equation does not show exact calculations of what could be expected at the end of the process; however, it gives an initial idea of how thermal output and mass flow rates need to be combined to achieve better results.

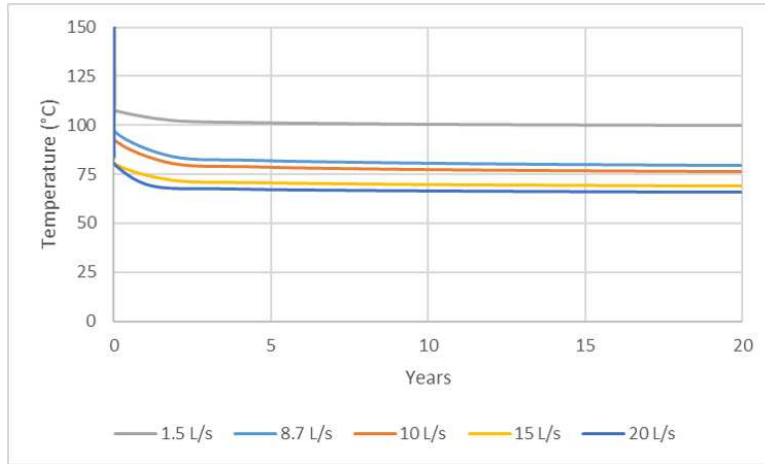


Figure 3.10: Surface fluid temperature output for 20 years of simulation for different flow rates in a pipe-in-pipe configuration.

Table 3.21: Temperature gain and potential thermal output for different flow rates using a pipe-in-pipe configuration

Flow rate (L/s)	ΔT (°C)	kWth
1.5	50	316
8.7	29	1,013
10	27	1,067
15	19	1,207
20	16	1,288

$$W_e = C_f * \dot{m} * (T_2 - T_1) * \eta \quad (3.1)$$

Where C_f is fluid heat capacity in J/(kg °C), \dot{m} is mass rate in kg/s, T_2 and T_1 are temperature outlet and inlet respectively from the loop in °C, η is Carnot's efficiency in fraction. Carnot's efficiency depends on the working fluid and the outlet temperature.

Higher temperature does not directly translate into high power generation. A combination of both, high flow rates and temperatures are needed to make CLG a feasible application. These cases show that maybe this type of concept is feasible for direct-use applications, rather than for power

generation. Nevertheless, this model does display a more realistic approach as it has a reservoir temperature of 187 °C, and it can be completed with today's technologies.

Lateral length

Besides the initial investment in HTHP reservoirs, there are engineering limitations as a cause of extreme temperatures and pressures. Most traditional drilling tools are designed to up to 150 °C (302 °F), while the newest technologies are capable of handling up to 175 °C (347 °F) (Krueger and Schoenborn 2020), for these reasons it is logical to increase the residence time of the fluid by moving horizontally in the same temperature, rather than going deeper at higher temperatures. This is also the typical configuration of unconventional reservoirs, which gives an advantage for this concept as it could be applied to abandoned wells.

To create the models, it needs to be specified that the toe of the well is exactly 90° with a turning radius of fewer than 2 ft. This is difficult to be completed in real operations, but for this specific research, it is assumed the completion of these types of wells.

This section presents the evaluation of the effect of lateral length between injector and producer wells on the fluid residence time, so it can gain more energy from the reservoir before it reaches the production tubular. An injection flow rate of 10 L/s is used for the following cases. To modify this parameter in the models, the grid size is modified in the I-direction, increasing and decreasing it depending on the lateral length. The completion information is being updated for the new well paths, so the model is adjusted to the new x, y, z, coordinates. Four different lateral lengths will be evaluated; 500 m (1,640 ft), 1,000 m (3,281 ft), 2,000 m (6,562 ft), and 3,000 m (9,843 ft). The cases are simulated for 20 years and the results are shown in Figure 3.11.

Results after 20 years show that the longer the lateral lengths, the higher the temperature output. Even with longer horizontal sections that are 3,000 m or 9,843 ft, the highest temperature output barely reaches 84 °C as it is shown in Table 3.22. After 6,660 m of fluid flow through the loop, the temperature gain is 34 °C, which might not represent a feasible investment. Nevertheless, this specific model has a reservoir temperature of 187 °C, which is closer to HPHT reservoirs, so taking into account these results it is worth to have a closer look to direct use applications for abandoned wells, which do not need a high investment at the beginning of the project, and also there are direct use applications for low-temperature fluid outputs.

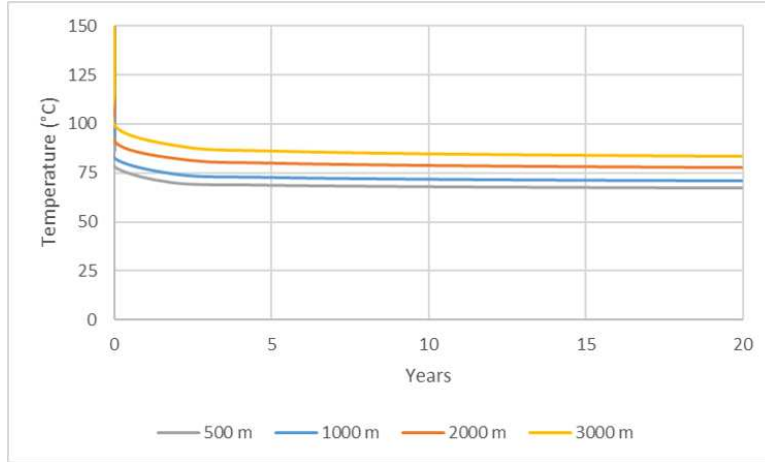


Figure 3.11: Surface fluid temperature output for 20 years of simulation for different lateral lengths in a pipe-in-pipe configuration.

Lateral length does not lead to higher temperature outputs. While the distance of the lateral is increased six times, the temperature gain barely increases by nearly 26%. The lateral length needs to be combined with higher temperatures to achieve better results, so cases with a deviation of less than 45° may lead to better results as the well keeps going deeper, which also means higher temperatures and longer residence time.

Table 3.22: Temperature gain for different lateral lengths using a pipe-in-pipe configuration

Lateral length (m)	Temperature outlet (°C)	ΔT (°C)
500	67	17
1,000	71	21
2,000	78	28
3,000	84	34

Reservoir temperature

This section will evaluate different reservoir temperatures at the same depth (3,658 m or 12,000 ft), so temperature gradients are adjusted to reach the proposed temperatures. Even if the objective of this section is to enhance the temperature output, 150 °C will be evaluated as it is a temperature that can be found in oil and gas reservoirs. It is important to mention that most of these cases show unrealistic reservoir temperatures at the given depth; nonetheless, one of the objectives of this research is to suggest ideal parameters that can be used in the future with better tools and hopefully in reservoirs with the given parameters.

Three different temperatures are evaluated; 150 °C, 250 °C, and 350 °C. Initially, 450 °C and 500 °C were proposed, but due to the high temperatures and interactions in the pipe-in-pipe configurations, simulation runs were not able to converge due to the high temperatures and pressures needed. Additionally, the preliminary results for 450 °C and 500 °C showed high material balance errors which could make those results unrealistic. Further modifications will be needed to evaluate those specific cases or maybe with a future enhancement of the modeling software, those proposed cases will be able to be evaluated. The three simulation results that run and converge are shown in Figure 3.12.

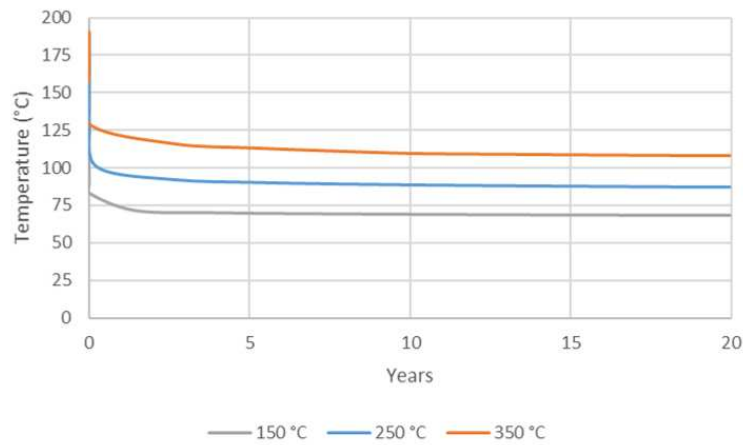


Figure 3.12: Surface fluid temperature output for 20 years of simulation for different reservoir temperatures in a pipe-in-pipe configuration.

As expected, the higher reservoir temperature case (350 °C) showed the highest temperature output, which allows producing fluid at 108 °C at the surface after 20 years of simulation. According to (Verkis Consulting Engineers 2014), that specific case shows feasible cases for electricity generation. On the other hand, at reservoir temperature ranges below 250 °C, the results show fluid temperatures of less than 90 °C, which is the minimum temperature outlet needed to be used for Organic Rankine Cycle (ORC) power plants. It is also important to mention, that the cases with high reservoir temperatures do need extra considerations as the drilling and completion tools for these targets are still under development and need to be proven in real environments.

Ideal pipe-in-pipe case

Building an ideal case is one of the objectives of this investigation to determined required conditions to make CLG a feasible concept for electricity generation. For the pipe-in-pipe configuration,

an ideal case will be proposed taking into account the technical difficulties and today's technologies, so an ideal, but implementable case is analyzed to be used in real and existing wells. Taking into account the results in the experimental matrix, an ideal case of 5,000 m (16,404 ft) of vertical depth, 2,000 m (6,561 ft) of lateral length, reservoir temperature of 250 °C (482 °F), and two injection rates will be analyzed; 15 L/s (8,579 bbl/day) and 10 L/s (5,434 bbl/day). All of the parameters chosen had the best output results in the experimental matrix, taking into account technical limitations due to high temperatures in the drilled rock. The remaining parameters remain the same as in the previous cases, as is shown in Table 3.24, as they display average rock properties and well configuration. It can be seen in Figure 3.13 the geometry of the model as well as the initial temperature distribution for the model.

Table 3.23: Temperature gain for different reservoir temperatures and depths in a pipe-in-pipe configuration

Reservoir temperature (°C)	Temperature outlet (°C)	ΔT (°C)
150	68	18
250	87	37
350	108	58

Table 3.24: Pipe-in-pipe ideal case input parameters

Parameter	Value
Vertical Depth	5,000 m
Surface Temperature	15 °C
Reservoir Temperature	250 °C
Geothermal Gradient	50 °C/km
Number of Laterals	1
Lateral length	2,000 m
Reservoir Thermal Conductivity	3 W/(m °C)
Reservoir Heat Capacity	950 J/(kg °C)
Reservoir Density	2,800 kg/ m ³
Production tubing inner diameter	0.1 m (4 in)
Production casing inner diameter	0.2 m (8.7 in)
Total Production Flow Rate	10 L/sec and 15 L/sec
Injection Temperature	50 °C
Lifetime	20 years

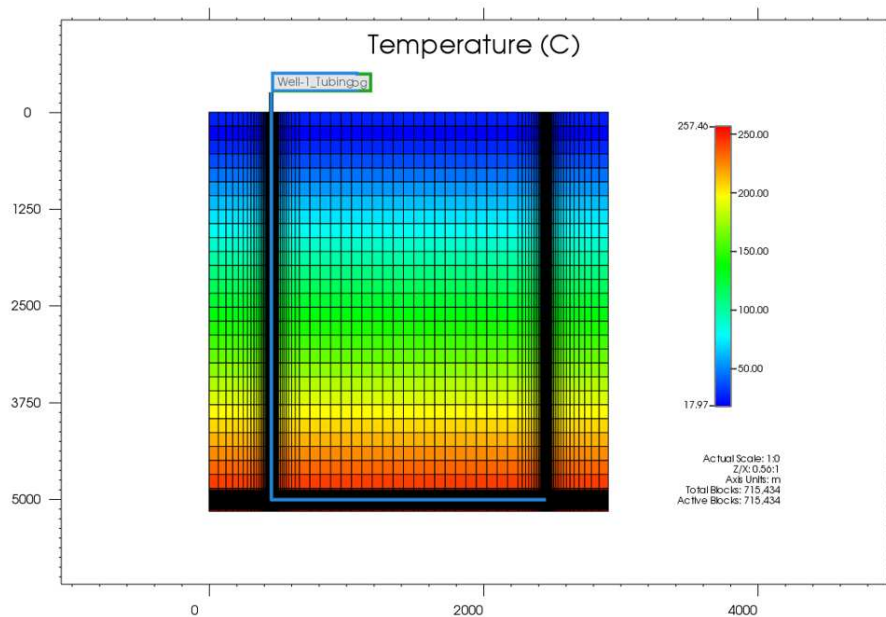


Figure 3.13: Surface fluid temperature output for 20 years of simulation for the ideal pipe-in-pipe case.

After 20 years of simulation, results show high temperature output at 10 L/s and 15 L/s. Figure 3.14 displays the surface temperature output for 20 years, where the temperature stabilizes at the first year of injection and production. As was expected, 10 L/s shows a higher temperature output. As shown in Table 3.25, it can be seen that this real case can provide a potential thermal power of 2 MW. Longer wells, combined with larger lateral lengths, higher reservoir temperatures, and precise flow rates, represent an applicable project for CLG.

Table 3.25: Temperature gain and potential thermal output for an ideal pipe-in-pipe case

Flow rate (m ³ /day)	Temperature output (°C)	ΔT (°C)	kWth
10 L/s	95	45	1,811
15 L/s	83	33	2,097

Most of these conditions need to be proven applicable to already drilled and completed wells. This is the main reason why this ideal case has reasonable parameters, so it could be applied to high temperature reservoirs that can be found in the oil and gas industry. This model will be used as a base case for the direct use application subsection in this research in a well drilled in the Haynesville Shale.

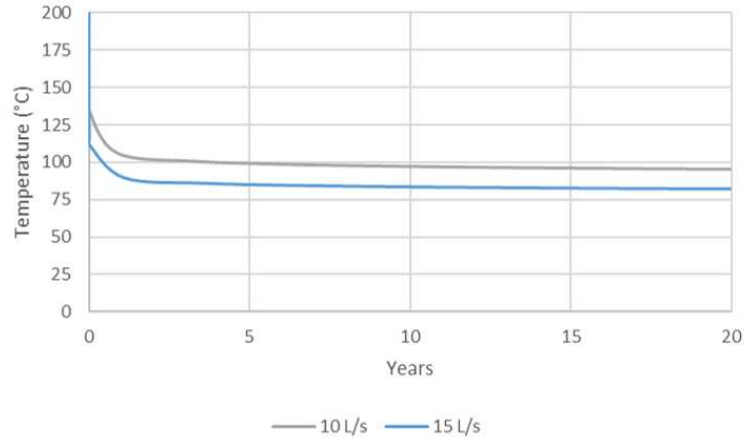


Figure 3.14: IK 2D view temperature distribution for a pipe-in-pipe ideal case.

3.2.2 U-Shaped

For this configuration, different parameters are proposed to evaluate an ideal case that could be used for electricity generation. The base case parameters are the same ones described in Table 3.12, except for the reservoir depth, reservoir temperature, lateral length, and injection flow rate. The parameter variations are described in the experimental matrix that is described as follows.

Injection flow rate

As mentioned in Nalla et al. (2005), varying the flow rate of the fluid is the most important factor as this type of concept does rely on the residence time that the fluid has to heat up. Nevertheless, having high fluid temperatures at surface does not precisely mean having a high thermal output. A combination of both, high temperature outputs and high flow rates are key aspects of the CLG concept. At first in this section, three different flow rates will be evaluated, and from those results, a more precise look will be taken to formulate ideal flow rates for real applications taking into account today's technology.

To model these new cases, the base case created in the previous section will be used. Only the flow rates are modified and the remaining parameters remain the same as in the base case. The first proposed flow rates will have a wide span in between each of the cases. 1.5 L/s (855 bbl/day), 15 L/s (8,579 bbl/day), and 75 L/s (40,758 bbl/day) flow rates are evaluated. As there is a sufficient difference of velocity between all of the flow rates, there will be a high difference in the thermal outputs and there is a clearer view of the most feasible range of rates.

The results after 20 years of simulation show that the higher the flow rate, the lower the temperature output. 1.5 L/s (855 bbl/day), which is the lowest flow rate, achieves an outlet temperature of 135 °C. The intermediate flow rate of 15 L/s (8,579 bbl/day) shows an outlet temperature of 79 °C, leading to an increase of 30 °C from the inlet temperature. The highest flow rate (75 L/s or 40,758 bbl/day) barely heats up along the wellbore as it generates an outlet temperature of 57 °C. Figure 3.15 displays the fluid temperature output after 20 years of simulation.

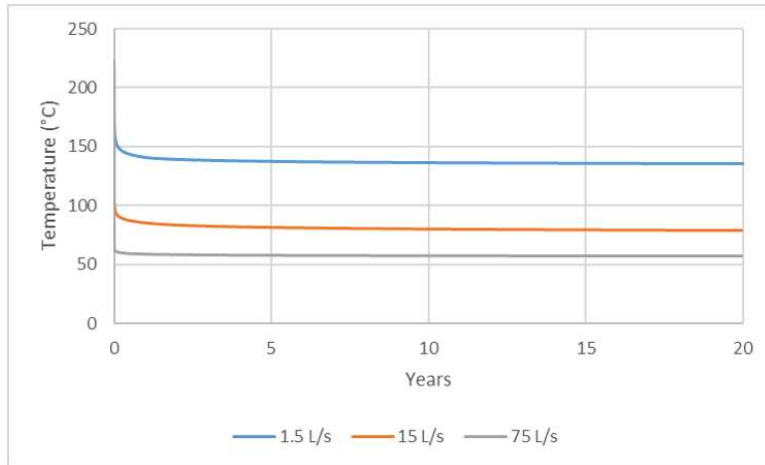


Figure 3.15: Surface fluid temperature output for 20 years of simulation for different flow rates in a U-shape configuration.

It is clear how the flow rate affects the temperature output, varying from 57 °C to 135 °C from the lowest flow rate case, to the highest. As mentioned in (Beckers 2016), the ideal temperature for electricity generation is above 130 °C; however, the flow rate that reaches this threshold is low and may not be feasible for energy generation.

Table 3.26: Temperature gain and potential thermal output for different flow rates using a U-shape configuration

Flow rate (L/s)	ΔT (°C)	kWth
1.5	85	538
15	29	1,843
75	7	2,113

Taking into account the thermal power output, it is clear that a combination of both temperature and flow rates is needed to achieve an efficient process for these types of concepts. Table 3.26 displays that even if the temperature output is high, it does not necessarily mean high power

generation. It is evident that a combination of both of these parameters is key to achieve better results.

From the initial results, three extra models will be expanded taking flow rates close to the best case simulated earlier. 8.7 L/s (4,717 bbl/day), 12.6 L/s (6,857 bbl/day), and 19 L/s (10,285 bbl/day) are the cases proposed to completely suggest an ideal flow rate. Figure 3.16 displays the surface fluid temperature output after 20 years of simulation.

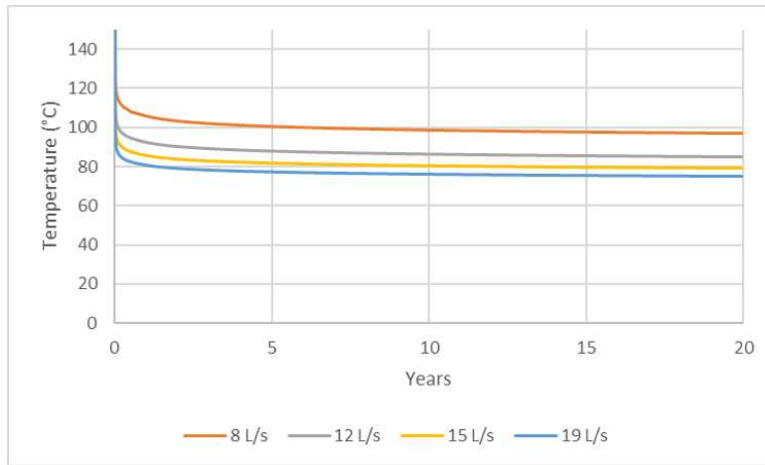


Figure 3.16: Surface fluid temperature output for 20 years of simulation for different flow rates in a U-shape configuration.

As expected, the lowest flow rate (8.7 L/s or 4,717 bbl/day) displays the highest temperature output, while 19 L/s (10,285 bbl/day) achieves the lowest temperature for this case. Table 3.27 displays the temperature output and temperature gain for each of the flow rates proposed. To understand deeply which case is better to be applied to future projects, technical analysis is performed in the next chapter of this research taking into account the results shown previously. Nonetheless, it is clear that having flow rates around 10 to 20 L/s displays the best scenario for the given parameters. This needs to be correlated to power plant capabilities and needs to choose an ideal flow rate.

Lateral length

This section evaluates the four different lateral lengths in between the 'Injector' and 'Producer' well. At first, the lateral length is evaluated from a theoretical point of view, so the toe of the well is exactly 90° with a turning radius of fewer than 2 ft for both of the wells - it is clear that this is not feasible in real operations; nonetheless, it helps to simplify the model as it is the main purpose

is to evaluate the reservoir and well schematics that will serve to develop these type of concept. For this specific parameter, the model looks to increase the residence time of the fluid as it has to flow for long distances through the hot reservoir. Four different lateral lengths will be evaluated; 500 m (1,640 ft), 1,000 m (3,281 ft), 2,000 m (6,562 ft), and 3,000 m (9,843 ft). 10 L/s of flow rate is used for all lateral length cases.

Table 3.27: Temperature gain and potential thermal output for flow rates varying from 8 to 19 L/s

Flow rate (L/s)	Temperature outlet (°C)	ΔT (°C)
8	99	49
12	85	35
15	79	29
19	75	25

At first, the models need to be modified to comply with these variations. To increase and decrease the lateral distance between the wells, the grid size is modified in the I-direction so the UBA's are not modified and the well trajectory is adjusted to these locations. Perforations are also revised so the model can run without issues. All of the cases use the same input parameters as in the base case with a flow rate of 15 L/s (8,579 ft) including the TVD of the well that is 3,000 m (9,843 ft). Figure 3.17 displays the temperature along 20 years of simulation.

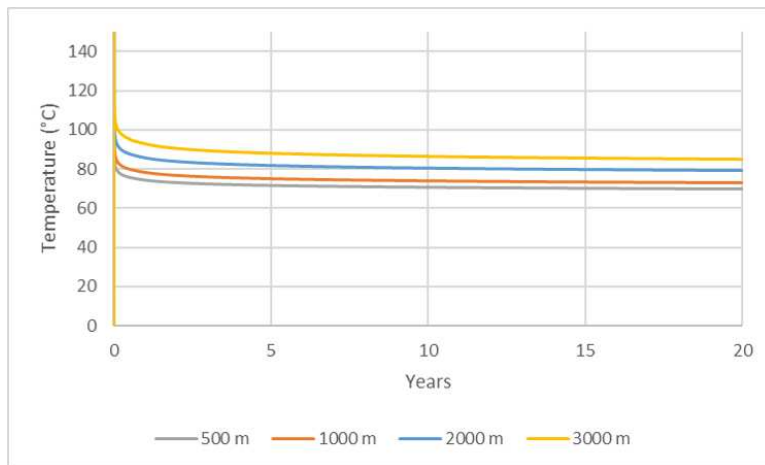


Figure 3.17: Surface fluid temperature output for 20 years of simulation for different lateral lengths.

After evaluating different distances between wells, results show what was expected from earlier studies. The longer the horizontal distance from well to well, the higher temperature output;

however, this difference is not as high as it could have been expected. There is a difference of 15 °C between all four cases, while the difference in distance is about 2500 m as it is shown in Table 3.28. Temperature profiles along the process show how the reservoir is unable to transfer enough energy to the working fluid. As it is shown in Figure 3.18, for the longest distance between wells the fluid is not able to reach more than 90 °C along the process, while the reservoir temperature is about 250 °C. It can also be seen, that about 1000 m from surface, in the injection well, the rock is cooling down the fluid, instead of heating it up, so it might be useful for future models to use an insulated pipe for that section of the well as it will enhance the temperature output and the complete process.

Table 3.28: Temperature gain and potential thermal output for different lateral lengths

Lateral length (m)	Temperature outlet (°C)	ΔT (°C)
500	70	20
1,000	73	23
2,000	79	29
3,000	85	35

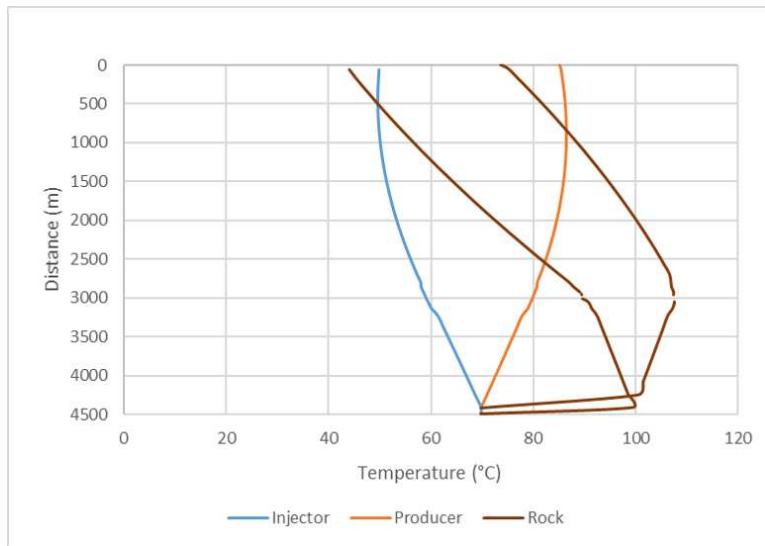


Figure 3.18: Temperature profile for the fluid and the rock through the well path.

This parameter variation shows that even if the residence time is increased along the process, there is still low convection between the source rock and the working fluid. In this specific case, it would be paramount to evaluate the need for horizontal sections while the temperature is not increasing as the temperature output does not increase accordingly to the increase of distance

between wells. An insulated pipe along with the production well will increase the temperature output.

Reservoir temperature

As it was mentioned in the pipe-in-pipe reservoir temperature models, 150 °C will be evaluated as it is a temperature that can be found in oil and gas reservoirs. A geothermal gradient of 50 °C/km is assumed to give a more realistic approach. To achieve the desired temperature at depth, the models will also have variations in the depth of the reservoir. Some of the cases show unrealistic well depths, that may not be drillable even with the most developed tools; nevertheless, it is part of this research to display ideal parameters to achieve temperature outputs that can be used for electricity generation. Table 3.29 displays the reservoir temperatures proposed and the depths calculated taking into account the assumed geothermal gradient.

Table 3.29: Reservoir temperature and depth for the experimental matrix

Reservoir temperature (°C)	Depth (m)
150	3,000
250	5,000
350	7,000
450	9,000
500	10,000

For this model, it is needed to adjust the pressures as well as the temperatures according to the depth of the model. The same process described in the base cases will be used but now changing the geothermal gradient to be 0.05 °C/m. Also, the BHP pressure should be adjusted to verify the desired depth. As in the lateral length cases, a flow rate of 15 L/s (8,579 ft) is assumed. Figure 3.19 displays the temperature along 20 years of simulation for the proposed models.

As temperature varies in the models, it is clear that the higher the temperature, the higher the temperature output at surface. As expected, the 500 °C and 450 °C reservoir temperatures give surface temperatures above 150 °C. According to (Beckers 2016), these are the ideal cases for electricity generation, and the flow rates used in these models are suitable for electricity generation. On the other hand, at temperatures ranges below 450 °C, the results show fluid temperatures of less than 150 °C. It is also important to mention, that the cases with higher temperature outputs do need extra considerations as the drilling and completion tools for these targets are still under

development and need to be proven in real environments.

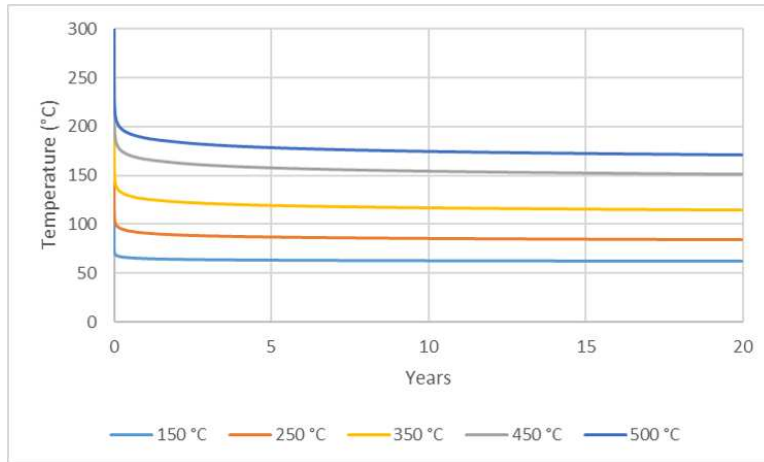


Figure 3.19: Surface fluid temperature output for 20 years of simulation for different reservoir temperatures.

Table 3.30: Temperature gain for different reservoir temperatures and depths

Reservoir temperature (°C)	Temperature outlet (°C)	ΔT (°C)
150	62	12
250	84	34
350	114	64
450	151	101
500	170	120

Ideal U-shape case

As part of this investigation, one of the objectives is to propose an ideal case where the CLG concept could be feasible from a technical point of view. Taking into account the results in the experimental matrix, an ideal case of 9,000 m (29,528 ft) of vertical depth, 3,000 m (9,843 ft) of lateral length, reservoir temperature of 450 °C (842 °F), and an injection flow rate of 15 L/s (8,579 bbl/day) is proposed. All of the parameters chosen, had the best output results in the experimental matrix, except for the reservoir temperature that was selected as it showed the minimum temperature output (150 °C or 302 °F) for electricity generation. The vertical section of the producer well will be insulated from 3,500 m as the rock temperature at that location is around 175 °C so the fluid does not has to interact with the colder sections of the configuration. Two different flow rates are evaluated; 15 L/s and 20 L/s. The remaining parameters remain the same as in the previous cases

as it is shown in Table 3.31. It can be seen in Figure 3.20 the geometry and the initial temperature distribution for the model.

Table 3.31: U-shape ideal case input parameters

Parameter	Value
Vertical Depth	9,000 m
Surface Temperature	15 °C
Reservoir Temperature	450 °C
Geothermal Gradient	50 °C/km
Number of Laterals	1
Surface Spacing Between Injection and Production Wells	3,000 m
Downhole Spacing Between Injection and Production Wells	3,000 m
Reservoir Thermal Conductivity	3 W/(m °C)
Reservoir Heat Capacity	950 J/(kg °C)
Reservoir Density	2,800 kg/ m ³
Well diameter	6 in
Total Production Flow Rate	15 L/s and 20 L/s
Injection Temperature	50 °C
Lifetime	20 years

After 20 years of simulation, results show high temperature output at both, 15 L/s and 20 L/s. As shown in Table 3.32, it can be seen that this real case can provide a potential thermal power of nearly 8 MW. Additionally, the insulated section gives extra temperature output as the heated fluid does not cool on the colder and shallow sections of the well path. It also shows an increase in temperature output as was expected, leading to the highest temperature output in this research. Deeper wells, combined with larger lateral lengths, higher reservoir temperatures, and precise flow rates, show an ideal project for CLG.

Table 3.32: Temperature gain and potential thermal output for an ideal U-shape case

Flow rate (L/s)	Temperature output (°C)	ΔT (°C)	MWth
15	167	117	7.4
20	148	98	7.9

However, most of these conditions need to be proven reachable. Drilling technology needs to prove the capability of reaching targets at 9,000 m (nearly 30,000 ft), and at reservoir temperatures of 450 °C (842 °F) to also connect the two conceptual wells. Also, the evaluated flow rates show the limit where the temperature output gets below 150 °C, which is the limit for electricity generation

applications according to (Beckers and McCabe 2019). Well diameter is a parameter not studied in this research that can be modified as well; nonetheless, all of the diameters used in this research are the ones proven to give stability in the well.

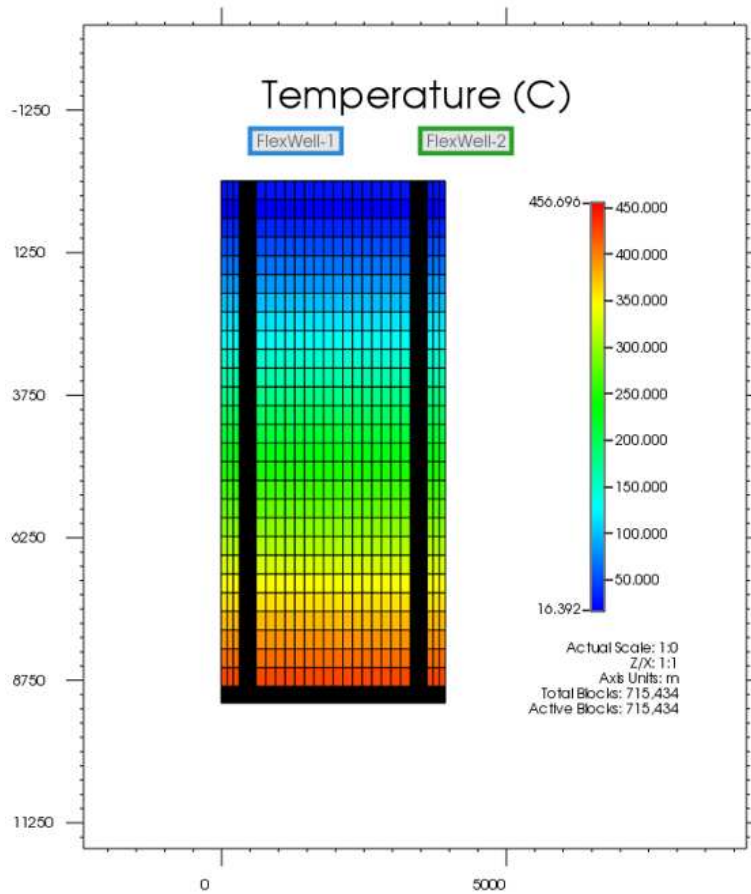


Figure 3.20: IK 2D view temperature distribution for an U-shape ideal case.

3.3 Working Fluids

As mentioned in the previous section, the working fluids could have been included as a part of the experimental matrix; however, its application and investigation shows an improvement that can be modified since the beginning of a project, and does not rely on the reservoir properties to be a feasible variable. After careful consideration, $s\text{CO}_2$, and water with nanoparticles of copper are selected to be evaluated. The following is the procedure and results for these models.

3.3.1 Supercritical Carbon Dioxide (sCO₂)

Water has been the most studied working fluid for CLG systems, but recent studies have shown sCO₂ as an alternative to achieve higher temperature outputs. The main goal of this section is to evaluate sCO₂ as an opportunity of enhancing the outlet temperature and its potential thermal power. (Amaya et al. 2020b) displays that sCO₂ showed promising results of 120 °C when injecting at a flow rate of 20 kg/s.

For this specific research, the fluid will be evaluated in the previously described pipe-in-pipe model as it has shown an easier implementation as it only needs to drill one well. The parameters used for this model are the ones shown in Table 3.20 where the only parameter changed is the working fluid. In addition to what has already been defined in the previous models, an extra component needs to be added. In the components section, CO₂ is selected from CMG’s library, gas is selected as the reference phase and the initial properties are left as default. The fluid enthalpy is entered from CMG’s user manual recommendations. The remaining tabs under the component section are not changed from the previous models.

Then, under the well section CO₂ is selected as the injected fluid and a 1-mole fraction is entered. For this case, the fluid will be injected at 20,000 kPa. After defining the injected fluid, the well producer constraints are defined as 8,000 kPa of minimum bottom hole pressure so the fluid maintains a supercritical state during the whole loop. For this specific model, three different flow rates will be evaluated taking into account as well the mass flow. Table 3.33 shows the proposed flow and mass rates to be evaluated.

Table 3.33: Cases proposed for sCO₂ as working fluid

Flow rate (m ³ /day)	Mass rate (kg/s)
147,416	2.5
737,080	12.3
3,685,400	61.5

The results for sCO₂ as working fluid, show a similar trend as the results for water. The higher the flow rate, the lower the temperature output and after one year of injection of the fluid, the temperature output seems to stabilize for the next 19 years. Figure 3.21 displays the temperature output for sCO₂ over 20 years.

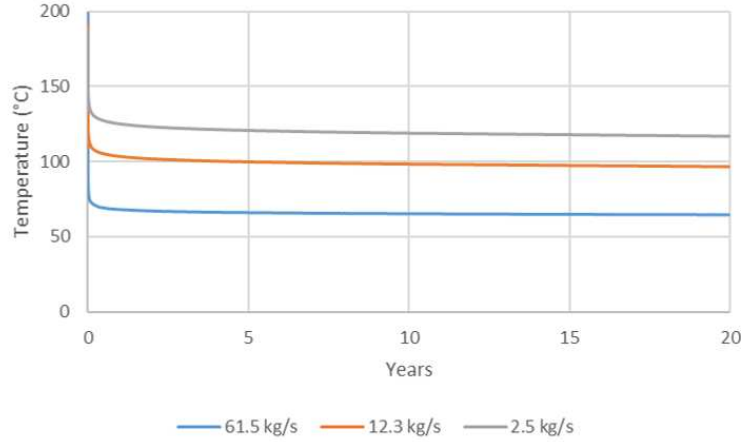


Figure 3.21: Surface fluid temperature output for 20 years of simulation for different mass rates using sCO₂ as working fluid.

On the other hand, the flow rates need to be interpreted taking into account the mass rate, so it can be converted into thermal power output. Table 3.34 displays the potential thermal output of the different cases proposed. While results do not show promising results, they are higher compared to the results displayed in Green-Fire’s ”Energy Closed-Loop Geothermal Demonstration using Supercritical Carbon Dioxide as Working Fluid” (Amaya et al. 2020b), (in this cases, thermal potential power is of 500 kW average).

Table 3.34: Temperature gain and potential thermal output for different flow rates using sCO₂ as working fluid

Flow rate (m ³ /day)	Mass rate (kg/s)	ΔT (°C)	kWth
147,416	2.5	67	151
737,080	12.3	47	530
3,685,400	61.5	15	846

Compared to water, sCO₂ shows lower results. While water cases showed a potential thermal power of 7 MW, sCO₂ shows a potential of 500 kW. Water does lead to better results while the logistics on handling and availability are easier compared to sCO₂. As the results on sCO₂ are not promising, water will be enhanced to achieve even better results than the ones proposed in the experimental matrix.

3.3.2 Water with Nanoparticles of Copper

To completely suggest ideal parameters for CLG, water will be enhanced taking advantage of today's technologies. (Bhanushali et al. 2017) performed a study to enhance the thermal conductivity of water using different particle shapes, where thermal conductivity was enhanced by 40% when using long nanowires, suggesting future developments in low filler fraction and high aspect ratio to increase even more the thermal conductivity of the working fluid. Based on the previous study, nanoparticles of copper could be used in CLG applications to enhance thermal output.

For this specific model, water conductivity and viscosity will be modified to simulate the addition of nanoparticles into the fluid taking into account the results shown in (Bhanushali et al. 2017). Water conductivity will be increased from 53,500 J/(m day °C) to 80,250 J/(m days °C) (50% increase). While water viscosity is also increased by 50% from 0.0047352 cp to 0.0071028 cp. All other parameters remain the same as in previous water cases assuming no other changes in the working fluid rather than conductivity and viscosity.

After 20 years of simulation, results display an average increase in the outlet temperature of 2 °C. Figure 3.22 displays a comparison of normal water versus water with nanoparticles of copper, these results show a small increase under already proven fluids. Additional cases can be run in the future for even enhanced results, where the fluid conductivity can be increased by more than 50%. This may be one of the main properties to be studied and enhanced for future application of the CLG concept.

When comparing the results into a potential power generation, the fluid with nanoparticles of copper may show an increased potential power as thermal conductivity is increased to 6300 J/(kg °C). Results for water with nanoparticles of copper show better results as not only the heat capacity is increased, also its density is increased which also enhances the thermal potential. However, these results need to be also compared to the cost of adding and treating the fluid, which will be higher than treating freshwater. Additionally, further studies need to be performed to evaluate its application into the CLG concept and power plants.

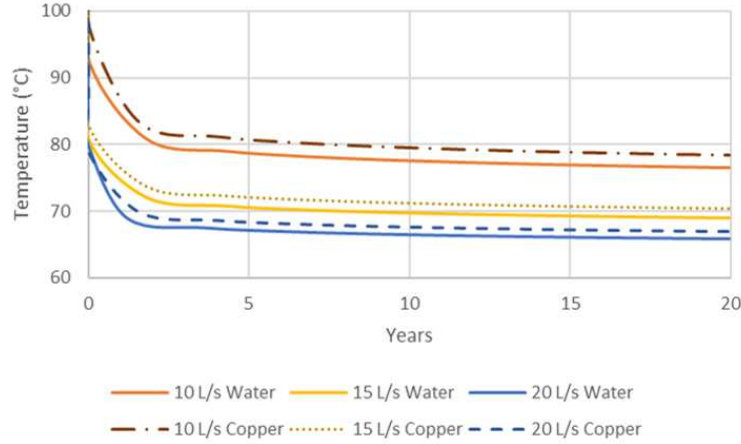


Figure 3.22: Surface fluid temperature output for 20 years of simulation for different mass rates using water with nanoparticles of copper as working fluid compared to normal water at the same flow rates.

Table 3.35: Temperature gain and potential thermal output comparison after 20 years of simulation for different flow rates of water and water with copper nanoparticles as working fluids

Working fluid	Flow rate (L/s)	Temperature outlet (°C)	kWth
Water	10	77	1,067
Water + NPCu	10	79	1,827
Water	15	69	1,207
Water + NPCu	15	71	2,083
Water	20	66	1,288
Water + NPCu	20	67	2,142

3.4 Haynesville Shale Real Application

From the experimental matrix results, outlet temperatures and flow rates suggested thermal outputs that can be utilized for direct-use applications. There are also new technology developments using temperature outputs as low as 75 °C where a binary power plant cycle can be used for electricity generation (Verkis Consulting Engineers 2014). A crucial point for these applications to be successful is to decrease the initial investment to put a geothermal well in production and being able to spend capital in power plants that can convert thermal power into electrical power.

Nowadays, there are oil and gas reservoirs with temperatures that can reach up to 350 °F. The abandoned and low productive wells in those locations can be recycled into either direct-use applications or electricity generation using binary power plants. As one of the main objectives of

this research is to evaluate the feasibility of the CLG concept in a real study, a well-known reservoir with high temperatures will be used to assess the applicability of a pipe-in-pipe CLG, An adaptation of an insulated tubing will be needed to implement the concept. Using resources available, and the models previously used in this research, a real case will be evaluated to understand the CLG concept applicability to a project that can be developed nowadays without the need for future technology developments.

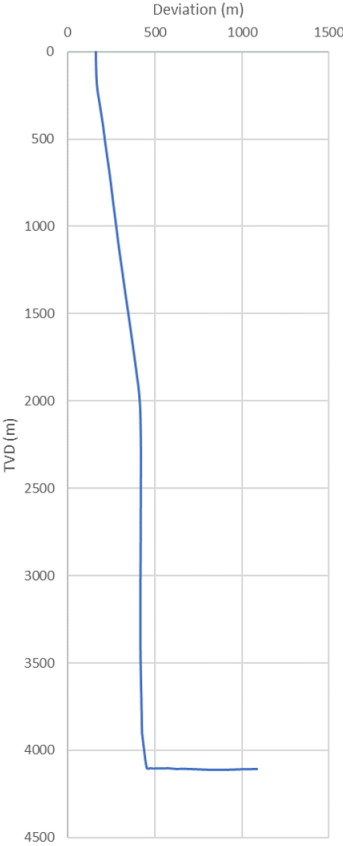


Figure 3.23: Haynesville well trajectory to be used in the real case.

The first step for this real case study is to identify an oil and gas resource with high temperatures with already drilled and produced wells, that unproductive wells can be recycled into geothermal applications. Haynesville Shale is selected for this study as its reservoir temperature can reach up to 168 °C or 335 °F (Franquet et al. 2019) and the measured and vertical depths of the wells drilled in this reservoir are long enough to provide residence time for the injected fluid in a CLG concept.

Once selected a reservoir that fits the minimum requirements for a CLG application, a real well and locations need to be selected. By merging and evaluating different papers where Haynesville Shale temperature is being discussed, it is identified that a suitable location with high temperatures in the Grogan field, in De Soto Parish, Louisiana where well depths can reach up to 13,000 ft (3,962 m) and horizontal sections of 3,000 ft (914 m). A well trajectory from this location is selected using Drilling Info database. The well trajectory identified is displayed in Figure 3.23 from a side view, the well trajectory selected only has TVD and deviation coordinates, it is assumed no change in the y-direction for this well.

As rock properties data is arduous to find, and most of the rock properties such as permeability and porosity are negligible for this concept, general assumptions will be used taking into account previous studies on geothermal applications for shale rocks, such as basal heat flux, formation thermal conductivity, and formation volume capacity, which fit the characteristics of the Haynesville Shale. Additionally, casing tubing diameters are selected according to well plans published from the selected location (Debrick 2015). Water will be used as working fluid as it has shown reliable results and it has proven to be practical for direct-use applications and binary power plants. Table 3.36 displays the input parameters for this case.

Table 3.36: Direct use scenario for vertical using parameters from an already drilled well in Haynesville Shale using a pipe-in-pipe configuration

Parameter	Value
Tubing Inner Diameter	0.0762 m (3 in)
Tubing Outer Diameter	0.0889 m (3.5 in)
Insulation Outer Diameter	0.1016 m (4 in)
Casing Inner Diameter	0.1778 m (7 in)
Casing Outer Diameter	0.1937 m (7.625 in)
Well Depth (TVD)	4,112 m (13,490 ft)
Lateral Length	693 m (2,245 ft)
Basal Heat Flux	0.1 W/m ²
Formation Thermal Conductivity	1.89 W/m °C
Formation Volume Capacity	1875.7 kJ/m ³ °C
Insulation Thermal Conductivity	0.07 W/m °C
Circulation Rates	5, 10, 15, and 20 L/s
Surface Temperature	25 °C (77 °F)
Bottom Hole Temperature	168.3 °C (335 °F)

To model this real case in CMG-STARs, the case used for the pipe-in-pipe configuration for different flow rates will be used as base. The grid depth needs to be readjusted in the k-direction so the model fits 4,112 m of reservoir depth. The reservoir temperature gradient is also adjusted to 0.041 °C/m. The well trajectory is adjusted to CMG input files so it also fits the base model. Finally, the FlexWell model needs to be created with the new pipe-in-pipe geometry, taking into account the parameters chosen from (Debrick 2015). Figure 3.25 displays a side view of the model created with the new well trajectory and FlexWell model.

Table 3.37: Temperature gain for different flow rates after 20 years of simulation for a case in Haynesville Shale

Flow rate (L/s)	Temperature outlet (°C)	ΔT (°C)
5	83	33
10	72	22
15	66	16
20	63	13

With all the previous modifications performed, the model is run for four different cases that were selected from the experimental matrix, varying different flow rates suitable for the pipe-in-pipe system and potential power output. While running the cases, the higher the flow rates the higher the frictional losses in the system, this also led to higher iterations for the model to run. Nevertheless, the proposed models were able to run for 20 years of simulation, and higher rates than 20 L/s were not studied as the thermal gain was expected to be less than 10 °C. Figure 3.24 show the simulation results for the proposed flow rates.

Results show that implementing a CLG concept into abandoned wells may lead to temperature outputs up to 83 °C. As it has been demonstrated in this research, this case also shows that the higher the flow rates, the lower the thermal outputs. For the flow models evaluated in this case, 5 L/s flow is the only rate where the temperature output is higher than 75 °C, which is the minimum temperature needed for binary cycle power plants.

However, many of these applications may be developed for direct use applications as the wells are already drilled, leading to a less initial investment. Additionally, these types of concepts may be able to extend the life of abandoned wells as they can supply the operations in the field with clean energy, that comes from the same operations. Also, further studies may evaluate the implication

of using a CLG loop when the reservoir surrounding the well is stimulated with artificial fractures, not only for a closed-loop concept, also using the previous stimulated fractures for oil and gas extraction.

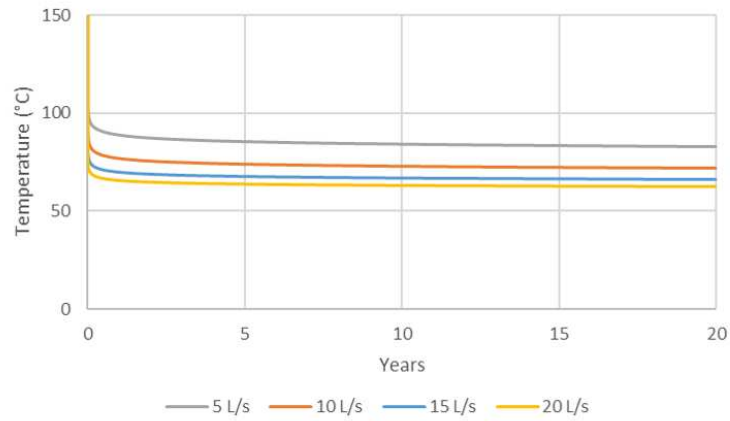


Figure 3.24: Surface fluid temperature output for 20 years of simulation for different flow rates for the Haynesville Shale real model.

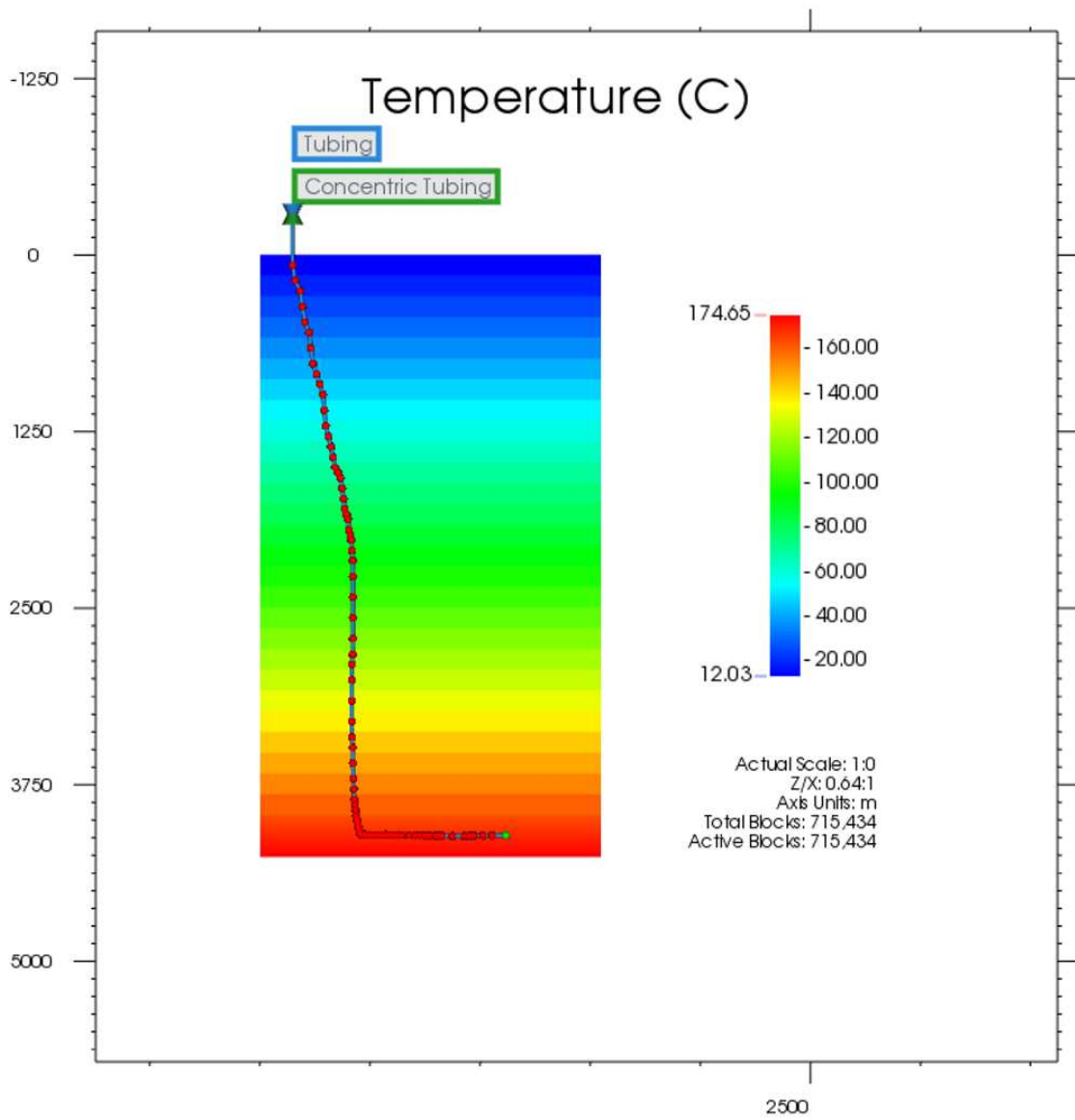


Figure 3.25: IK 2D view temperature distribution for Haynesville Shale case.

CHAPTER 4

TECHNICAL EVALUATION

This chapter presents and discusses a technical analysis on CLG, taking into account the numerous models evaluated in this research. At first, a techno-economical analysis was proposed using geothermal GEOPHIRES software; due to the main nature of CLG where no fracture systems are needed, the software may lead to miscalculations and over assumptions already included in the reservoir model. Many of the assumptions and calculations used in GEOPHIRES will be used in this technical analysis. To implement a complete technical analysis, economic aspects will be taken into account; nevertheless, the main focus of this chapter is to assess the feasible application of the different models proposed in the previous chapters.

A relation between the simulation results, power conversion, technological, and logistical aspects will be needed to recommend a final utilization of the proposed models. To address a technical analysis, at first, the models simulated will be evaluated taking into account the outlet parameters after the simulation - working fluid, outlet temperature, and flow rate. Secondly, each model will be analyzed to know the availability of constructing a power plant and its possible initial adaptations or constructions needed to develop the final utilization application. Finally, two end-use applications are recommended taking into account the outlet parameters - direct use or electricity generation.

As the simulation results are already complete, the first step in this analysis is to determine the thermal power for each of the cases. As thermal efficiency is not included in this first analysis, this helps to evaluate the potential thermal power that could be used for direct use application. No electrical conversion is performed for these thermal calculations. Eq. 3.1 is used for the thermal power determination, where η is not taken into account as there is no electrical power conversion.

Once the thermal power is calculated, it is correlated with the temperature output on the model to determine the potential power conversion into electricity. Efficiencies are calculated from Beckers and McCabe (2019), where the lower limit temperature is 100 °C for electricity generation applications; however, as it is mentioned in (Verkis Consulting Engineers 2014), temperatures as low as 90 °C are also included for feasible electricity generation in this research. Temperature ranges below 180 °C are suitable for ORC or binary plants, while temperatures above 180 °C are appropriate for single and double flash power plants. Cases with temperatures below 90 °C are discarded for

electricity generation and will be recommended for direct-use applications. To determine efficiency, subcritical ORC power plants are assumed for all the water cases and supercritical ORC is assumed for the sCO₂ cases. Efficiencies are calculated from GEOPHIRES as its calculations includes enthalpy and entropy variation depending on the fluids temperature and pressure. GEOPHIRES is only used to calculate the efficiencies, and the remaining output values from the software are discarded.

After power conversion is calculated, an implementation aspect is added to the analysis. While this specific aspect does not evaluate directly the results from the models in this research, it depicts the possible needs of implementing the cases studied earlier. Two different implementations are identified in this analysis - re-adaptation of abandoned wells, which will need possible surface modification or construction of new facilities, and new field construction, which will require exploration, drilling, completion, surface facilities construction, etc. While there is not a detailed investment analysis, this aspect gives an initial idea of what additional financing is needed to develop the proposed cases in this research.

For this analysis, pumping injection, fluid treatment, power plants working flow rates, and power plant availability are assumed as negligible. No power loss is assumed due to re-injection into the well as it is expected for a CLG system to achieve an initial thermosiphon effect where the fluid can flow through the loop without a continuous pump (Muir 2020). As in the proposed concept, the injected fluid does not have direct interaction with the rock because it is expected to have no special treatments through the process as the fluid composition will not change through the loop. The recommended working flow rates for ORC power plants are 40 L/s; nonetheless, the proposed cases have maximum injection rates of 20 L/s. To comply with the minimum requirement for power plants, each case will have a recommended amount of wells to ideally achieve a total of 40 L/s in the process so these types of plants can be used for electricity generation. Finally, all the suggested and mentioned plants are assumed to be possibly implemented in the proposed cases, as well as their ideal efficiency in the power conversion. The analysis results for all the cases simulated in this research are displayed in Appendix ??.

From forty-one cases run in this research, twelve of them are suitable for electricity generation, taking into account their temperature output, five of them from a pipe-in-pipe configuration, and the remaining seven from a U-shape configuration. The remaining twenty-nine cases may be useful

for direct use applications, where most of them can be re-adapted from abandoned oil and gas reservoirs if a pipe-in-pipe configuration is adjusted in those wells. The proposed direct-use re-adapted cases can reach up to 2 MW of thermal power when using water with nanoparticles of copper and freshwater as working fluids. From the twelve cases suitable for electricity generation, four of them can be re-adapted from abandoned oil and gas reservoirs with today's technologies; however, from those four cases, two of them need around 25 wells with an adapted pipe-in-pipe configuration to be able to produce electricity. The remaining two cases need fewer than four surrounding wells feeding the electricity generator. One of them is the ideal case of a pipe-in-pipe configuration and the remaining is the one using 12.3 kg/s of sCO₂ as working fluid.

The remaining eight cases that can be used for electricity generation need future technology to be developed or new wells to be drilled. One of them is the 350 °C of reservoir temperature using a pipe-in-pipe configuration, which displays the minimum requirements for a pipe-in-pipe to be useful for electricity generation. The remaining seven cases that need further development are U-shape configurations that include the five models where the reservoir temperature is higher or equal to 350 °C. Only two cases can reach more than 150 °C of outlet temperature after 20 years of simulation.

In this research, the ideal cases proposed for the pipe-in-pipe configuration had the objective to determine the minimum requirements for electricity generation. From the two proposed cases, one of them can be used for an electrical generation when using four wells and when joining the four wells, over 1 MW is achieved as potential electrical power. The remaining ideal pipe-in-pipe case marks the limit where the CLG concept may not be feasible for electricity generation, and it may need more than four wells in the same cluster to justify the construction of an electrical power plant.

The U-shape ideal cases in this research had the main purpose of developing the highest potential power generation. While the cases proposed (15 and 20 L/s) show high temperature outputs, both of them mark the limit between having more than 150 °C as outlet temperature. This also displays that a single U-shape well at the proposed depth and temperature can generate 7 MW of thermal power and around 1.2 MW of electrical power. A future implementation may include having different parallel wells so the converted mass rate increases while the potential power is also increased.

The Haynesville Shale cases do not show promising results. All of them have an outlet temperature of less than 90 °C; however, the thermal output is higher than 2 MW that can be applied for many direct use applications. On the other hand, with future developments on ORC power plants, lower temperatures may be feasible for electrical power conversion. Additionally, these cases can be used as a base to determine the minimum requirements for recycling oil and gas wells into other types of applications that can reduce carbon footprint.

Figure 4.1 displays the distribution of the cases taking into account the outlet temperature and the potential thermal power. The red line displays the minimum temperature needed for the cases to be determined for electricity generation. The right side displays the twelve cases recommended for electricity generation where ten of them display 350 °C as minimum reservoir temperature and the remaining two assume flow rates lower than 10 L/s where at least five wells are needed to feed the electrical power plant.

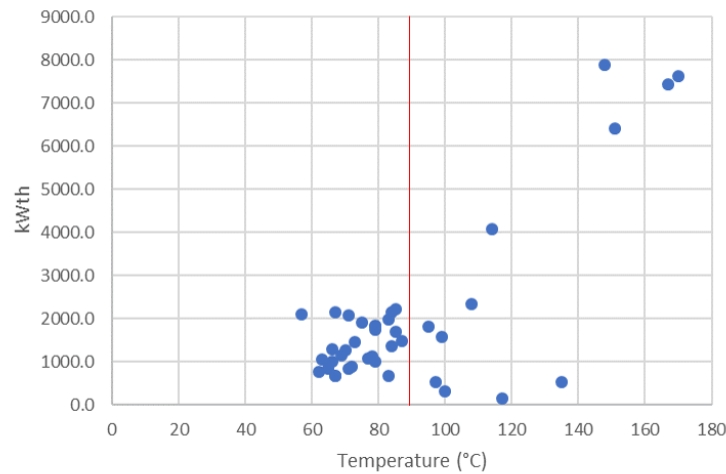


Figure 4.1: Utilization efficiency for different power plant types as a function of wellhead temperature and dry-bulb ambient temperature.

350 °C is the ideal reservoir temperature for electricity generation. All of the cases that were simulated with that minimum reservoir temperature showed the potential of electricity generation. Additionally, with the proposed casing and tubular diameters, ranges between 10 to 20 L/s of injection flow rate show the ideal combination of temperature output and power generation. Those flow rates have enough residence time to gain heat from the reservoir and also generate decent temperature outputs. When decreasing the minimum temperature needed for electricity conversion

from 90 °C to 75 °C, the number of cases with electrical potential increases significantly, suggesting that the main variable to keep researching on is to augment the power plant capacities.

CHAPTER 5

SUMMARY AND CONCLUSIONS

This thesis presents a numerical modeling study of two Closed-Loop Geothermal concepts, a pipe-in-pipe and a U-shape configuration, where the working fluid does not interact directly with the rock of the geothermal reservoir. In CLG configurations, the working fluid flows within a well and it gains temperature by heat conduction from the hot reservoir rock. A thermal reservoir simulation software, CMG-STARS, is used to perform the numerical modeling of the CLG concepts. Models created using CMG-STARS were verified against previously reported analytical modeling results before a sensitivity analysis was performed to determine the required conditions that make CLG concepts feasible for electricity generation. Additionally, different working fluids were studied, including water, supercritical CO₂, and a fluid with nanoparticles of copper, to compare their relative performance in improving the thermal efficiency of the process.

CMG-STARS simulation software was able to reproduce previous and alternate results, showing more precise results than the compared models. The CMG-STARS pipe-in-pipe model can verify the previous work performed by Nalla et al. (2005), with a 4.6% relative difference in output temperature, as CMG-STARS takes into account friction losses during fluid flow in the well tubulars. For the U-shape case, the results obtained using CMG-STARS were comparable with the analytical solution by the SBT model, with a 3.17% relative difference as CMG-STARS takes into account pipe and cement resistance to heat transfer from the reservoir to the working fluid. The numerical simulations of both CLG configurations exhibit more realistic results than their alternate models.

The base case models were modified to evaluate different parameters that could enhance the thermal output of the CLG configurations. The parameters modified included lateral lengths up to 3,000 m (9843 ft), well depths up to 10,000 m (32,808 ft), reservoir temperatures up to 500 °C, and flow rates up to 75 L/s. However, the modeling software does show limitations when the models have reservoir temperatures above 350 °C and flow rates higher than 50 L/s, especially in pipe-in-pipe configurations as the simulated working fluid tends to change its state, leading to high-pressure changes that cause convergence problems in the numerical solution.

Different working fluids were analyzed for the CLG concepts. sCO₂ models displayed fair results where potential electrical power of 50 kW may be achieved. Additionally, modeling water

with nanoparticles of copper shows that not only this specific fluid can be used, but also increasing the fluid conductivity will eventually increase the power output of the system regardless of the fluid.

Results confirmed that the main parameters affecting the concept results were residence time, injection flow rate, and reservoir temperature, in descending order of importance. The longer the wells, the higher residence time that the working fluid had to gain heat from the reservoir; however, at bottom depth, the rock still displays double the temperature of the working fluid, suggesting that the heat transfer in this concept is not efficient. Flow rates from 10 to 20 L/s entice ideal work for the proposed casing diameters, as they can gain enough heat from the reservoir as well as being able to generate thermal power from 1 to 2 MW. Reservoir temperature plays a major role in this concept, as all of the cases with electrical power generation potential, had reservoir temperature of at least 250 °C. Most of the cases with temperatures below 250 °C were found not suitable for electrical generation.

The ideal cases proposed accomplished their purpose of maximizing the thermal output. The ideal pipe-in-pipe showed the minimum parameters to justify an electrical power plant when using four nearby wells and taking into account current technology developments and the possible re-use of abandoned oil and gas wells with a potential electrical power generation of 1 MW. The ideal U-shape cases proposed were the only ones able to display potential electrical power above 1 MW from a single well, when having reservoir temperatures above 450 °C.

Insulated pipes in both of the models show their desired purpose, to isolate the heated fluid with nearly no heat loss on its flow back to the surface. Initially, the pipe-in-pipe configuration intended to have an insulated tubular pipe, so there was no heat exchange between the fluid flowing to the bottom of the reservoir and the heated fluid flowing to the surface. However, the results show how the insulated pipe can impede the fluid to cool down, having less than 1 °C of temperature loss. For the U-shaped configuration, the initial models did not intend insulated pipes; however, after analyzing early cases, the production flow showed heat loss on its produced fluids. Understanding the grid location where the fluid stopped gaining heat (where both the working fluid and the reservoir temperatures were the same), and applying an insulated pipe from that location, proved a most efficient system and higher temperature outputs at the surface.

Haynesville Shale's real applications were successfully modeled for a CLG concept. Introducing a well trajectory and thermal parameters from this unconventional play into a pipe-in-pipe model displayed that CLG can be used for direct use applications. Thermal power outputs up to 1 MW were demonstrated assuming a re-adaptation of abandoned and unproductive wells. Using low flow rates of less than 5 L/s may lead to output temperature differences of 90 °C or more, allowing a cluster of wells to be feasible to implement either an ORC plant or a direct use distribution network. Additionally, the artificial fractures created in the early stages of the well may lead to higher temperature outputs and models, where the fracture network is analyzed, which may completely suggest Haynesville's application for electricity generation.

The technical analysis demonstrated the feasibility of CLG, giving the actual state and application of the concept and it was also able to recommend the minimum parameters required to upgrade from direct use applications to electrical power generation. Re-adaptation of depleted petroleum wells for geothermal applications is feasible with today's technologies, when a group of wells is considered in locations where the reservoir temperature exceeds 170 °C with flow rates between 10 to 20 L/s. sCO₂ also proved reliable thermal outputs at mass rates close to 12 kg/s. Both working fluids may have higher temperature outputs if higher diameters in the pipe network can be applied to the CLG concept. Finally, when having reservoir temperatures above 350 °C, a single well configuration with sufficient flow rates (>10 L/s) can generate enough heat to justify a power conversion plant capable of generating more than 1 MW per well.

CHAPTER 6

FUTURE WORK

The following topics that can be further developed with the proposed models and configurations. Future work to enhance CLG include analysis of the fracture network surrounding the well, double loop systems where the heated fluid is re-injected into the wellbore, multiple parallel wells in a CLG concept, and development of more efficient power plants. The following are the ideas proposed:

1. Construction of cases where a Discrete Fracture Network (DFN) is modeled, allowing to understand the possible enhancement of thermal output in both closed-loop systems or open-loop systems in a coaxial heat exchanger with fractures as proposed in Wang et al. (2009).
2. Double-loop systems where the fluid is injected as explained in this research, and when the fluid is being produced it can flow again in-depth to gain more heat from the reservoir, this system may be feasible using a combination of both pipe-in-pipe systems and U-shaped configurations.
3. Multiple parallel wells in both CLG configurations proposed in this research. When the wells have the same vertical parent well its diameter can be increased in shallower depths, while its sidetrack wells have smaller diameters drilled into different locations of the hot source rock. This allows the system to process higher rates on surface while the temperature output is maintained.
4. As mentioned in Chapter 2, there are limitations with power plant efficiencies. This proposed topic goes beyond reservoir engineering and petroleum engineering; however, if the power plants can convert power in with higher efficiencies, lower temperature processes may be feasible, leading to better geothermal systems. Better studies and development in the Kalina cycle may lead to applicable systems that lead to higher conversion efficiencies.

REFERENCES CITED

- Amaya, A., Higgins, B., Muir, J., and Scherer, J. 2020a. GreenFire Energy Closed-Loop Geothermal Demonstration at the Coso Geothermal Field. *Proc.*, 45th Workshop on Geothermal Reservoir Engineering, Stanford University, Stanford, California, February 10-12, 2020.
- Amaya, A., Higgins, B., Muir, J., and Scherer, J. 2020b. GreenFire Energy Closed-Loop Geothermal Demonstration using Supercritical Carbon Dioxide as Working Fluid. *Proc.*, 45th Workshop on Geothermal Reservoir Engineering, Stanford University, Stanford, California, February 10-12, 2020.
- Beckers, K. 2016. *Low-Temperature Geothermal Energy: Systems Modeling, Reservoir Simulation, And Economic Analysis*. Ph.D. thesis, Cornell University, Ithaca, New York (May 2016).
- Beckers, K. 2018. Closed-Loop Geothermal Heat Extraction. Technical report, National Renewable Energy Laboratory, Golden, Colorado (January 2018).
- Beckers, K. 2020. Closed-Loop Geothermal Base Case Scenario. Technical report, National Renewable Energy Laboratory, Golden, Colorado (February 2020).
- Beckers, K., Koch, D., and Tester, J. 2015. Slender-body theory for transient heat conduction: theoretical basis, numerical implementation and case studies. <http://doi.org/10.1098/rspa.2015.0494>. *Proceedings Royal Society*, **471**(2184).
- Beckers, K. F. and McCabe, K. 2019. GEOPHIRES v2.0: updated geothermal techno-economic simulation tool. *Geothermal Energy*, **7**.
- Bhanushali, S., Noah Jason, N., Ghosh, P., Ganesh, A., P Simon, G., and Cheng, W. 2017. Enhanced Thermal Conductivity of Copper Nanofluids: The Effect of Filler Geometry. *ACS Applied Material Interfaces*, **9**.
- Choi, S. and Eastman, J. 1995. Enhancing Thermal Conductivity of Fluids with Nanoparticles. Presented at the 1995 International mechanical engineering congress and exhibition, San Francisco, CA, 12-17 Nov 1995.
- Choi, S., Eastman, J., Li, S., and Yu, W. 2001. Anomalously increased effective thermal conductivities of ethylene glycol-based nanofluids containing copper nanoparticles. *Applied Physics Letters*, **78 - 6**: 718–720.
- Computer Modeling Group Ltd. 2009. *User's Guide STARS, Advanced Process and Thermal Reservoir Simulation*. Calgary, Alberta, Canada: Computer Modelling Group Ltd.
- Computer Modeling Group Ltd. 2015. Advanced processes thermal reservoir: Product overview, <https://www.cmgl.ca/uploads/files/pdf/software/2015>.

- Debrick, C. S. 2015. Well planning and construction: Haynesville shale – east texas, <https://www.epa.gov/sites/production/files/documents/wellplanningandconstructiontechniques.pdf> (accessed 4 March 2021).
- Dincer, I. and Demir, M. E. 2018. Gas Turbine Cycles. *Comprehensive Energy Systems*, **4**: 209–263.
- Fanchi, J. 2018. *Principles of Applied Reservoir Simulation, fourth edition*. Gulf Professional Publishing.
- Franquet, J. A., Moronkeji, D. A., and Morton, J. 2019. Straddle Packer MicroFrac Testing in High Temperature Unconventional Well: A Case Study in the Bossier/Haynesville Shale. Presented at the 53rd U.S. Rock Mechanics/Geomechanics Symposium, New York City, New York, June 2019.
- Horne, R. N. 1980. Design Considerations of a Down-Hole Geothermal Heat Exchanger. *Geothermal Resources Council Transactions*, **4**: 569–572.
- Krueger, S. and Schoenborn, K. 2020. New High Temperature Coiled Tubing Drilling Bottom Hole Assembly Enables Slimhole Re-Entry Drilling in Challenging High Temperature Wells. Presented at the SPE/ICoTA Well Intervention Conference and Exhibition, The Woodlands, Texas, USA, March 2020.
- Lund, J., Freeston, D., and Boyd, T. 2005. Direct application of geothermal energy. *Geothermics*, **34**: 691–727.
- Muir, J. R. 2020. New Opportunities and Applications for Closed-Loop Geothermal Energy Systems. *Geothermal Rising Bulletin*, **49-4**: 12–16.
- Nalla, G., Shook, M., Mines, G., and Bloomfield, K. 2005. Parametric sensitivity study of operating and design variables in wellbore heat exchangers. *Geothermics*, **34**: 330–346.
- National Renewable Energy Laboratory. 2020. Sedimentary and Enhanced Geothermal Systems, <https://www.nrel.gov/geothermal/sedimentary-egs.html> (accessed 4 November 2020).
- Oldenburg, C., Pan, L., Muir, M., Eastman, A., and Higgins, B. 2016. Numerical Simulation of Critical Factors Controlling Heat Extraction from Geothermal Systems Using a Closed-Loop Heat Exchange Method. 41st Workshop on Geothermal Reservoir Engineering, Stanford, California, February 22-24.
- Parker, M., Buller, D., Petre, J. E., and Dreher, D. T. 2009. Haynesville Shale-Petrophysical Evaluation. Paper presented at the SPE Rocky Mountain Petroleum Technology Conference, Denver, Colorado, April 2009.
- Phuoc, T., Massoudi, M., Wang, P., Oryshchyn, D., and McKoy, M. L. 2017. The Exergy of Geothermal Fluids: CO₂ versus Water. *GRC Transactions*, **41**.
- Riahi, A., Moncarz, P., Kolbe, W., and Damjanac, B. 2017. Innovative Closed-Loop Geothermal Well Designs Using Water and Super Critical Carbon Dioxide as Working Fluids. 42nd Workshop on Geothermal Reservoir Engineering, Stanford, California, February 13-15, 2017.

- Schiegg, H., Rødland, A., Zhu, G., and Yuen, D. 2015. Electro-pulse-boring (EPB): Novel super-deep drilling technology for low cost electricity. *Earth Science*, **26**: 37–46.
- Tester, J., Reber, T., Beckers, K., and Lukawski, M. 2015. Deep geothermal energy for district heating: Lessons learned from the U.S. and beyond. *Advanced District Heating and Cooling (DHC) Systems*, **1**: 75–98.
- United States Department of Energy. 2016. Geothermal energy – direct-use, <https://www.wbdg.org/resources/geothermal-energy-direct-use> (accessed 2 February 2021).
- Verkis Consulting Engineers. 2014. Geothermal Binary Power Plants> Preliminary study of low temperature utilization, cost estimates and energy cost. Technical report, Verkis Consulting Engineers with funding from the Icelandic International Development Agency (ICEIDA), (August 2014).
- Wang, Z., McClure, M. W., and Horne, R. N. 2009. A single-well EGS Configuration Using a Thermosiphon. Presented at the Thirty-Fourth Workshop on Geothermal Reservoir Engineering, Stanford University, Stanford, California, February 9-11, 2009.
- Winsloe, R., Richter, A., and Vany, J. 2020. The Emerging (and Proven) Technologies that Could Finally Make Geothermal Scalable. Paper presented at World Geothermal Congress, Reykjavik, April 27 – May 1, 2020. 37022. International Geothermal Association.

APPENDIX A

TECHNICAL ANALYSIS MATRIX

Figure A.1 displays the technical analysis matrix. All the 41 cases are described, depending on the main parameter evaluated with its thermal power, as well as its efficiency, electrical power, number of wells, and implementation, when the cases were selected for electricity generation. This matrix was discussed, explained, and analyzed in Chapter 4.

		Temperature output (°C)	Application	kWth	Efficiency	kWe	# Wells	Implementation
Pipe-in-pipe configuration	Flow rate (L/s)	1.6	ORC power plant	316.79	0.09	27.16	25	Re-adaptation
		8.7	Direct use	1,013.26	-	-	-	Re-adaptation
		10	Direct use	1,086.77	-	-	-	Re-adaptation
		15	Direct use	1,147.14	-	-	-	Re-adaptation
		20	Direct use	1,288.02	-	-	-	Re-adaptation
	Lateral length (m)	500	Direct use	684.26	-	-	-	Re-adaptation
		1000	Direct use	845.26	-	-	-	Re-adaptation
		2000	Direct use	1,127.02	-	-	-	Re-adaptation
		3000	Direct use	1,368.52	-	-	-	Re-adaptation
	Reservoir Temperature (°C)	150	Direct use	684.26	-	-	-	Re-adaptation
		250	Direct use	1,489.28	-	-	-	New project
		350	ORC power plant	2,334.54	0.10	224.34	4	New project
	Ideal case	10 L/s	ORC power plant	1,811.28	0.08	143.54	4	Re-adaptation
		15 L/s	Direct use	1,992.41	-	-	-	Re-adaptation
	sCO ₂	2.5 kg/s	ORC power plant	151.19	0.11	16.29	16	Re-adaptation
		12.3 kg/s	ORC power plant	530.29	0.08	43.40	3	Re-adaptation
		61.5 kg/s	Direct use	846.21	-	-	-	Re-adaptation
	Water/NPCu	10 L/s	Direct use	1,827.00	-	-	-	Re-adaptation
		15 L/s	Direct use	2,082.50	-	-	-	Re-adaptation
		20 L/s	Direct use	2,142.00	-	-	-	Re-adaptation

U-shape configuration	Flow rate (L/s)	1.6	135	ORC power plant	538.54	0.13	70.60	25	New project
		8	99	ORC power plant	1,577.83	0.08	133.22	5	New project
		12	85	Direct use	1,690.53	-	-	-	New project
		15	79	Direct use	1,750.91	-	-	-	New project
		19	75	Direct use	1,911.91	-	-	-	New project
		75	57	Direct use	2,113.16	-	-	-	New project
	Lateral length (m)	500	70	Direct use	1,270.88	-	-	-	New project
		1000	73	Direct use	1,461.51	-	-	-	New project
		2000	79	Direct use	1,842.77	-	-	-	New project
		3000	85	Direct use	2,224.04	-	-	-	New project
	Reservoir Temperature (°C)	150	62	Direct use	762.53	-	-	-	New project
		250	84	Direct use	2,160.49	-	-	-	New project
		350	114	ORC power plant	4,066.81	0.10	422.43	3	New project
		450	151	Flash power plant	6,417.94	0.15	974.40	3	New project
		500	170	Flash power plant	7,625.27	0.18	1,345.46	3	New project
	Ideal case	15 L/s	167	Flash power plant	7,434.64	0.17	1,282.92	3	New project
		20 L/s	148	ORC power plant	7,889.14	0.15	1,167.09	2	New project
	Haynesville	5 L/s	83	Direct use	664.14	-	-	-	Re-adaptation
		10 L/s	72	Direct use	885.52	-	-	-	Re-adaptation
		15 L/s	66	Direct use	1,016.70	-	-	-	Re-adaptation
20 L/s		63	Direct use	1,046.52	-	-	-	Re-adaptation	

Figure A.1: Technical analysis matrix displaying all the parameters calculated and analyzed for all the cases run in the research.

APPENDIX B
PIPE-IN-PIPE CASE .DAT CODE

The following is the code used by CMG-STARs to read and run the pipe-in-pipe model evaluated in Chapter 3. The .dat file shown in this appendix is for the pipe-in-pipe configuration described in Table 3.20:

```

** 2020-11-06, 9:12:42 AM, santiagorocha
RESULTS SIMULATOR STARS 201910

WPRN FLEXWELL GRID 1
INUNIT SI
WSRF WELL 10
WSRF GRID 100
WPRN ITER 1
OUTPRN WELL ALL
OUTPRN RES NONE
OUTSRF GRID MASNENW PRES SG SW TEMP
OUTSRF FLEXLAYER ALL
OUTPRN ITER NEWTON
** Distance units: m
RESULTS XOFFSET          0.0000
RESULTS YOFFSET          0.0000
RESULTS ROTATION          0.0000 ** (DEGREES)
RESULTS AXES-DIRECTIONS 1.0 -1.0 1.0
** *****
** Definition of fundamental cartesian grid
** *****
GRID VARI 141 59 86
KDIR DOWN
DI IVAR
66.48  56.78  48.49  41.41  35.37  30.21  25.8  22.04  18.82  16.07
13.73  11.72  10.01  8.55  7.3  6.24  5.33  4.55  3.89  3.32
2.83  2.42  2.07  1.77  1.51  1.29  1.1  0.94  0.8  0.69
0.59  0.5  1  0.5  0.59  0.69  0.8  0.94  1.1  1.29
1.51  1.77  2.07  2.42  2.83  3.32  3.89  4.55  5.33  6.24
7.3  8.55  10.01  11.72  13.73  16.07  18.82  22.04  25.8  30.21
35.37  41.41  48.49  56.78  66.48  83.87  83.87  83.87  83.87  83.87
83.87  83.87  83.87  83.87  83.87  83.87  66.48  56.78  48.49  41.41
35.37  30.21  25.8  22.04  18.82  16.07  13.73  11.72  10.01  8.55
7.3  6.24  5.33  4.55  3.89  3.32  2.83  2.42  2.07  1.77
1.51  1.29  1.1  0.94  0.8  0.69  0.59  0.5  1  0.5
0.59  0.69  0.8  0.94  1.1  1.29  1.51  1.77  2.07  2.42
2.83  3.32  3.89  4.55  5.33  6.24  7.3  8.55  10.01  11.72
13.73  16.07  18.82  22.04  25.8  30.21  35.37  41.41  48.49  56.78
66.48

```

DJ JVAR
14.42 13.11 11.92 10.83 9.85 8.95 8.14 7.40 6.73
6.12 5.56 5.05 4.59 4.18 3.80 3.45 3.14 2.85
2.59 2.36 2.14 1.95 1.77 1.61 1.46 1.33 1.21
1.10 0.5 1 0.5 1.10
1.21 1.33 1.46 1.61 1.77 1.95 2.14 2.36 2.59
2.85 3.14 3.45 3.80 4.18 4.59 5.05 5.56 6.12
6.73 7.40 8.14 8.95 9.85 10.83 11.92 13.11 14.42

DK KVAR
27*129.9626
14.42 13.11 11.92 10.83 9.85 8.95 8.14 7.40 6.73
6.12 5.56 5.05 4.59 4.18 3.80 3.45 3.14 2.85
2.59 2.36 2.14 1.95 1.77 1.61 1.46 1.33 1.21
1.10 0.5 1.0 0.5 1.10
1.21 1.33 1.46 1.61 1.77 1.95 2.14 2.36 2.59
2.85 3.14 3.45 3.80 4.18 4.59 5.05 5.56 6.12
6.73 7.40 8.14 8.95 9.85 10.83 11.92 13.11 14.42

DTOP
8319*0
PERMI CON 0.001
PERMJ EQUALSI
PERMK EQUALSI
** 0 = null block, 1 = active block
NULL CON 1
POR CON 0.05
** 0 = pinched block, 1 = active block
PINCHOUTARRAY CON 1
END-GRID
ROCKTYPE 1
CPOR 4.35e-7
ROCKCP 2.66e6 0
THCONR 2.59e5
THCONW 53500
** Model and number of components
MODEL 2 2 1 1
COMPNAME 'H2O' 'CO2'
CMM
0 0.04401
PCRIT
0 7376
TCRIT
0 31.05
CPG1
0 21.08550
CPG2
0 0.06709
CPG3
0 -4.74505E-05
CPG4
0 1.49183E-08
CPG5
0 -1.27083E-12
MASSDEN
0

CP
 0
 CT1
 0
 CT2
 0
 CPT
 0
 AVISC
 0.0047352
 BVISC
 1515.7
 PRSR 36677
 TEMR 187
 PSURF 101
 TSURF 15
 XNACL 0
 PVT DEPARTURE ON
 WAITPENTH
 ACEN 0.3480 0.2310
 ROCKFLUID
 RPT 1 WAITWEI
 ** Sw krw krow
 SWT
 0 0 1
 1 1 0
 ** Sl krg krog
 SLT
 0 1 0
 1 0 1
 INITIAL
 VERTICAL OFF

 **
 INITREGION 1
 REFPRES 36677
 REFDEPTH 3657.6
 PRES KVAR
 750.8 2050.4 3350.1 4649.7 5949.3 7248.9 8548.6 9848.2 11147.8
 12447.4 13747.1 15046.7 16346.3 17646.0 18945.6 20245.2 21544.8 22844.5
 24144.1 25443.7 26743.3 28043.0 29342.6 30642.2 31941.8 33241.5 34541.1
 35263.0 35400.7 35525.8 35639.6 35743.0 35837.0 35922.4 36000.1 36070.8
 36135.0 36193.4 36246.5 36294.7 36338.5 36378.4 36414.7 36447.6 36477.6
 36504.8 36529.5 36552.0 36572.5 36591.1 36608.0 36623.3 36637.3 36650.0
 36661.5 36669.5 36677.0 36684.5 36692.5 36704.1 36716.8 36730.7 36746.1
 36763.0 36781.6 36802.0 36824.5 36849.3 36876.5 36906.4 36939.4 36975.6
 37015.5 37059.4 37107.6 37160.6 37219.0 37283.3 37353.9 37431.6 37517.1
 37611.1 37714.5 37828.2 37953.4 38091.0
 TEMP KVAR
 18.1 24.2 30.3 36.4 42.5 48.6 54.7 60.8 66.9
 73.1 79.2 85.3 91.4 97.5 103.6 109.7 115.8 122.0
 128.1 134.2 140.3 146.4 152.5 158.6 164.7 170.8 177.0
 180.4 181.0 181.6 182.1 182.6 183.0 183.5 183.8 184.1
 184.5 184.7 185.0 185.2 185.4 185.6 185.8 185.9 186.1
 186.2 186.3 186.4 186.5 186.6 186.7 186.7 186.8 186.9

186.9	187.0	187.0	187.0	187.1	187.1	187.2	187.3	187.3
187.4	187.5	187.6	187.7	187.8	187.9	188.1	188.2	188.4
188.6	188.8	189.0	189.3	189.5	189.9	190.2	190.5	191.0
191.4	191.9	192.4	193.0	193.6				

```

SW CON          1
SO CON          0
SG CON          0
MFRAC_WAT 'H2O' CON      1
MFRAC_GAS 'CO2' CON      1

```

```

NUMERICAL
RUN
DATE 2020 1 1
DTWELL 1E-4
DTMAX 0.1

```

```

**
WELL 'Well-1_Annulus'
PRODUCER 'Well-1_Annulus'
OPERATE MAX STW 0.0 CONT

```

```

**          rad geofac wfrac skin
GEOMETRY K 0.115 0.249 1.0 0.0
PERF_FLX   GEOA 'Well-1_Annulus'

```

```

** UBA          ff          Status Connection
33 30 1          1.0 CLOSED FLOW-TO 'SURFACE' REFLAYER
33 30 2          1.0 CLOSED FLOW-TO 1
33 30 3          1.0 CLOSED FLOW-TO 2
33 30 4          1.0 CLOSED FLOW-TO 3
33 30 5          1.0 CLOSED FLOW-TO 4
33 30 6          1.0 CLOSED FLOW-TO 5
33 30 7          1.0 CLOSED FLOW-TO 6
33 30 8          1.0 CLOSED FLOW-TO 7
33 30 9          1.0 CLOSED FLOW-TO 8
33 30 10         1.0 CLOSED FLOW-TO 9
33 30 11         1.0 CLOSED FLOW-TO 10
33 30 12         1.0 CLOSED FLOW-TO 11
33 30 13         1.0 CLOSED FLOW-TO 12
33 30 14         1.0 CLOSED FLOW-TO 13
33 30 15         1.0 CLOSED FLOW-TO 14
33 30 16         1.0 CLOSED FLOW-TO 15
33 30 17         1.0 CLOSED FLOW-TO 16
33 30 18         1.0 CLOSED FLOW-TO 17
33 30 19         1.0 CLOSED FLOW-TO 18
33 30 20         1.0 CLOSED FLOW-TO 19
33 30 21         1.0 CLOSED FLOW-TO 20
33 30 22         1.0 CLOSED FLOW-TO 21
33 30 23         1.0 CLOSED FLOW-TO 22
33 30 24         1.0 CLOSED FLOW-TO 23
33 30 25         1.0 CLOSED FLOW-TO 24
33 30 26         1.0 CLOSED FLOW-TO 25
33 30 27         1.0 CLOSED FLOW-TO 26
33 30 28         1.0 CLOSED FLOW-TO 27
33 30 29         1.0 CLOSED FLOW-TO 28
33 30 30         1.0 CLOSED FLOW-TO 29
33 30 31         1.0 CLOSED FLOW-TO 30
33 30 32         1.0 CLOSED FLOW-TO 31
33 30 33         1.0 CLOSED FLOW-TO 32

```

33	30	34	1.0	CLOSED	FLOW-TO	33
33	30	35	1.0	CLOSED	FLOW-TO	34
33	30	36	1.0	CLOSED	FLOW-TO	35
33	30	37	1.0	CLOSED	FLOW-TO	36
33	30	38	1.0	CLOSED	FLOW-TO	37
33	30	39	1.0	CLOSED	FLOW-TO	38
33	30	40	1.0	CLOSED	FLOW-TO	39
33	30	41	1.0	CLOSED	FLOW-TO	40
33	30	42	1.0	CLOSED	FLOW-TO	41
33	30	43	1.0	CLOSED	FLOW-TO	42
33	30	44	1.0	CLOSED	FLOW-TO	43
33	30	45	1.0	CLOSED	FLOW-TO	44
33	30	46	1.0	CLOSED	FLOW-TO	45
33	30	47	1.0	CLOSED	FLOW-TO	46
33	30	48	1.0	CLOSED	FLOW-TO	47
33	30	49	1.0	CLOSED	FLOW-TO	48
33	30	50	1.0	CLOSED	FLOW-TO	49
33	30	51	1.0	CLOSED	FLOW-TO	50
33	30	52	1.0	CLOSED	FLOW-TO	51
33	30	53	1.0	CLOSED	FLOW-TO	52
33	30	54	1.0	CLOSED	FLOW-TO	53
33	30	55	1.0	CLOSED	FLOW-TO	54
33	30	56	1.0	CLOSED	FLOW-TO	55
33	30	57	1.0	CLOSED	FLOW-TO	56
34	30	57	1.0	CLOSED	FLOW-TO	57
35	30	57	1.0	CLOSED	FLOW-TO	58
36	30	57	1.0	CLOSED	FLOW-TO	59
37	30	57	1.0	CLOSED	FLOW-TO	60
38	30	57	1.0	CLOSED	FLOW-TO	61
39	30	57	1.0	CLOSED	FLOW-TO	62
40	30	57	1.0	CLOSED	FLOW-TO	63
41	30	57	1.0	CLOSED	FLOW-TO	64
42	30	57	1.0	CLOSED	FLOW-TO	65
43	30	57	1.0	CLOSED	FLOW-TO	66
44	30	57	1.0	CLOSED	FLOW-TO	67
45	30	57	1.0	CLOSED	FLOW-TO	68
46	30	57	1.0	CLOSED	FLOW-TO	69
47	30	57	1.0	CLOSED	FLOW-TO	70
48	30	57	1.0	CLOSED	FLOW-TO	71
49	30	57	1.0	CLOSED	FLOW-TO	72
50	30	57	1.0	CLOSED	FLOW-TO	73
51	30	57	1.0	CLOSED	FLOW-TO	74
52	30	57	1.0	CLOSED	FLOW-TO	75
53	30	57	1.0	CLOSED	FLOW-TO	76
54	30	57	1.0	CLOSED	FLOW-TO	77
55	30	57	1.0	CLOSED	FLOW-TO	78
56	30	57	1.0	CLOSED	FLOW-TO	79
57	30	57	1.0	CLOSED	FLOW-TO	80
58	30	57	1.0	CLOSED	FLOW-TO	81
59	30	57	1.0	CLOSED	FLOW-TO	82
60	30	57	1.0	CLOSED	FLOW-TO	83
61	30	57	1.0	CLOSED	FLOW-TO	84
62	30	57	1.0	CLOSED	FLOW-TO	85
63	30	57	1.0	CLOSED	FLOW-TO	86
64	30	57	1.0	CLOSED	FLOW-TO	87

65	30	57	1.0	CLOSED	FLOW-TO	88
66	30	57	1.0	CLOSED	FLOW-TO	89
67	30	57	1.0	CLOSED	FLOW-TO	90
68	30	57	1.0	CLOSED	FLOW-TO	91
69	30	57	1.0	CLOSED	FLOW-TO	92
70	30	57	1.0	CLOSED	FLOW-TO	93
71	30	57	1.0	CLOSED	FLOW-TO	94
72	30	57	1.0	CLOSED	FLOW-TO	95
73	30	57	1.0	CLOSED	FLOW-TO	96
74	30	57	1.0	CLOSED	FLOW-TO	97
75	30	57	1.0	CLOSED	FLOW-TO	98
76	30	57	1.0	CLOSED	FLOW-TO	99
77	30	57	1.0	CLOSED	FLOW-TO	100
78	30	57	1.0	CLOSED	FLOW-TO	101
79	30	57	1.0	CLOSED	FLOW-TO	102
80	30	57	1.0	CLOSED	FLOW-TO	103
81	30	57	1.0	CLOSED	FLOW-TO	104
82	30	57	1.0	CLOSED	FLOW-TO	105
83	30	57	1.0	CLOSED	FLOW-TO	106
84	30	57	1.0	CLOSED	FLOW-TO	107
85	30	57	1.0	CLOSED	FLOW-TO	108
86	30	57	1.0	CLOSED	FLOW-TO	109
87	30	57	1.0	CLOSED	FLOW-TO	110
88	30	57	1.0	CLOSED	FLOW-TO	111
89	30	57	1.0	CLOSED	FLOW-TO	112
90	30	57	1.0	CLOSED	FLOW-TO	113
91	30	57	1.0	CLOSED	FLOW-TO	114
92	30	57	1.0	CLOSED	FLOW-TO	115
93	30	57	1.0	CLOSED	FLOW-TO	116
94	30	57	1.0	CLOSED	FLOW-TO	117
95	30	57	1.0	CLOSED	FLOW-TO	118
96	30	57	1.0	CLOSED	FLOW-TO	119
97	30	57	1.0	CLOSED	FLOW-TO	120
98	30	57	1.0	CLOSED	FLOW-TO	121
99	30	57	1.0	CLOSED	FLOW-TO	122
100	30	57	1.0	CLOSED	FLOW-TO	123
101	30	57	1.0	CLOSED	FLOW-TO	124
102	30	57	1.0	CLOSED	FLOW-TO	125
103	30	57	1.0	CLOSED	FLOW-TO	126
104	30	57	1.0	CLOSED	FLOW-TO	127
105	30	57	1.0	CLOSED	FLOW-TO	128
106	30	57	1.0	CLOSED	FLOW-TO	129
107	30	57	1.0	CLOSED	FLOW-TO	130
108	30	57	1.0	CLOSED	FLOW-TO	131
109	30	57	1.0	CLOSED	FLOW-TO	132
110	30	57	1.0	OPEN	FLOW-TO	133

LAYERXYZ 'Well-1-Annulus'

** perf geometric data: UBA, block entry(x,y,z) block exit(x,y,z), length

33	30	1	453.120001	148.610000	0.000000	453.120001	148.610000		
			129.962601	129.962601					
33	30	2	453.120001	148.610000	129.962601	453.120001	148.610000		
			259.925201	129.962601					
33	30	3	453.120001	148.610000	259.925201	453.120001	148.610000		
			389.887802	129.962601					

33	30	4	453.120001	148.610000	389.887802	453.120001	148.610000
			519.850403	129.962601			
33	30	5	453.120001	148.610000	519.850403	453.120001	148.610000
			649.813004	129.962601			
33	30	6	453.120001	148.610000	649.813004	453.120001	148.610000
			779.775604	129.962601			
33	30	7	453.120001	148.610000	779.775604	453.120001	148.610000
			909.738205	129.962601			
33	30	8	453.120001	148.610000	909.738205	453.120001	148.610000
			1039.700806	129.962601			
33	30	9	453.120001	148.610000	1039.700806	453.120001	148.610000
			1169.663406	129.962601			
33	30	10	453.120001	148.610000	1169.663406	453.120001	148.610000
			1299.626007	129.962601			
33	30	11	453.120001	148.610000	1299.626007	453.120001	148.610000
			1429.588608	129.962601			
33	30	12	453.120001	148.610000	1429.588608	453.120001	148.610000
			1559.551208	129.962601			
33	30	13	453.120001	148.610000	1559.551208	453.120001	148.610000
			1689.513809	129.962601			
33	30	14	453.120001	148.610000	1689.513809	453.120001	148.610000
			1819.476410	129.962601			
33	30	15	453.120001	148.610000	1819.476410	453.120001	148.610000
			1949.439011	129.962601			
33	30	16	453.120001	148.610000	1949.439011	453.120001	148.610000
			2079.401611	129.962601			
33	30	17	453.120001	148.610000	2079.401611	453.120001	148.610000
			2209.364212	129.962601			
33	30	18	453.120001	148.610000	2209.364212	453.120001	148.610000
			2339.326813	129.962601			
33	30	19	453.120001	148.610000	2339.326813	453.120001	148.610000
			2469.289413	129.962601			
33	30	20	453.120001	148.610000	2469.289413	453.120001	148.610000
			2599.252014	129.962601			
33	30	21	453.120001	148.610000	2599.252014	453.120001	148.610000
			2729.214615	129.962601			
33	30	22	453.120001	148.610000	2729.214615	453.120001	148.610000
			2859.177216	129.962601			
33	30	23	453.120001	148.610000	2859.177216	453.120001	148.610000
			2989.139816	129.962601			
33	30	24	453.120001	148.610000	2989.139816	453.120001	148.610000
			3119.102417	129.962601			
33	30	25	453.120001	148.610000	3119.102417	453.120001	148.610000
			3249.065018	129.962601			
33	30	26	453.120001	148.610000	3249.065018	453.120001	148.610000
			3379.027618	129.962601			
33	30	27	453.120001	148.610000	3379.027618	453.120001	148.610000
			3508.990219	129.962601			
33	30	28	453.120001	148.610000	3508.990219	453.120001	148.610000
			3523.410219	14.420000			
33	30	29	453.120001	148.610000	3523.410219	453.120001	148.610000
			3536.520219	13.110000			
33	30	30	453.120001	148.610000	3536.520219	453.120001	148.610000
			3548.440219	11.920000			

33	30	31	453.120001	148.610000	3548.440219	453.120001	148.610000
			3559.270219	10.830000			
33	30	32	453.120001	148.610000	3559.270219	453.120001	148.610000
			3569.120219	9.850000			
33	30	33	453.120001	148.610000	3569.120219	453.120001	148.610000
			3578.070219	8.950000			
33	30	34	453.120001	148.610000	3578.070219	453.120001	148.610000
			3586.210219	8.140000			
33	30	35	453.120001	148.610000	3586.210219	453.120001	148.610000
			3593.610219	7.400000			
33	30	36	453.120001	148.610000	3593.610219	453.120001	148.610000
			3600.340219	6.730000			
33	30	37	453.120001	148.610000	3600.340219	453.120001	148.610000
			3606.460219	6.120000			
33	30	38	453.120001	148.610000	3606.460219	453.120001	148.610000
			3612.020219	5.560000			
33	30	39	453.120001	148.610000	3612.020219	453.120001	148.610000
			3617.070220	5.050000			
33	30	40	453.120001	148.610000	3617.070220	453.120001	148.610000
			3621.660220	4.590000			
33	30	41	453.120001	148.610000	3621.660220	453.120001	148.610000
			3625.840219	4.180000			
33	30	42	453.120001	148.610000	3625.840219	453.120001	148.610000
			3629.640219	3.800000			
33	30	43	453.120001	148.610000	3629.640219	453.120001	148.610000
			3633.090219	3.450000			
33	30	44	453.120001	148.610000	3633.090219	453.120001	148.610000
			3636.230220	3.140000			
33	30	45	453.120001	148.610000	3636.230220	453.120001	148.610000
			3639.080220	2.850000			
33	30	46	453.120001	148.610000	3639.080220	453.120001	148.610000
			3641.670219	2.590000			
33	30	47	453.120001	148.610000	3641.670219	453.120001	148.610000
			3644.030219	2.360000			
33	30	48	453.120001	148.610000	3644.030219	453.120001	148.610000
			3646.170219	2.140000			
33	30	49	453.120001	148.610000	3646.170219	453.120001	148.610000
			3648.120219	1.950000			
33	30	50	453.120001	148.610000	3648.120219	453.120001	148.610000
			3649.890219	1.770000			
33	30	51	453.120001	148.610000	3649.890219	453.120001	148.610000
			3651.500219	1.610000			
33	30	52	453.120001	148.610000	3651.500219	453.120001	148.610000
			3652.960220	1.460000			
33	30	53	453.120001	148.610000	3652.960220	453.120001	148.610000
			3654.290220	1.330000			
33	30	54	453.120001	148.610000	3654.290220	453.120001	148.610000
			3655.500220	1.210000			
33	30	55	453.120001	148.610000	3655.500220	453.120001	148.610000
			3656.600220	1.100000			
33	30	56	453.120001	148.610000	3656.600220	453.245001	148.610000
			3657.100220	0.529508			
33	30	57	453.245001	148.610000	3657.100220	453.620001	148.610000
			3657.475220	0.559017			

34	30	57	453.620001	148.610000	3657.475220	454.120001	148.610000
			3657.600220	0.529508			
35	30	57	454.120001	148.610000	3657.600220	454.710001	148.610000
			3657.600220	0.590000			
36	30	57	454.710001	148.610000	3657.600220	455.400001	148.610000
			3657.600220	0.690000			
37	30	57	455.400001	148.610000	3657.600220	456.200001	148.610000
			3657.600220	0.800000			
38	30	57	456.200001	148.610000	3657.600220	457.140001	148.610000
			3657.600220	0.940000			
39	30	57	457.140001	148.610000	3657.600220	458.240001	148.610000
			3657.600220	1.100000			
40	30	57	458.240001	148.610000	3657.600220	459.530001	148.610000
			3657.600220	1.290000			
41	30	57	459.530001	148.610000	3657.600220	461.040001	148.610000
			3657.600220	1.510000			
42	30	57	461.040001	148.610000	3657.600220	462.810001	148.610000
			3657.600220	1.770000			
43	30	57	462.810001	148.610000	3657.600220	464.880001	148.610000
			3657.600220	2.070000			
44	30	57	464.880001	148.610000	3657.600220	467.300001	148.610000
			3657.600220	2.420000			
45	30	57	467.300001	148.610000	3657.600220	470.130001	148.610000
			3657.600220	2.830000			
46	30	57	470.130001	148.610000	3657.600220	473.450001	148.610000
			3657.600220	3.320000			
47	30	57	473.450001	148.610000	3657.600220	477.340001	148.610000
			3657.600220	3.890000			
48	30	57	477.340001	148.610000	3657.600220	481.890002	148.610000
			3657.600220	4.550000			
49	30	57	481.890002	148.610000	3657.600220	487.220001	148.610000
			3657.600220	5.330000			
50	30	57	487.220001	148.610000	3657.600220	493.460001	148.610000
			3657.600220	6.240000			
51	30	57	493.460001	148.610000	3657.600220	500.760001	148.610000
			3657.600220	7.300000			
52	30	57	500.760001	148.610000	3657.600220	509.310002	148.610000
			3657.600220	8.550000			
53	30	57	509.310002	148.610000	3657.600220	519.320002	148.610000
			3657.600220	10.010000			
54	30	57	519.320002	148.610000	3657.600220	531.040002	148.610000
			3657.600220	11.720000			
55	30	57	531.040002	148.610000	3657.600220	544.770002	148.610000
			3657.600220	13.730000			
56	30	57	544.770002	148.610000	3657.600220	560.840001	148.610000
			3657.600220	16.070000			
57	30	57	560.840001	148.610000	3657.600220	579.660001	148.610000
			3657.600220	18.820000			
58	30	57	579.660001	148.610000	3657.600220	601.700002	148.610000
			3657.600220	22.040001			
59	30	57	601.700002	148.610000	3657.600220	627.500001	148.610000
			3657.600220	25.799999			
60	30	57	627.500001	148.610000	3657.600220	657.710000	148.610000
			3657.600220	30.209999			

61	30	57	657.710000	148.610000	3657.600220	693.079999	148.610000
			3657.600220	35.369999			
62	30	57	693.079999	148.610000	3657.600220	734.489999	148.610000
			3657.600220	41.410000			
63	30	57	734.489999	148.610000	3657.600220	782.980001	148.610000
			3657.600220	48.490002			
64	30	57	782.980001	148.610000	3657.600220	839.760000	148.610000
			3657.600220	56.779999			
65	30	57	839.760000	148.610000	3657.600220	906.240003	148.610000
			3657.600220	66.480003			
66	30	57	906.240003	148.610000	3657.600220	990.110006	148.610000
			3657.600220	83.870003			
67	30	57	990.110006	148.610000	3657.600220	1073.980008	148.610000
			3657.600220	83.870003			
68	30	57	1073.980008	148.610000	3657.600220	1157.850011	148.610000
			3657.600220	83.870003			
69	30	57	1157.850011	148.610000	3657.600220	1241.720014	148.610000
			3657.600220	83.870003			
70	30	57	1241.720014	148.610000	3657.600220	1325.590017	148.610000
			3657.600220	83.870003			
71	30	57	1325.590017	148.610000	3657.600220	1409.460019	148.610000
			3657.600220	83.870003			
72	30	57	1409.460019	148.610000	3657.600220	1493.330022	148.610000
			3657.600220	83.870003			
73	30	57	1493.330022	148.610000	3657.600220	1577.200025	148.610000
			3657.600220	83.870003			
74	30	57	1577.200025	148.610000	3657.600220	1661.070028	148.610000
			3657.600220	83.870003			
75	30	57	1661.070028	148.610000	3657.600220	1744.940030	148.610000
			3657.600220	83.870003			
76	30	57	1744.940030	148.610000	3657.600220	1828.810033	148.610000
			3657.600220	83.870003			
77	30	57	1828.810033	148.610000	3657.600220	1895.290036	148.610000
			3657.600220	66.480003			
78	30	57	1895.290036	148.610000	3657.600220	1952.070035	148.610000
			3657.600220	56.779999			
79	30	57	1952.070035	148.610000	3657.600220	2000.560037	148.610000
			3657.600220	48.490002			
80	30	57	2000.560037	148.610000	3657.600220	2041.970037	148.610000
			3657.600220	41.410000			
81	30	57	2041.970037	148.610000	3657.600220	2077.340036	148.610000
			3657.600220	35.369999			
82	30	57	2077.340036	148.610000	3657.600220	2107.550035	148.610000
			3657.600220	30.209999			
83	30	57	2107.550035	148.610000	3657.600220	2133.350034	148.610000
			3657.600220	25.799999			
84	30	57	2133.350034	148.610000	3657.600220	2155.390035	148.610000
			3657.600220	22.040001			
85	30	57	2155.390035	148.610000	3657.600220	2174.210035	148.610000
			3657.600220	18.820000			
86	30	57	2174.210035	148.610000	3657.600220	2190.280034	148.610000
			3657.600220	16.070000			
87	30	57	2190.280034	148.610000	3657.600220	2204.010034	148.610000
			3657.600220	13.730000			

88	30	57	2204.010034	148.610000	3657.600220	2215.730034	148.610000
			3657.600220	11.720000			
89	30	57	2215.730034	148.610000	3657.600220	2225.740034	148.610000
			3657.600220	10.010000			
90	30	57	2225.740034	148.610000	3657.600220	2234.290035	148.610000
			3657.600220	8.550000			
91	30	57	2234.290035	148.610000	3657.600220	2241.590035	148.610000
			3657.600220	7.300000			
92	30	57	2241.590035	148.610000	3657.600220	2247.830034	148.610000
			3657.600220	6.240000			
93	30	57	2247.830034	148.610000	3657.600220	2253.160034	148.610000
			3657.600220	5.330000			
94	30	57	2253.160034	148.610000	3657.600220	2257.710035	148.610000
			3657.600220	4.550000			
95	30	57	2257.710035	148.610000	3657.600220	2261.600035	148.610000
			3657.600220	3.890000			
96	30	57	2261.600035	148.610000	3657.600220	2264.920035	148.610000
			3657.600220	3.320000			
97	30	57	2264.920035	148.610000	3657.600220	2267.750035	148.610000
			3657.600220	2.830000			
98	30	57	2267.750035	148.610000	3657.600220	2270.170035	148.610000
			3657.600220	2.420000			
99	30	57	2270.170035	148.610000	3657.600220	2272.240035	148.610000
			3657.600220	2.070000			
100	30	57	2272.240035	148.610000	3657.600220	2274.010035	148.610000
			3657.600220	1.770000			
101	30	57	2274.010035	148.610000	3657.600220	2275.520035	148.610000
			3657.600220	1.510000			
102	30	57	2275.520035	148.610000	3657.600220	2276.810035	148.610000
			3657.600220	1.290000			
103	30	57	2276.810035	148.610000	3657.600220	2277.910035	148.610000
			3657.600220	1.100000			
104	30	57	2277.910035	148.610000	3657.600220	2278.850035	148.610000
			3657.600220	0.940000			
105	30	57	2278.850035	148.610000	3657.600220	2279.650035	148.610000
			3657.600220	0.800000			
106	30	57	2279.650035	148.610000	3657.600220	2280.340035	148.610000
			3657.600220	0.690000			
107	30	57	2280.340035	148.610000	3657.600220	2280.930035	148.610000
			3657.600220	0.590000			
108	30	57	2280.930035	148.610000	3657.600220	2281.430035	148.610000
			3657.600220	0.500000			
109	30	57	2281.430035	148.610000	3657.600220	2282.430035	148.610000
			3657.600220	1.000000			
110	30	57	2282.430035	148.610000	3657.600220	2282.930035	148.610000
			3657.600220	0.500000			

SHUTIN 'Well-1_Annulus'

**

WELL 'Well-1_ConcTbg'

**50000.0 CONT

PRODUCER 'Well-1_ConcTbg'

OPERATE MIN BHP 5000.0 CONT

** rad geofac wfrac skin

GEOMETRY K 0.0505 0.249 1.0 0.0

PERF_FLX GEOA 'Well-1_ConcTbg'

** UBA	ff	Status	Connection
33 30 1	1.0	CLOSED	FLOW-TO 'SURFACE' REFLAYER
33 30 2	1.0	CLOSED	FLOW-TO 1
33 30 3	1.0	CLOSED	FLOW-TO 2
33 30 4	1.0	CLOSED	FLOW-TO 3
33 30 5	1.0	CLOSED	FLOW-TO 4
33 30 6	1.0	CLOSED	FLOW-TO 5
33 30 7	1.0	CLOSED	FLOW-TO 6
33 30 8	1.0	CLOSED	FLOW-TO 7
33 30 9	1.0	CLOSED	FLOW-TO 8
33 30 10	1.0	CLOSED	FLOW-TO 9
33 30 11	1.0	CLOSED	FLOW-TO 10
33 30 12	1.0	CLOSED	FLOW-TO 11
33 30 13	1.0	CLOSED	FLOW-TO 12
33 30 14	1.0	CLOSED	FLOW-TO 13
33 30 15	1.0	CLOSED	FLOW-TO 14
33 30 16	1.0	CLOSED	FLOW-TO 15
33 30 17	1.0	CLOSED	FLOW-TO 16
33 30 18	1.0	CLOSED	FLOW-TO 17
33 30 19	1.0	CLOSED	FLOW-TO 18
33 30 20	1.0	CLOSED	FLOW-TO 19
33 30 21	1.0	CLOSED	FLOW-TO 20
33 30 22	1.0	CLOSED	FLOW-TO 21
33 30 23	1.0	CLOSED	FLOW-TO 22
33 30 24	1.0	CLOSED	FLOW-TO 23
33 30 25	1.0	CLOSED	FLOW-TO 24
33 30 26	1.0	CLOSED	FLOW-TO 25
33 30 27	1.0	CLOSED	FLOW-TO 26
33 30 28	1.0	CLOSED	FLOW-TO 27
33 30 29	1.0	CLOSED	FLOW-TO 28
33 30 30	1.0	CLOSED	FLOW-TO 29
33 30 31	1.0	CLOSED	FLOW-TO 30
33 30 32	1.0	CLOSED	FLOW-TO 31
33 30 33	1.0	CLOSED	FLOW-TO 32
33 30 34	1.0	CLOSED	FLOW-TO 33
33 30 35	1.0	CLOSED	FLOW-TO 34
33 30 36	1.0	CLOSED	FLOW-TO 35
33 30 37	1.0	CLOSED	FLOW-TO 36
33 30 38	1.0	CLOSED	FLOW-TO 37
33 30 39	1.0	CLOSED	FLOW-TO 38
33 30 40	1.0	CLOSED	FLOW-TO 39
33 30 41	1.0	CLOSED	FLOW-TO 40
33 30 42	1.0	CLOSED	FLOW-TO 41
33 30 43	1.0	CLOSED	FLOW-TO 42
33 30 44	1.0	CLOSED	FLOW-TO 43
33 30 45	1.0	CLOSED	FLOW-TO 44
33 30 46	1.0	CLOSED	FLOW-TO 45
33 30 47	1.0	CLOSED	FLOW-TO 46
33 30 48	1.0	CLOSED	FLOW-TO 47
33 30 49	1.0	CLOSED	FLOW-TO 48
33 30 50	1.0	CLOSED	FLOW-TO 49
33 30 51	1.0	CLOSED	FLOW-TO 50
33 30 52	1.0	CLOSED	FLOW-TO 51
33 30 53	1.0	CLOSED	FLOW-TO 52
33 30 54	1.0	CLOSED	FLOW-TO 53

33	30	55	1.0	CLOSED	FLOW-TO	54
33	30	56	1.0	CLOSED	FLOW-TO	55
33	30	57	1.0	CLOSED	FLOW-TO	56
34	30	57	1.0	CLOSED	FLOW-TO	57
35	30	57	1.0	CLOSED	FLOW-TO	58
36	30	57	1.0	CLOSED	FLOW-TO	59
37	30	57	1.0	CLOSED	FLOW-TO	60
38	30	57	1.0	CLOSED	FLOW-TO	61
39	30	57	1.0	CLOSED	FLOW-TO	62
40	30	57	1.0	CLOSED	FLOW-TO	63
41	30	57	1.0	CLOSED	FLOW-TO	64
42	30	57	1.0	CLOSED	FLOW-TO	65
43	30	57	1.0	CLOSED	FLOW-TO	66
44	30	57	1.0	CLOSED	FLOW-TO	67
45	30	57	1.0	CLOSED	FLOW-TO	68
46	30	57	1.0	CLOSED	FLOW-TO	69
47	30	57	1.0	CLOSED	FLOW-TO	70
48	30	57	1.0	CLOSED	FLOW-TO	71
49	30	57	1.0	CLOSED	FLOW-TO	72
50	30	57	1.0	CLOSED	FLOW-TO	73
51	30	57	1.0	CLOSED	FLOW-TO	74
52	30	57	1.0	CLOSED	FLOW-TO	75
53	30	57	1.0	CLOSED	FLOW-TO	76
54	30	57	1.0	CLOSED	FLOW-TO	77
55	30	57	1.0	CLOSED	FLOW-TO	78
56	30	57	1.0	CLOSED	FLOW-TO	79
57	30	57	1.0	CLOSED	FLOW-TO	80
58	30	57	1.0	CLOSED	FLOW-TO	81
59	30	57	1.0	CLOSED	FLOW-TO	82
60	30	57	1.0	CLOSED	FLOW-TO	83
61	30	57	1.0	CLOSED	FLOW-TO	84
62	30	57	1.0	CLOSED	FLOW-TO	85
63	30	57	1.0	CLOSED	FLOW-TO	86
64	30	57	1.0	CLOSED	FLOW-TO	87
65	30	57	1.0	CLOSED	FLOW-TO	88
66	30	57	1.0	CLOSED	FLOW-TO	89
67	30	57	1.0	CLOSED	FLOW-TO	90
68	30	57	1.0	CLOSED	FLOW-TO	91
69	30	57	1.0	CLOSED	FLOW-TO	92
70	30	57	1.0	CLOSED	FLOW-TO	93
71	30	57	1.0	CLOSED	FLOW-TO	94
72	30	57	1.0	CLOSED	FLOW-TO	95
73	30	57	1.0	CLOSED	FLOW-TO	96
74	30	57	1.0	CLOSED	FLOW-TO	97
75	30	57	1.0	CLOSED	FLOW-TO	98
76	30	57	1.0	CLOSED	FLOW-TO	99
77	30	57	1.0	CLOSED	FLOW-TO	100
78	30	57	1.0	CLOSED	FLOW-TO	101
79	30	57	1.0	CLOSED	FLOW-TO	102
80	30	57	1.0	CLOSED	FLOW-TO	103
81	30	57	1.0	CLOSED	FLOW-TO	104
82	30	57	1.0	CLOSED	FLOW-TO	105
83	30	57	1.0	CLOSED	FLOW-TO	106
84	30	57	1.0	CLOSED	FLOW-TO	107
85	30	57	1.0	CLOSED	FLOW-TO	108

86	30	57	1.0	CLOSED	FLOW-TO	109
87	30	57	1.0	CLOSED	FLOW-TO	110
88	30	57	1.0	CLOSED	FLOW-TO	111
89	30	57	1.0	CLOSED	FLOW-TO	112
90	30	57	1.0	CLOSED	FLOW-TO	113
91	30	57	1.0	CLOSED	FLOW-TO	114
92	30	57	1.0	CLOSED	FLOW-TO	115
93	30	57	1.0	CLOSED	FLOW-TO	116
94	30	57	1.0	CLOSED	FLOW-TO	117
95	30	57	1.0	CLOSED	FLOW-TO	118
96	30	57	1.0	CLOSED	FLOW-TO	119
97	30	57	1.0	CLOSED	FLOW-TO	120
98	30	57	1.0	CLOSED	FLOW-TO	121
99	30	57	1.0	CLOSED	FLOW-TO	122
100	30	57	1.0	CLOSED	FLOW-TO	123
101	30	57	1.0	CLOSED	FLOW-TO	124
102	30	57	1.0	CLOSED	FLOW-TO	125
103	30	57	1.0	CLOSED	FLOW-TO	126
104	30	57	1.0	CLOSED	FLOW-TO	127
105	30	57	1.0	CLOSED	FLOW-TO	128
106	30	57	1.0	CLOSED	FLOW-TO	129
107	30	57	1.0	CLOSED	FLOW-TO	130
108	30	57	1.0	CLOSED	FLOW-TO	131
109	30	57	1.0	OPEN	FLOW-TO	132

LAYERXYZ 'Well-1-ConcTbg'

** perf geometric data: UBA, block entry(x,y,z) block exit(x,y,z), length

33	30	1	453.120001	148.610000	0.000000	453.120001	148.610000	
			129.962601	129.962601				
33	30	2	453.120001	148.610000	129.962601	453.120001	148.610000	
			259.925201	129.962601				
33	30	3	453.120001	148.610000	259.925201	453.120001	148.610000	
			389.887802	129.962601				
33	30	4	453.120001	148.610000	389.887802	453.120001	148.610000	
			519.850403	129.962601				
33	30	5	453.120001	148.610000	519.850403	453.120001	148.610000	
			649.813004	129.962601				
33	30	6	453.120001	148.610000	649.813004	453.120001	148.610000	
			779.775604	129.962601				
33	30	7	453.120001	148.610000	779.775604	453.120001	148.610000	
			909.738205	129.962601				
33	30	8	453.120001	148.610000	909.738205	453.120001	148.610000	
			1039.700806	129.962601				
33	30	9	453.120001	148.610000	1039.700806	453.120001	148.610000	
			1169.663406	129.962601				
33	30	10	453.120001	148.610000	1169.663406	453.120001	148.610000	
			1299.626007	129.962601				
33	30	11	453.120001	148.610000	1299.626007	453.120001	148.610000	
			1429.588608	129.962601				
33	30	12	453.120001	148.610000	1429.588608	453.120001	148.610000	
			1559.551208	129.962601				
33	30	13	453.120001	148.610000	1559.551208	453.120001	148.610000	
			1689.513809	129.962601				
33	30	14	453.120001	148.610000	1689.513809	453.120001	148.610000	
			1819.476410	129.962601				

33	30	15	453.120001	148.610000	1819.476410	453.120001	148.610000
			1949.439011	129.962601			
33	30	16	453.120001	148.610000	1949.439011	453.120001	148.610000
			2079.401611	129.962601			
33	30	17	453.120001	148.610000	2079.401611	453.120001	148.610000
			2209.364212	129.962601			
33	30	18	453.120001	148.610000	2209.364212	453.120001	148.610000
			2339.326813	129.962601			
33	30	19	453.120001	148.610000	2339.326813	453.120001	148.610000
			2469.289413	129.962601			
33	30	20	453.120001	148.610000	2469.289413	453.120001	148.610000
			2599.252014	129.962601			
33	30	21	453.120001	148.610000	2599.252014	453.120001	148.610000
			2729.214615	129.962601			
33	30	22	453.120001	148.610000	2729.214615	453.120001	148.610000
			2859.177216	129.962601			
33	30	23	453.120001	148.610000	2859.177216	453.120001	148.610000
			2989.139816	129.962601			
33	30	24	453.120001	148.610000	2989.139816	453.120001	148.610000
			3119.102417	129.962601			
33	30	25	453.120001	148.610000	3119.102417	453.120001	148.610000
			3249.065018	129.962601			
33	30	26	453.120001	148.610000	3249.065018	453.120001	148.610000
			3379.027618	129.962601			
33	30	27	453.120001	148.610000	3379.027618	453.120001	148.610000
			3508.990219	129.962601			
33	30	28	453.120001	148.610000	3508.990219	453.120001	148.610000
			3523.410219	14.420000			
33	30	29	453.120001	148.610000	3523.410219	453.120001	148.610000
			3536.520219	13.110000			
33	30	30	453.120001	148.610000	3536.520219	453.120001	148.610000
			3548.440219	11.920000			
33	30	31	453.120001	148.610000	3548.440219	453.120001	148.610000
			3559.270219	10.830000			
33	30	32	453.120001	148.610000	3559.270219	453.120001	148.610000
			3569.120219	9.850000			
33	30	33	453.120001	148.610000	3569.120219	453.120001	148.610000
			3578.070219	8.950000			
33	30	34	453.120001	148.610000	3578.070219	453.120001	148.610000
			3586.210219	8.140000			
33	30	35	453.120001	148.610000	3586.210219	453.120001	148.610000
			3593.610219	7.400000			
33	30	36	453.120001	148.610000	3593.610219	453.120001	148.610000
			3600.340219	6.730000			
33	30	37	453.120001	148.610000	3600.340219	453.120001	148.610000
			3606.460219	6.120000			
33	30	38	453.120001	148.610000	3606.460219	453.120001	148.610000
			3612.020219	5.560000			
33	30	39	453.120001	148.610000	3612.020219	453.120001	148.610000
			3617.070220	5.050000			
33	30	40	453.120001	148.610000	3617.070220	453.120001	148.610000
			3621.660220	4.590000			
33	30	41	453.120001	148.610000	3621.660220	453.120001	148.610000
			3625.840219	4.180000			

33	30	42	453.120001	148.610000	3625.840219	453.120001	148.610000
			3629.640219	3.800000			
33	30	43	453.120001	148.610000	3629.640219	453.120001	148.610000
			3633.090219	3.450000			
33	30	44	453.120001	148.610000	3633.090219	453.120001	148.610000
			3636.230220	3.140000			
33	30	45	453.120001	148.610000	3636.230220	453.120001	148.610000
			3639.080220	2.850000			
33	30	46	453.120001	148.610000	3639.080220	453.120001	148.610000
			3641.670219	2.590000			
33	30	47	453.120001	148.610000	3641.670219	453.120001	148.610000
			3644.030219	2.360000			
33	30	48	453.120001	148.610000	3644.030219	453.120001	148.610000
			3646.170219	2.140000			
33	30	49	453.120001	148.610000	3646.170219	453.120001	148.610000
			3648.120219	1.950000			
33	30	50	453.120001	148.610000	3648.120219	453.120001	148.610000
			3649.890219	1.770000			
33	30	51	453.120001	148.610000	3649.890219	453.120001	148.610000
			3651.500219	1.610000			
33	30	52	453.120001	148.610000	3651.500219	453.120001	148.610000
			3652.960220	1.460000			
33	30	53	453.120001	148.610000	3652.960220	453.120001	148.610000
			3654.290220	1.330000			
33	30	54	453.120001	148.610000	3654.290220	453.120001	148.610000
			3655.500220	1.210000			
33	30	55	453.120001	148.610000	3655.500220	453.120001	148.610000
			3656.600220	1.100000			
33	30	56	453.120001	148.610000	3656.600220	453.245001	148.610000
			3657.100220	0.529508			
33	30	57	453.245001	148.610000	3657.100220	453.620001	148.610000
			3657.475220	0.559017			
34	30	57	453.620001	148.610000	3657.475220	454.120001	148.610000
			3657.600220	0.529508			
35	30	57	454.120001	148.610000	3657.600220	454.710001	148.610000
			3657.600220	0.590000			
36	30	57	454.710001	148.610000	3657.600220	455.400001	148.610000
			3657.600220	0.690000			
37	30	57	455.400001	148.610000	3657.600220	456.200001	148.610000
			3657.600220	0.800000			
38	30	57	456.200001	148.610000	3657.600220	457.140001	148.610000
			3657.600220	0.940000			
39	30	57	457.140001	148.610000	3657.600220	458.240001	148.610000
			3657.600220	1.100000			
40	30	57	458.240001	148.610000	3657.600220	459.530001	148.610000
			3657.600220	1.290000			
41	30	57	459.530001	148.610000	3657.600220	461.040001	148.610000
			3657.600220	1.510000			
42	30	57	461.040001	148.610000	3657.600220	462.810001	148.610000
			3657.600220	1.770000			
43	30	57	462.810001	148.610000	3657.600220	464.880001	148.610000
			3657.600220	2.070000			
44	30	57	464.880001	148.610000	3657.600220	467.300001	148.610000
			3657.600220	2.420000			

45	30	57	467.300001	148.610000	3657.600220	470.130001	148.610000
			3657.600220	2.830000			
46	30	57	470.130001	148.610000	3657.600220	473.450001	148.610000
			3657.600220	3.320000			
47	30	57	473.450001	148.610000	3657.600220	477.340001	148.610000
			3657.600220	3.890000			
48	30	57	477.340001	148.610000	3657.600220	481.890002	148.610000
			3657.600220	4.550000			
49	30	57	481.890002	148.610000	3657.600220	487.220001	148.610000
			3657.600220	5.330000			
50	30	57	487.220001	148.610000	3657.600220	493.460001	148.610000
			3657.600220	6.240000			
51	30	57	493.460001	148.610000	3657.600220	500.760001	148.610000
			3657.600220	7.300000			
52	30	57	500.760001	148.610000	3657.600220	509.310002	148.610000
			3657.600220	8.550000			
53	30	57	509.310002	148.610000	3657.600220	519.320002	148.610000
			3657.600220	10.010000			
54	30	57	519.320002	148.610000	3657.600220	531.040002	148.610000
			3657.600220	11.720000			
55	30	57	531.040002	148.610000	3657.600220	544.770002	148.610000
			3657.600220	13.730000			
56	30	57	544.770002	148.610000	3657.600220	560.840001	148.610000
			3657.600220	16.070000			
57	30	57	560.840001	148.610000	3657.600220	579.660001	148.610000
			3657.600220	18.820000			
58	30	57	579.660001	148.610000	3657.600220	601.700002	148.610000
			3657.600220	22.040001			
59	30	57	601.700002	148.610000	3657.600220	627.500001	148.610000
			3657.600220	25.799999			
60	30	57	627.500001	148.610000	3657.600220	657.710000	148.610000
			3657.600220	30.209999			
61	30	57	657.710000	148.610000	3657.600220	693.079999	148.610000
			3657.600220	35.369999			
62	30	57	693.079999	148.610000	3657.600220	734.489999	148.610000
			3657.600220	41.410000			
63	30	57	734.489999	148.610000	3657.600220	782.980001	148.610000
			3657.600220	48.490002			
64	30	57	782.980001	148.610000	3657.600220	839.760000	148.610000
			3657.600220	56.779999			
65	30	57	839.760000	148.610000	3657.600220	906.240003	148.610000
			3657.600220	66.480003			
66	30	57	906.240003	148.610000	3657.600220	990.110006	148.610000
			3657.600220	83.870003			
67	30	57	990.110006	148.610000	3657.600220	1073.980008	148.610000
			3657.600220	83.870003			
68	30	57	1073.980008	148.610000	3657.600220	1157.850011	148.610000
			3657.600220	83.870003			
69	30	57	1157.850011	148.610000	3657.600220	1241.720014	148.610000
			3657.600220	83.870003			
70	30	57	1241.720014	148.610000	3657.600220	1325.590017	148.610000
			3657.600220	83.870003			
71	30	57	1325.590017	148.610000	3657.600220	1409.460019	148.610000
			3657.600220	83.870003			

72	30	57	1409.460019	148.610000	3657.600220	1493.330022	148.610000
			3657.600220	83.870003			
73	30	57	1493.330022	148.610000	3657.600220	1577.200025	148.610000
			3657.600220	83.870003			
74	30	57	1577.200025	148.610000	3657.600220	1661.070028	148.610000
			3657.600220	83.870003			
75	30	57	1661.070028	148.610000	3657.600220	1744.940030	148.610000
			3657.600220	83.870003			
76	30	57	1744.940030	148.610000	3657.600220	1828.810033	148.610000
			3657.600220	83.870003			
77	30	57	1828.810033	148.610000	3657.600220	1895.290036	148.610000
			3657.600220	66.480003			
78	30	57	1895.290036	148.610000	3657.600220	1952.070035	148.610000
			3657.600220	56.779999			
79	30	57	1952.070035	148.610000	3657.600220	2000.560037	148.610000
			3657.600220	48.490002			
80	30	57	2000.560037	148.610000	3657.600220	2041.970037	148.610000
			3657.600220	41.410000			
81	30	57	2041.970037	148.610000	3657.600220	2077.340036	148.610000
			3657.600220	35.369999			
82	30	57	2077.340036	148.610000	3657.600220	2107.550035	148.610000
			3657.600220	30.209999			
83	30	57	2107.550035	148.610000	3657.600220	2133.350034	148.610000
			3657.600220	25.799999			
84	30	57	2133.350034	148.610000	3657.600220	2155.390035	148.610000
			3657.600220	22.040001			
85	30	57	2155.390035	148.610000	3657.600220	2174.210035	148.610000
			3657.600220	18.820000			
86	30	57	2174.210035	148.610000	3657.600220	2190.280034	148.610000
			3657.600220	16.070000			
87	30	57	2190.280034	148.610000	3657.600220	2204.010034	148.610000
			3657.600220	13.730000			
88	30	57	2204.010034	148.610000	3657.600220	2215.730034	148.610000
			3657.600220	11.720000			
89	30	57	2215.730034	148.610000	3657.600220	2225.740034	148.610000
			3657.600220	10.010000			
90	30	57	2225.740034	148.610000	3657.600220	2234.290035	148.610000
			3657.600220	8.550000			
91	30	57	2234.290035	148.610000	3657.600220	2241.590035	148.610000
			3657.600220	7.300000			
92	30	57	2241.590035	148.610000	3657.600220	2247.830034	148.610000
			3657.600220	6.240000			
93	30	57	2247.830034	148.610000	3657.600220	2253.160034	148.610000
			3657.600220	5.330000			
94	30	57	2253.160034	148.610000	3657.600220	2257.710035	148.610000
			3657.600220	4.550000			
95	30	57	2257.710035	148.610000	3657.600220	2261.600035	148.610000
			3657.600220	3.890000			
96	30	57	2261.600035	148.610000	3657.600220	2264.920035	148.610000
			3657.600220	3.320000			
97	30	57	2264.920035	148.610000	3657.600220	2267.750035	148.610000
			3657.600220	2.830000			
98	30	57	2267.750035	148.610000	3657.600220	2270.170035	148.610000
			3657.600220	2.420000			

99	30	57	2270.170035	148.610000	3657.600220	2272.240035	148.610000
			3657.600220	2.070000			
100	30	57	2272.240035	148.610000	3657.600220	2274.010035	148.610000
			3657.600220	1.770000			
101	30	57	2274.010035	148.610000	3657.600220	2275.520035	148.610000
			3657.600220	1.510000			
102	30	57	2275.520035	148.610000	3657.600220	2276.810035	148.610000
			3657.600220	1.290000			
103	30	57	2276.810035	148.610000	3657.600220	2277.910035	148.610000
			3657.600220	1.100000			
104	30	57	2277.910035	148.610000	3657.600220	2278.850035	148.610000
			3657.600220	0.940000			
105	30	57	2278.850035	148.610000	3657.600220	2279.650035	148.610000
			3657.600220	0.800000			
106	30	57	2279.650035	148.610000	3657.600220	2280.340035	148.610000
			3657.600220	0.690000			
107	30	57	2280.340035	148.610000	3657.600220	2280.930035	148.610000
			3657.600220	0.590000			
108	30	57	2280.930035	148.610000	3657.600220	2281.430035	148.610000
			3657.600220	0.500000			
109	30	57	2281.430035	148.610000	3657.600220	2282.430035	148.610000
			3657.600220	1.000000			

**

WELL 'Well-1_Tubing'
 INJECTOR MOBWEIGHT IMPLICIT 'Well-1_Tubing'
 INCOMP WATER 1.0
 TINJW 50.0
 QUAL 0.0
 PINJW 20000.0

OPERATE MAX SIW 864 CONT
 OPERATE MAX BHP 100000.0 CONT

** rad geofac wfrac skin

GEOMETRY K 0.11 0.249 1.0 0.0

PERF_FLX GEOA 'Well-1_Tubing'

** UBA	ff	Status	Connection
33 30 1	1.0	CLOSED	FLOW-FROM 'SURFACE' REFLAYER
33 30 2	1.0	CLOSED	FLOW-FROM 1
33 30 3	1.0	CLOSED	FLOW-FROM 2
33 30 4	1.0	CLOSED	FLOW-FROM 3
33 30 5	1.0	CLOSED	FLOW-FROM 4
33 30 6	1.0	CLOSED	FLOW-FROM 5
33 30 7	1.0	CLOSED	FLOW-FROM 6
33 30 8	1.0	CLOSED	FLOW-FROM 7
33 30 9	1.0	CLOSED	FLOW-FROM 8
33 30 10	1.0	CLOSED	FLOW-FROM 9
33 30 11	1.0	CLOSED	FLOW-FROM 10
33 30 12	1.0	CLOSED	FLOW-FROM 11
33 30 13	1.0	CLOSED	FLOW-FROM 12
33 30 14	1.0	CLOSED	FLOW-FROM 13
33 30 15	1.0	CLOSED	FLOW-FROM 14
33 30 16	1.0	CLOSED	FLOW-FROM 15
33 30 17	1.0	CLOSED	FLOW-FROM 16
33 30 18	1.0	CLOSED	FLOW-FROM 17
33 30 19	1.0	CLOSED	FLOW-FROM 18
33 30 20	1.0	CLOSED	FLOW-FROM 19

33	30	21	1.0	CLOSED	FLOW-FROM	20
33	30	22	1.0	CLOSED	FLOW-FROM	21
33	30	23	1.0	CLOSED	FLOW-FROM	22
33	30	24	1.0	CLOSED	FLOW-FROM	23
33	30	25	1.0	CLOSED	FLOW-FROM	24
33	30	26	1.0	CLOSED	FLOW-FROM	25
33	30	27	1.0	CLOSED	FLOW-FROM	26
33	30	28	1.0	CLOSED	FLOW-FROM	27
33	30	29	1.0	CLOSED	FLOW-FROM	28
33	30	30	1.0	CLOSED	FLOW-FROM	29
33	30	31	1.0	CLOSED	FLOW-FROM	30
33	30	32	1.0	CLOSED	FLOW-FROM	31
33	30	33	1.0	CLOSED	FLOW-FROM	32
33	30	34	1.0	CLOSED	FLOW-FROM	33
33	30	35	1.0	CLOSED	FLOW-FROM	34
33	30	36	1.0	CLOSED	FLOW-FROM	35
33	30	37	1.0	CLOSED	FLOW-FROM	36
33	30	38	1.0	CLOSED	FLOW-FROM	37
33	30	39	1.0	CLOSED	FLOW-FROM	38
33	30	40	1.0	CLOSED	FLOW-FROM	39
33	30	41	1.0	CLOSED	FLOW-FROM	40
33	30	42	1.0	CLOSED	FLOW-FROM	41
33	30	43	1.0	CLOSED	FLOW-FROM	42
33	30	44	1.0	CLOSED	FLOW-FROM	43
33	30	45	1.0	CLOSED	FLOW-FROM	44
33	30	46	1.0	CLOSED	FLOW-FROM	45
33	30	47	1.0	CLOSED	FLOW-FROM	46
33	30	48	1.0	CLOSED	FLOW-FROM	47
33	30	49	1.0	CLOSED	FLOW-FROM	48
33	30	50	1.0	CLOSED	FLOW-FROM	49
33	30	51	1.0	CLOSED	FLOW-FROM	50
33	30	52	1.0	CLOSED	FLOW-FROM	51
33	30	53	1.0	CLOSED	FLOW-FROM	52
33	30	54	1.0	CLOSED	FLOW-FROM	53
33	30	55	1.0	CLOSED	FLOW-FROM	54
33	30	56	1.0	CLOSED	FLOW-FROM	55
33	30	57	1.0	CLOSED	FLOW-FROM	56
34	30	57	1.0	CLOSED	FLOW-FROM	57
35	30	57	1.0	CLOSED	FLOW-FROM	58
36	30	57	1.0	CLOSED	FLOW-FROM	59
37	30	57	1.0	CLOSED	FLOW-FROM	60
38	30	57	1.0	CLOSED	FLOW-FROM	61
39	30	57	1.0	CLOSED	FLOW-FROM	62
40	30	57	1.0	CLOSED	FLOW-FROM	63
41	30	57	1.0	CLOSED	FLOW-FROM	64
42	30	57	1.0	CLOSED	FLOW-FROM	65
43	30	57	1.0	CLOSED	FLOW-FROM	66
44	30	57	1.0	CLOSED	FLOW-FROM	67
45	30	57	1.0	CLOSED	FLOW-FROM	68
46	30	57	1.0	CLOSED	FLOW-FROM	69
47	30	57	1.0	CLOSED	FLOW-FROM	70
48	30	57	1.0	CLOSED	FLOW-FROM	71
49	30	57	1.0	CLOSED	FLOW-FROM	72
50	30	57	1.0	CLOSED	FLOW-FROM	73
51	30	57	1.0	CLOSED	FLOW-FROM	74

52	30	57	1.0	CLOSED	FLOW-FROM	75
53	30	57	1.0	CLOSED	FLOW-FROM	76
54	30	57	1.0	CLOSED	FLOW-FROM	77
55	30	57	1.0	CLOSED	FLOW-FROM	78
56	30	57	1.0	CLOSED	FLOW-FROM	79
57	30	57	1.0	CLOSED	FLOW-FROM	80
58	30	57	1.0	CLOSED	FLOW-FROM	81
59	30	57	1.0	CLOSED	FLOW-FROM	82
60	30	57	1.0	CLOSED	FLOW-FROM	83
61	30	57	1.0	CLOSED	FLOW-FROM	84
62	30	57	1.0	CLOSED	FLOW-FROM	85
63	30	57	1.0	CLOSED	FLOW-FROM	86
64	30	57	1.0	CLOSED	FLOW-FROM	87
65	30	57	1.0	CLOSED	FLOW-FROM	88
66	30	57	1.0	CLOSED	FLOW-FROM	89
67	30	57	1.0	CLOSED	FLOW-FROM	90
68	30	57	1.0	CLOSED	FLOW-FROM	91
69	30	57	1.0	CLOSED	FLOW-FROM	92
70	30	57	1.0	CLOSED	FLOW-FROM	93
71	30	57	1.0	CLOSED	FLOW-FROM	94
72	30	57	1.0	CLOSED	FLOW-FROM	95
73	30	57	1.0	CLOSED	FLOW-FROM	96
74	30	57	1.0	CLOSED	FLOW-FROM	97
75	30	57	1.0	CLOSED	FLOW-FROM	98
76	30	57	1.0	CLOSED	FLOW-FROM	99
77	30	57	1.0	CLOSED	FLOW-FROM	100
78	30	57	1.0	CLOSED	FLOW-FROM	101
79	30	57	1.0	CLOSED	FLOW-FROM	102
80	30	57	1.0	CLOSED	FLOW-FROM	103
81	30	57	1.0	CLOSED	FLOW-FROM	104
82	30	57	1.0	CLOSED	FLOW-FROM	105
83	30	57	1.0	CLOSED	FLOW-FROM	106
84	30	57	1.0	CLOSED	FLOW-FROM	107
85	30	57	1.0	CLOSED	FLOW-FROM	108
86	30	57	1.0	CLOSED	FLOW-FROM	109
87	30	57	1.0	CLOSED	FLOW-FROM	110
88	30	57	1.0	CLOSED	FLOW-FROM	111
89	30	57	1.0	CLOSED	FLOW-FROM	112
90	30	57	1.0	CLOSED	FLOW-FROM	113
91	30	57	1.0	CLOSED	FLOW-FROM	114
92	30	57	1.0	CLOSED	FLOW-FROM	115
93	30	57	1.0	CLOSED	FLOW-FROM	116
94	30	57	1.0	CLOSED	FLOW-FROM	117
95	30	57	1.0	CLOSED	FLOW-FROM	118
96	30	57	1.0	CLOSED	FLOW-FROM	119
97	30	57	1.0	CLOSED	FLOW-FROM	120
98	30	57	1.0	CLOSED	FLOW-FROM	121
99	30	57	1.0	CLOSED	FLOW-FROM	122
100	30	57	1.0	CLOSED	FLOW-FROM	123
101	30	57	1.0	CLOSED	FLOW-FROM	124
102	30	57	1.0	CLOSED	FLOW-FROM	125
103	30	57	1.0	CLOSED	FLOW-FROM	126
104	30	57	1.0	CLOSED	FLOW-FROM	127
105	30	57	1.0	CLOSED	FLOW-FROM	128
106	30	57	1.0	CLOSED	FLOW-FROM	129

107 30 57 1.0 CLOSED FLOW-FROM 130
 108 30 57 1.0 CLOSED FLOW-FROM 131
 109 30 57 1.0 OPEN FLOW-FROM 132

LAYERXYZ 'Well-1_Tubing'

** perf geometric data: UBA, block entry(x,y,z) block exit(x,y,z), length

33	30	1	453.120001	148.610000	0.000000	453.120001	148.610000	
			129.962601	129.962601				
33	30	2	453.120001	148.610000	129.962601	453.120001	148.610000	
			259.925201	129.962601				
33	30	3	453.120001	148.610000	259.925201	453.120001	148.610000	
			389.887802	129.962601				
33	30	4	453.120001	148.610000	389.887802	453.120001	148.610000	
			519.850403	129.962601				
33	30	5	453.120001	148.610000	519.850403	453.120001	148.610000	
			649.813004	129.962601				
33	30	6	453.120001	148.610000	649.813004	453.120001	148.610000	
			779.775604	129.962601				
33	30	7	453.120001	148.610000	779.775604	453.120001	148.610000	
			909.738205	129.962601				
33	30	8	453.120001	148.610000	909.738205	453.120001	148.610000	
			1039.700806	129.962601				
33	30	9	453.120001	148.610000	1039.700806	453.120001	148.610000	
			1169.663406	129.962601				
33	30	10	453.120001	148.610000	1169.663406	453.120001	148.610000	
			1299.626007	129.962601				
33	30	11	453.120001	148.610000	1299.626007	453.120001	148.610000	
			1429.588608	129.962601				
33	30	12	453.120001	148.610000	1429.588608	453.120001	148.610000	
			1559.551208	129.962601				
33	30	13	453.120001	148.610000	1559.551208	453.120001	148.610000	
			1689.513809	129.962601				
33	30	14	453.120001	148.610000	1689.513809	453.120001	148.610000	
			1819.476410	129.962601				
33	30	15	453.120001	148.610000	1819.476410	453.120001	148.610000	
			1949.439011	129.962601				
33	30	16	453.120001	148.610000	1949.439011	453.120001	148.610000	
			2079.401611	129.962601				
33	30	17	453.120001	148.610000	2079.401611	453.120001	148.610000	
			2209.364212	129.962601				
33	30	18	453.120001	148.610000	2209.364212	453.120001	148.610000	
			2339.326813	129.962601				
33	30	19	453.120001	148.610000	2339.326813	453.120001	148.610000	
			2469.289413	129.962601				
33	30	20	453.120001	148.610000	2469.289413	453.120001	148.610000	
			2599.252014	129.962601				
33	30	21	453.120001	148.610000	2599.252014	453.120001	148.610000	
			2729.214615	129.962601				
33	30	22	453.120001	148.610000	2729.214615	453.120001	148.610000	
			2859.177216	129.962601				
33	30	23	453.120001	148.610000	2859.177216	453.120001	148.610000	
			2989.139816	129.962601				
33	30	24	453.120001	148.610000	2989.139816	453.120001	148.610000	
			3119.102417	129.962601				
33	30	25	453.120001	148.610000	3119.102417	453.120001	148.610000	
			3249.065018	129.962601				

33	30	26	453.120001	148.610000	3249.065018	453.120001	148.610000
			3379.027618	129.962601			
33	30	27	453.120001	148.610000	3379.027618	453.120001	148.610000
			3508.990219	129.962601			
33	30	28	453.120001	148.610000	3508.990219	453.120001	148.610000
			3523.410219	14.420000			
33	30	29	453.120001	148.610000	3523.410219	453.120001	148.610000
			3536.520219	13.110000			
33	30	30	453.120001	148.610000	3536.520219	453.120001	148.610000
			3548.440219	11.920000			
33	30	31	453.120001	148.610000	3548.440219	453.120001	148.610000
			3559.270219	10.830000			
33	30	32	453.120001	148.610000	3559.270219	453.120001	148.610000
			3569.120219	9.850000			
33	30	33	453.120001	148.610000	3569.120219	453.120001	148.610000
			3578.070219	8.950000			
33	30	34	453.120001	148.610000	3578.070219	453.120001	148.610000
			3586.210219	8.140000			
33	30	35	453.120001	148.610000	3586.210219	453.120001	148.610000
			3593.610219	7.400000			
33	30	36	453.120001	148.610000	3593.610219	453.120001	148.610000
			3600.340219	6.730000			
33	30	37	453.120001	148.610000	3600.340219	453.120001	148.610000
			3606.460219	6.120000			
33	30	38	453.120001	148.610000	3606.460219	453.120001	148.610000
			3612.020219	5.560000			
33	30	39	453.120001	148.610000	3612.020219	453.120001	148.610000
			3617.070220	5.050000			
33	30	40	453.120001	148.610000	3617.070220	453.120001	148.610000
			3621.660220	4.590000			
33	30	41	453.120001	148.610000	3621.660220	453.120001	148.610000
			3625.840219	4.180000			
33	30	42	453.120001	148.610000	3625.840219	453.120001	148.610000
			3629.640219	3.800000			
33	30	43	453.120001	148.610000	3629.640219	453.120001	148.610000
			3633.090219	3.450000			
33	30	44	453.120001	148.610000	3633.090219	453.120001	148.610000
			3636.230220	3.140000			
33	30	45	453.120001	148.610000	3636.230220	453.120001	148.610000
			3639.080220	2.850000			
33	30	46	453.120001	148.610000	3639.080220	453.120001	148.610000
			3641.670219	2.590000			
33	30	47	453.120001	148.610000	3641.670219	453.120001	148.610000
			3644.030219	2.360000			
33	30	48	453.120001	148.610000	3644.030219	453.120001	148.610000
			3646.170219	2.140000			
33	30	49	453.120001	148.610000	3646.170219	453.120001	148.610000
			3648.120219	1.950000			
33	30	50	453.120001	148.610000	3648.120219	453.120001	148.610000
			3649.890219	1.770000			
33	30	51	453.120001	148.610000	3649.890219	453.120001	148.610000
			3651.500219	1.610000			
33	30	52	453.120001	148.610000	3651.500219	453.120001	148.610000
			3652.960220	1.460000			

33	30	53	453.120001	148.610000	3652.960220	453.120001	148.610000
			3654.290220	1.330000			
33	30	54	453.120001	148.610000	3654.290220	453.120001	148.610000
			3655.500220	1.210000			
33	30	55	453.120001	148.610000	3655.500220	453.120001	148.610000
			3656.600220	1.100000			
33	30	56	453.120001	148.610000	3656.600220	453.245001	148.610000
			3657.100220	0.529508			
33	30	57	453.245001	148.610000	3657.100220	453.620001	148.610000
			3657.475220	0.559017			
34	30	57	453.620001	148.610000	3657.475220	454.120001	148.610000
			3657.600220	0.529508			
35	30	57	454.120001	148.610000	3657.600220	454.710001	148.610000
			3657.600220	0.590000			
36	30	57	454.710001	148.610000	3657.600220	455.400001	148.610000
			3657.600220	0.690000			
37	30	57	455.400001	148.610000	3657.600220	456.200001	148.610000
			3657.600220	0.800000			
38	30	57	456.200001	148.610000	3657.600220	457.140001	148.610000
			3657.600220	0.940000			
39	30	57	457.140001	148.610000	3657.600220	458.240001	148.610000
			3657.600220	1.100000			
40	30	57	458.240001	148.610000	3657.600220	459.530001	148.610000
			3657.600220	1.290000			
41	30	57	459.530001	148.610000	3657.600220	461.040001	148.610000
			3657.600220	1.510000			
42	30	57	461.040001	148.610000	3657.600220	462.810001	148.610000
			3657.600220	1.770000			
43	30	57	462.810001	148.610000	3657.600220	464.880001	148.610000
			3657.600220	2.070000			
44	30	57	464.880001	148.610000	3657.600220	467.300001	148.610000
			3657.600220	2.420000			
45	30	57	467.300001	148.610000	3657.600220	470.130001	148.610000
			3657.600220	2.830000			
46	30	57	470.130001	148.610000	3657.600220	473.450001	148.610000
			3657.600220	3.320000			
47	30	57	473.450001	148.610000	3657.600220	477.340001	148.610000
			3657.600220	3.890000			
48	30	57	477.340001	148.610000	3657.600220	481.890002	148.610000
			3657.600220	4.550000			
49	30	57	481.890002	148.610000	3657.600220	487.220001	148.610000
			3657.600220	5.330000			
50	30	57	487.220001	148.610000	3657.600220	493.460001	148.610000
			3657.600220	6.240000			
51	30	57	493.460001	148.610000	3657.600220	500.760001	148.610000
			3657.600220	7.300000			
52	30	57	500.760001	148.610000	3657.600220	509.310002	148.610000
			3657.600220	8.550000			
53	30	57	509.310002	148.610000	3657.600220	519.320002	148.610000
			3657.600220	10.010000			
54	30	57	519.320002	148.610000	3657.600220	531.040002	148.610000
			3657.600220	11.720000			
55	30	57	531.040002	148.610000	3657.600220	544.770002	148.610000
			3657.600220	13.730000			

56	30	57	544.770002	148.610000	3657.600220	560.840001	148.610000
			3657.600220	16.070000			
57	30	57	560.840001	148.610000	3657.600220	579.660001	148.610000
			3657.600220	18.820000			
58	30	57	579.660001	148.610000	3657.600220	601.700002	148.610000
			3657.600220	22.040001			
59	30	57	601.700002	148.610000	3657.600220	627.500001	148.610000
			3657.600220	25.799999			
60	30	57	627.500001	148.610000	3657.600220	657.710000	148.610000
			3657.600220	30.209999			
61	30	57	657.710000	148.610000	3657.600220	693.079999	148.610000
			3657.600220	35.369999			
62	30	57	693.079999	148.610000	3657.600220	734.489999	148.610000
			3657.600220	41.410000			
63	30	57	734.489999	148.610000	3657.600220	782.980001	148.610000
			3657.600220	48.490002			
64	30	57	782.980001	148.610000	3657.600220	839.760000	148.610000
			3657.600220	56.779999			
65	30	57	839.760000	148.610000	3657.600220	906.240003	148.610000
			3657.600220	66.480003			
66	30	57	906.240003	148.610000	3657.600220	990.110006	148.610000
			3657.600220	83.870003			
67	30	57	990.110006	148.610000	3657.600220	1073.980008	148.610000
			3657.600220	83.870003			
68	30	57	1073.980008	148.610000	3657.600220	1157.850011	148.610000
			3657.600220	83.870003			
69	30	57	1157.850011	148.610000	3657.600220	1241.720014	148.610000
			3657.600220	83.870003			
70	30	57	1241.720014	148.610000	3657.600220	1325.590017	148.610000
			3657.600220	83.870003			
71	30	57	1325.590017	148.610000	3657.600220	1409.460019	148.610000
			3657.600220	83.870003			
72	30	57	1409.460019	148.610000	3657.600220	1493.330022	148.610000
			3657.600220	83.870003			
73	30	57	1493.330022	148.610000	3657.600220	1577.200025	148.610000
			3657.600220	83.870003			
74	30	57	1577.200025	148.610000	3657.600220	1661.070028	148.610000
			3657.600220	83.870003			
75	30	57	1661.070028	148.610000	3657.600220	1744.940030	148.610000
			3657.600220	83.870003			
76	30	57	1744.940030	148.610000	3657.600220	1828.810033	148.610000
			3657.600220	83.870003			
77	30	57	1828.810033	148.610000	3657.600220	1895.290036	148.610000
			3657.600220	66.480003			
78	30	57	1895.290036	148.610000	3657.600220	1952.070035	148.610000
			3657.600220	56.779999			
79	30	57	1952.070035	148.610000	3657.600220	2000.560037	148.610000
			3657.600220	48.490002			
80	30	57	2000.560037	148.610000	3657.600220	2041.970037	148.610000
			3657.600220	41.410000			
81	30	57	2041.970037	148.610000	3657.600220	2077.340036	148.610000
			3657.600220	35.369999			
82	30	57	2077.340036	148.610000	3657.600220	2107.550035	148.610000
			3657.600220	30.209999			

83	30	57	2107.550035	148.610000	3657.600220	2133.350034	148.610000
			3657.600220	25.799999			
84	30	57	2133.350034	148.610000	3657.600220	2155.390035	148.610000
			3657.600220	22.040001			
85	30	57	2155.390035	148.610000	3657.600220	2174.210035	148.610000
			3657.600220	18.820000			
86	30	57	2174.210035	148.610000	3657.600220	2190.280034	148.610000
			3657.600220	16.070000			
87	30	57	2190.280034	148.610000	3657.600220	2204.010034	148.610000
			3657.600220	13.730000			
88	30	57	2204.010034	148.610000	3657.600220	2215.730034	148.610000
			3657.600220	11.720000			
89	30	57	2215.730034	148.610000	3657.600220	2225.740034	148.610000
			3657.600220	10.010000			
90	30	57	2225.740034	148.610000	3657.600220	2234.290035	148.610000
			3657.600220	8.550000			
91	30	57	2234.290035	148.610000	3657.600220	2241.590035	148.610000
			3657.600220	7.300000			
92	30	57	2241.590035	148.610000	3657.600220	2247.830034	148.610000
			3657.600220	6.240000			
93	30	57	2247.830034	148.610000	3657.600220	2253.160034	148.610000
			3657.600220	5.330000			
94	30	57	2253.160034	148.610000	3657.600220	2257.710035	148.610000
			3657.600220	4.550000			
95	30	57	2257.710035	148.610000	3657.600220	2261.600035	148.610000
			3657.600220	3.890000			
96	30	57	2261.600035	148.610000	3657.600220	2264.920035	148.610000
			3657.600220	3.320000			
97	30	57	2264.920035	148.610000	3657.600220	2267.750035	148.610000
			3657.600220	2.830000			
98	30	57	2267.750035	148.610000	3657.600220	2270.170035	148.610000
			3657.600220	2.420000			
99	30	57	2270.170035	148.610000	3657.600220	2272.240035	148.610000
			3657.600220	2.070000			
100	30	57	2272.240035	148.610000	3657.600220	2274.010035	148.610000
			3657.600220	1.770000			
101	30	57	2274.010035	148.610000	3657.600220	2275.520035	148.610000
			3657.600220	1.510000			
102	30	57	2275.520035	148.610000	3657.600220	2276.810035	148.610000
			3657.600220	1.290000			
103	30	57	2276.810035	148.610000	3657.600220	2277.910035	148.610000
			3657.600220	1.100000			
104	30	57	2277.910035	148.610000	3657.600220	2278.850035	148.610000
			3657.600220	0.940000			
105	30	57	2278.850035	148.610000	3657.600220	2279.650035	148.610000
			3657.600220	0.800000			
106	30	57	2279.650035	148.610000	3657.600220	2280.340035	148.610000
			3657.600220	0.690000			
107	30	57	2280.340035	148.610000	3657.600220	2280.930035	148.610000
			3657.600220	0.590000			
108	30	57	2280.930035	148.610000	3657.600220	2281.430035	148.610000
			3657.600220	0.500000			
109	30	57	2281.430035	148.610000	3657.600220	2282.430035	148.610000
			3657.600220	1.000000			

WALLCP 1.63e+06
WALLHCN 4320
INSULATION_HEAT_PROP 3283 168
RELROUGH 0.0001
MAX_NUSSELT 100

**
REPORTING_GROUP 'FlexWell: FlexWell-1'
'Well-1_Annulus' 'Well-1_Tubing' 'Well-1_ConcTbg'
1.0 1.0 1.0
DTMAX 0.1

**
DATE 2020 1 2
DTMAX 1.0

**
DATE 2020 1 3
DTMAX 90.0

**
DATE 2040 1 1.00000
STOP

RESULTS FLEXWELL BEGIN
RESULTS FLEXWELL FLEXWELLNAME 'FlexWell-1'
RESULTS FLEXWELL AUTO_COMPLETE_PERFS 'YES'
RESULTS FLEXWELL TUBING_WELLNAME 'Well-1_Tubing'
SELECTED_ANNULUS_COMPLETION_BRANCH 'Annulus Main Branch ending with UBA
[110,30,57] : 2020-01-01'
RESULTS FLEXWELL CONCENTRIC_TUBING_WELLNAME 'Well-1_ConcTbg'
SELECTED_ANNULUS_COMPLETION_BRANCH 'Annulus Main Branch ending with UBA
[110,30,57] : 2020-01-01'
RESULTS FLEXWELL END

RESULTS SPEC 'Permeability K'
RESULTS SPEC SPECNOTCALCVAL -99999
RESULTS SPEC REGION 'All Layers (Whole Grid)'
RESULTS SPEC REGIONTYPE 'REGION_WHOLEGRID'
RESULTS SPEC LAYERNUMB 0
RESULTS SPEC PORTYPE 1
RESULTS SPEC EQUALSI 0 1
RESULTS SPEC SPECKEEMOD 'YES'
RESULTS SPEC STOP

RESULTS SPEC 'Permeability J'
RESULTS SPEC SPECNOTCALCVAL -99999
RESULTS SPEC REGION 'All Layers (Whole Grid)'
RESULTS SPEC REGIONTYPE 'REGION_WHOLEGRID'
RESULTS SPEC LAYERNUMB 0
RESULTS SPEC PORTYPE 1
RESULTS SPEC EQUALSI 0 1
RESULTS SPEC SPECKEEMOD 'YES'
RESULTS SPEC STOP

APPENDIX C
U-SHAPE CASE .DAT CODE

The following is the code used by CMG-STARs to read and run the u-shape model evaluated in Chapter 3. The .dat file shown in this appendix is for the pipe-in-pipe configuration described in Table 3.12:

```

RESULTS SIMULATOR STARS 201910
WPRN FLEXWELL GRID 1
INUNIT SI
WSRF WELL 1
WSRF GRID 1
OUTPRN WELL ALL
OUTSRF GRID PRES TEMP
OUTSRF FLEXLAYER ALL
** Distance units: m
RESULTS XOFFSET          0.0000
RESULTS YOFFSET          0.0000
RESULTS ROTATION          0.0000 ** (DEGREES)
RESULTS AXES-DIRECTIONS 1.0 -1.0 1.0
** *****
** Definition of fundamental cartesian grid
** *****
GRID VARI 141 59 86
KDIR DOWN
DI IVAR
106.42  106.42  106.42  14.42  13.11  11.92  10.83  9.85  8.95
8.14    7.4    6.73  6.12  5.56  5.05  4.59  4.18  3.8
3.45    3.14  2.85  2.59  2.36  2.14  1.95  1.77  1.61
1.46    1.33  1.21  1.1   0.5   0.5   0.5   1.1   1.21
1.33    1.46  1.61  1.77  1.95  2.14  2.36  2.59  2.85
3.14    3.45  3.8   4.18  4.59  5.05  5.56  6.12  6.73
7.4     8.14  8.95  9.85  10.83 11.92 13.11 14.42 106.42
106.42  106.42 106.42 106.42 106.42 106.42 106.42 0.5  106.42
106.42  106.42 106.42 106.42 106.42 106.42 106.42 14.42 13.11
11.92   10.83 9.85  8.95  8.14  7.4   6.73  6.12  5.56
5.05   4.59  4.18  3.8   3.45  3.14  2.85  2.59  2.36
2.14   1.95  1.77  1.61  1.46  1.33  1.21  1.1   0.5
0.5    0.5   1.1   1.21  1.33  1.46  1.61  1.77  1.95
2.14   2.36  2.59  2.85  3.14  3.45  3.8   4.18  4.59
5.05   5.56  6.12  6.73  7.4   8.14  8.95  9.85  10.83
11.92  13.11 14.42 106.42 106.42 106.42

DJ JVAR
14.42  13.11  11.92  10.83  9.85  8.95  8.14  7.40  6.73
6.12   5.56  5.05  4.59  4.18  3.80  3.45  3.14  2.85
2.59   2.36  2.14  1.95  1.77  1.61  1.46  1.33  1.21

```

1.10	0.5	0.5	0.5	1.10				
1.21	1.33	1.46	1.61	1.77	1.95	2.14	2.36	2.59
2.85	3.14	3.45	3.80	4.18	4.59	5.05	5.56	6.12
6.73	7.40	8.14	8.95	9.85	10.83	11.92	13.11	14.42

DK KVAR

27*105.6155

14.42	13.11	11.92	10.83	9.85	8.95	8.14	7.40	6.73
6.12	5.56	5.05	4.59	4.18	3.80	3.45	3.14	2.85
2.59	2.36	2.14	1.95	1.77	1.61	1.46	1.33	1.21
1.10	0.5	0.5	0.5	1.10				
1.21	1.33	1.46	1.61	1.77	1.95	2.14	2.36	2.59
2.85	3.14	3.45	3.80	4.18	4.59	5.05	5.56	6.12
6.73	7.40	8.14	8.95	9.85	10.83	11.92	13.11	14.42

DTOP

8319*0

PERMI CON 0.00000

MOD 71 30 57 = 10000.0

PERMJ EQUALSI

PERMK EQUALSI

** 0 = null block, 1 = active block

NULL CON 1

POR CON 0.050

MOD 71 30 57 = 0.999

** 0 = pinched block, 1 = active block

PINCHOUTARRAY CON 1

END-GRID

ROCKTYPE 1

CPOR 4.35e-7

ROCKCP 2.66e6 0

THCONR 2.59e5

THCONW 53500

** Model and number of components

MODEL 1 1 1 1

COMPNAME 'H2O'

CMM

0

PCRIT

0

TCRIT

0

MASSDEN

1000

AVISC

0.0047352

BVISC

1515.7

ROCKFLUID

RPT 1 WATWET

** Sw krw krow

SWT

0 0 1

1 1 0

** S1 krg krog

SLT

0 1 0
 1 0 1

INITIAL
 VERTICAL OFF

INITREGION 1
 REFPRES 30000
 REFDEPTH 3000
 PRES KVAR

528	1584	2640	3697	4753	5809	6865	7921	8977	10033
11090	12146	13202	14258	15314	16370	17427	18483	19539	20595
21651	22707	23763	24820	25876	26932	27988	28588	28726	28851
28965	29068	29162	29248	29325	29396	29460	29519	29572	29620
29664	29704	29740	29773	29803	29830	29855	29877	29898	29916
29933	29949	29963	29975	29987	29995	30000	30005	30013	30025
30037	30051	30067	30084	30102	30123	30145	30170	30197	30227
30260	30296	30336	30380	30428	30481	30540	30604	30675	30752
30838	30932	31035	31149	31274	31412				

TEMP KVAR

14.2	22.7	31.1	39.6	48.0	56.5	64.9	73.4	81.8	90.3
98.7	107.2	115.6	124.1	132.5	141.0	149.4	157.9	166.3	174.8
183.2	191.7	200.1	208.6	217.0	225.5	233.9	238.7	239.8	240.8
241.7	242.5	243.3	244.0	244.6	245.2	245.7	246.1	246.6	247.0
247.3	247.6	247.9	248.2	248.4	248.6	248.8	249.0	249.2	249.3
249.5	249.6	249.7	249.8	249.9	250.0	250.0	250.0	250.1	250.2
250.3	250.4	250.5	250.7	250.8	251.0	251.2	251.4	251.6	251.8
252.1	252.4	252.7	253.0	253.4	253.9	254.3	254.8	255.4	256.0
256.7	257.5	258.3	259.2	260.2	261.3				

SW CON 1
 SO CON 0
 SG CON 0
 MFRAC_WAT 'H2O' CON 1
 MFRAC_GAS 'H2O' CON 0

NUMERICAL

AUTOTUNE

RUN

DATE 2020 1 1

DTWELL 0.0001

DIMAX 0.001

**

WELL 'FlexWell-1'

INJECTOR MOBWEIGHT IMPLICIT 'FlexWell-1'

INCOMP WATER 1.0

TINJW 50.0

QUAL 0.0

PINJW 3875.0

OPERATE MAX STW 1364 CONT

** rad geofac wfrac skin

GEOMETRY K 0.0762 0.249 1.0 0.0

PERF_FLX GEOA 'FlexWell-1'

** UBA ff Status Connection

33 30 1 1.0 CLOSED FLOW-FROM 'SURFACE' REFLAYER

33 30 2 1.0 CLOSED FLOW-FROM 1

33 30 3 1.0 CLOSED FLOW-FROM 2

33 30 4	1.0	CLOSED	FLOW-FROM	3
33 30 5	1.0	CLOSED	FLOW-FROM	4
33 30 6	1.0	CLOSED	FLOW-FROM	5
33 30 7	1.0	CLOSED	FLOW-FROM	6
33 30 8	1.0	CLOSED	FLOW-FROM	7
33 30 9	1.0	CLOSED	FLOW-FROM	8
33 30 10	1.0	CLOSED	FLOW-FROM	9
33 30 11	1.0	CLOSED	FLOW-FROM	10
33 30 12	1.0	CLOSED	FLOW-FROM	11
33 30 13	1.0	CLOSED	FLOW-FROM	12
33 30 14	1.0	CLOSED	FLOW-FROM	13
33 30 15	1.0	CLOSED	FLOW-FROM	14
33 30 16	1.0	CLOSED	FLOW-FROM	15
33 30 17	1.0	CLOSED	FLOW-FROM	16
33 30 18	1.0	CLOSED	FLOW-FROM	17
33 30 19	1.0	CLOSED	FLOW-FROM	18
33 30 20	1.0	CLOSED	FLOW-FROM	19
33 30 21	1.0	CLOSED	FLOW-FROM	20
33 30 22	1.0	CLOSED	FLOW-FROM	21
33 30 23	1.0	CLOSED	FLOW-FROM	22
33 30 24	1.0	CLOSED	FLOW-FROM	23
33 30 25	1.0	CLOSED	FLOW-FROM	24
33 30 26	1.0	CLOSED	FLOW-FROM	25
33 30 27	1.0	CLOSED	FLOW-FROM	26
33 30 28	1.0	CLOSED	FLOW-FROM	27
33 30 29	1.0	CLOSED	FLOW-FROM	28
33 30 30	1.0	CLOSED	FLOW-FROM	29
33 30 31	1.0	CLOSED	FLOW-FROM	30
33 30 32	1.0	CLOSED	FLOW-FROM	31
33 30 33	1.0	CLOSED	FLOW-FROM	32
33 30 34	1.0	CLOSED	FLOW-FROM	33
33 30 35	1.0	CLOSED	FLOW-FROM	34
33 30 36	1.0	CLOSED	FLOW-FROM	35
33 30 37	1.0	CLOSED	FLOW-FROM	36
33 30 38	1.0	CLOSED	FLOW-FROM	37
33 30 39	1.0	CLOSED	FLOW-FROM	38
33 30 40	1.0	CLOSED	FLOW-FROM	39
33 30 41	1.0	CLOSED	FLOW-FROM	40
33 30 42	1.0	CLOSED	FLOW-FROM	41
33 30 43	1.0	CLOSED	FLOW-FROM	42
33 30 44	1.0	CLOSED	FLOW-FROM	43
33 30 45	1.0	CLOSED	FLOW-FROM	44
33 30 46	1.0	CLOSED	FLOW-FROM	45
33 30 47	1.0	CLOSED	FLOW-FROM	46
33 30 48	1.0	CLOSED	FLOW-FROM	47
33 30 49	1.0	CLOSED	FLOW-FROM	48
33 30 50	1.0	CLOSED	FLOW-FROM	49
33 30 51	1.0	CLOSED	FLOW-FROM	50
33 30 52	1.0	CLOSED	FLOW-FROM	51
33 30 53	1.0	CLOSED	FLOW-FROM	52
33 30 54	1.0	CLOSED	FLOW-FROM	53
33 30 55	1.0	CLOSED	FLOW-FROM	54
33 30 56	1.0	CLOSED	FLOW-FROM	55
33 30 57	1.0	CLOSED	FLOW-FROM	56
34 30 57	1.0	CLOSED	FLOW-FROM	57

35	30	57	1.0	CLOSED	FLOW-FROM	58
36	30	57	1.0	CLOSED	FLOW-FROM	59
37	30	57	1.0	CLOSED	FLOW-FROM	60
38	30	57	1.0	CLOSED	FLOW-FROM	61
39	30	57	1.0	CLOSED	FLOW-FROM	62
40	30	57	1.0	CLOSED	FLOW-FROM	63
41	30	57	1.0	CLOSED	FLOW-FROM	64
42	30	57	1.0	CLOSED	FLOW-FROM	65
43	30	57	1.0	CLOSED	FLOW-FROM	66
44	30	57	1.0	CLOSED	FLOW-FROM	67
45	30	57	1.0	CLOSED	FLOW-FROM	68
46	30	57	1.0	CLOSED	FLOW-FROM	69
47	30	57	1.0	CLOSED	FLOW-FROM	70
48	30	57	1.0	CLOSED	FLOW-FROM	71
49	30	57	1.0	CLOSED	FLOW-FROM	72
50	30	57	1.0	CLOSED	FLOW-FROM	73
51	30	57	1.0	CLOSED	FLOW-FROM	74
52	30	57	1.0	CLOSED	FLOW-FROM	75
53	30	57	1.0	CLOSED	FLOW-FROM	76
54	30	57	1.0	CLOSED	FLOW-FROM	77
55	30	57	1.0	CLOSED	FLOW-FROM	78
56	30	57	1.0	CLOSED	FLOW-FROM	79
57	30	57	1.0	CLOSED	FLOW-FROM	80
58	30	57	1.0	CLOSED	FLOW-FROM	81
59	30	57	1.0	CLOSED	FLOW-FROM	82
60	30	57	1.0	CLOSED	FLOW-FROM	83
61	30	57	1.0	CLOSED	FLOW-FROM	84
62	30	57	1.0	CLOSED	FLOW-FROM	85
63	30	57	1.0	CLOSED	FLOW-FROM	86
64	30	57	1.0	CLOSED	FLOW-FROM	87
65	30	57	1.0	CLOSED	FLOW-FROM	88
66	30	57	1.0	CLOSED	FLOW-FROM	89
67	30	57	1.0	CLOSED	FLOW-FROM	90
68	30	57	1.0	CLOSED	FLOW-FROM	91
69	30	57	1.0	CLOSED	FLOW-FROM	92
70	30	57	1.0	CLOSED	FLOW-FROM	93
71	30	57	1.0	OPEN	FLOW-FROM	94

LAYERXYZ 'FlexWell-1'

** perf geometric data: UBA, block entry(x,y,z) block exit(x,y,z), length

33	30	1	467.619995	148.360000	0.000000	467.619995	148.360000	105.615501
			105.615501					
33	30	2	467.619995	148.360000	105.615501	467.619995	148.360000	
			211.231003	105.615501				
33	30	3	467.619995	148.360000	211.231003	467.619995	148.360000	
			316.846504	105.615501				
33	30	4	467.619995	148.360000	316.846504	467.619995	148.360000	
			422.462006	105.615501				
33	30	5	467.619995	148.360000	422.462006	467.619995	148.360000	
			528.077507	105.615501				
33	30	6	467.619995	148.360000	528.077507	467.619995	148.360000	
			633.693008	105.615501				
33	30	7	467.619995	148.360000	633.693008	467.619995	148.360000	
			739.308510	105.615501				
33	30	8	467.619995	148.360000	739.308510	467.619995	148.360000	
			844.924011	105.615501				

33	30	9	467.619995	148.360000	844.924011	467.619995	148.360000
			950.539513	105.615501			
33	30	10	467.619995	148.360000	950.539513	467.619995	148.360000
			1056.155014	105.615501			
33	30	11	467.619995	148.360000	1056.155014	467.619995	148.360000
			1161.770515	105.615501			
33	30	12	467.619995	148.360000	1161.770515	467.619995	148.360000
			1267.386017	105.615501			
33	30	13	467.619995	148.360000	1267.386017	467.619995	148.360000
			1373.001518	105.615501			
33	30	14	467.619995	148.360000	1373.001518	467.619995	148.360000
			1478.617020	105.615501			
33	30	15	467.619995	148.360000	1478.617020	467.619995	148.360000
			1584.232521	105.615501			
33	30	16	467.619995	148.360000	1584.232521	467.619995	148.360000
			1689.848022	105.615501			
33	30	17	467.619995	148.360000	1689.848022	467.619995	148.360000
			1795.463524	105.615501			
33	30	18	467.619995	148.360000	1795.463524	467.619995	148.360000
			1901.079025	105.615501			
33	30	19	467.619995	148.360000	1901.079025	467.619995	148.360000
			2006.694527	105.615501			
33	30	20	467.619995	148.360000	2006.694527	467.619995	148.360000
			2112.310028	105.615501			
33	30	21	467.619995	148.360000	2112.310028	467.619995	148.360000
			2217.925529	105.615501			
33	30	22	467.619995	148.360000	2217.925529	467.619995	148.360000
			2323.541031	105.615501			
33	30	23	467.619995	148.360000	2323.541031	467.619995	148.360000
			2429.156532	105.615501			
33	30	24	467.619995	148.360000	2429.156532	467.619995	148.360000
			2534.772034	105.615501			
33	30	25	467.619995	148.360000	2534.772034	467.619995	148.360000
			2640.387535	105.615501			
33	30	26	467.619995	148.360000	2640.387535	467.619995	148.360000
			2746.003036	105.615501			
33	30	27	467.619995	148.360000	2746.003036	467.619995	148.360000
			2851.618538	105.615501			
33	30	28	467.619995	148.360000	2851.618538	467.619995	148.360000
			2866.038538	14.420000			
33	30	29	467.619995	148.360000	2866.038538	467.619995	148.360000
			2879.148538	13.110000			
33	30	30	467.619995	148.360000	2879.148538	467.619995	148.360000
			2891.068538	11.920000			
33	30	31	467.619995	148.360000	2891.068538	467.619995	148.360000
			2901.898538	10.830000			
33	30	32	467.619995	148.360000	2901.898538	467.619995	148.360000
			2911.748538	9.850000			
33	30	33	467.619995	148.360000	2911.748538	467.619995	148.360000
			2920.698538	8.950000			
33	30	34	467.619995	148.360000	2920.698538	467.619995	148.360000
			2928.838538	8.140000			
33	30	35	467.619995	148.360000	2928.838538	467.619995	148.360000
			2936.238538	7.400000			

33	30	36	467.619995	148.360000	2936.238538	467.619995	148.360000
			2942.968538	6.730000			
33	30	37	467.619995	148.360000	2942.968538	467.619995	148.360000
			2949.088538	6.120000			
33	30	38	467.619995	148.360000	2949.088538	467.619995	148.360000
			2954.648538	5.560000			
33	30	39	467.619995	148.360000	2954.648538	467.619995	148.360000
			2959.698538	5.050000			
33	30	40	467.619995	148.360000	2959.698538	467.619995	148.360000
			2964.288538	4.590000			
33	30	41	467.619995	148.360000	2964.288538	467.619995	148.360000
			2968.468538	4.180000			
33	30	42	467.619995	148.360000	2968.468538	467.619995	148.360000
			2972.268538	3.800000			
33	30	43	467.619995	148.360000	2972.268538	467.619995	148.360000
			2975.718538	3.450000			
33	30	44	467.619995	148.360000	2975.718538	467.619995	148.360000
			2978.858538	3.140000			
33	30	45	467.619995	148.360000	2978.858538	467.619995	148.360000
			2981.708538	2.850000			
33	30	46	467.619995	148.360000	2981.708538	467.619995	148.360000
			2984.298538	2.590000			
33	30	47	467.619995	148.360000	2984.298538	467.619995	148.360000
			2986.658538	2.360000			
33	30	48	467.619995	148.360000	2986.658538	467.619995	148.360000
			2988.798538	2.140000			
33	30	49	467.619995	148.360000	2988.798538	467.619995	148.360000
			2990.748538	1.950000			
33	30	50	467.619995	148.360000	2990.748538	467.619995	148.360000
			2992.518538	1.770000			
33	30	51	467.619995	148.360000	2992.518538	467.619995	148.360000
			2994.128538	1.610000			
33	30	52	467.619995	148.360000	2994.128538	467.619995	148.360000
			2995.588538	1.460000			
33	30	53	467.619995	148.360000	2995.588538	467.619995	148.360000
			2996.918538	1.330000			
33	30	54	467.619995	148.360000	2996.918538	467.619995	148.360000
			2998.128538	1.210000			
33	30	55	467.619995	148.360000	2998.128538	467.619995	148.360000
			2999.228538	1.100000			
33	30	56	467.619995	148.360000	2999.228538	467.703328	148.360000
			2999.728538	0.513523			
33	30	57	467.703328	148.360000	2999.728538	467.869995	148.360000
			2999.895205	0.263523			
34	30	57	467.869995	148.360000	2999.895205	468.369995	148.360000
			2999.978538	0.513523			
35	30	57	468.369995	148.360000	2999.978538	469.469995	148.360000
			2999.978538	1.100000			
36	30	57	469.469995	148.360000	2999.978538	470.679995	148.360000
			2999.978538	1.210000			
37	30	57	470.679995	148.360000	2999.978538	472.009995	148.360000
			2999.978538	1.330000			
38	30	57	472.009995	148.360000	2999.978538	473.469995	148.360000
			2999.978538	1.460000			

39	30	57	473.469995	148.360000	2999.978538	475.079995	148.360000
			2999.978538	1.610000			
40	30	57	475.079995	148.360000	2999.978538	476.849995	148.360000
			2999.978538	1.770000			
41	30	57	476.849995	148.360000	2999.978538	478.799995	148.360000
			2999.978538	1.950000			
42	30	57	478.799995	148.360000	2999.978538	480.939995	148.360000
			2999.978538	2.140000			
43	30	57	480.939995	148.360000	2999.978538	483.299995	148.360000
			2999.978538	2.360000			
44	30	57	483.299995	148.360000	2999.978538	485.889995	148.360000
			2999.978538	2.590000			
45	30	57	485.889995	148.360000	2999.978538	488.739995	148.360000
			2999.978538	2.850000			
46	30	57	488.739995	148.360000	2999.978538	491.879995	148.360000
			2999.978538	3.140000			
47	30	57	491.879995	148.360000	2999.978538	495.329995	148.360000
			2999.978538	3.450000			
48	30	57	495.329995	148.360000	2999.978538	499.129995	148.360000
			2999.978538	3.800000			
49	30	57	499.129995	148.360000	2999.978538	503.309995	148.360000
			2999.978538	4.180000			
50	30	57	503.309995	148.360000	2999.978538	507.899995	148.360000
			2999.978538	4.590000			
51	30	57	507.899995	148.360000	2999.978538	512.949995	148.360000
			2999.978538	5.050000			
52	30	57	512.949995	148.360000	2999.978538	518.509995	148.360000
			2999.978538	5.560000			
53	30	57	518.509995	148.360000	2999.978538	524.629995	148.360000
			2999.978538	6.120000			
54	30	57	524.629995	148.360000	2999.978538	531.359995	148.360000
			2999.978538	6.730000			
55	30	57	531.359995	148.360000	2999.978538	538.759995	148.360000
			2999.978538	7.400000			
56	30	57	538.759995	148.360000	2999.978538	546.899996	148.360000
			2999.978538	8.140000			
57	30	57	546.899996	148.360000	2999.978538	555.849995	148.360000
			2999.978538	8.950000			
58	30	57	555.849995	148.360000	2999.978538	565.699996	148.360000
			2999.978538	9.850000			
59	30	57	565.699996	148.360000	2999.978538	576.529996	148.360000
			2999.978538	10.830000			
60	30	57	576.529996	148.360000	2999.978538	588.449996	148.360000
			2999.978538	11.920000			
61	30	57	588.449996	148.360000	2999.978538	601.559995	148.360000
			2999.978538	13.110000			
62	30	57	601.559995	148.360000	2999.978538	615.979995	148.360000
			2999.978538	14.420000			
63	30	57	615.979995	148.360000	2999.978538	722.399994	148.360000
			2999.978538	106.419998			
64	30	57	722.399994	148.360000	2999.978538	828.819992	148.360000
			2999.978538	106.419998			
65	30	57	828.819992	148.360000	2999.978538	935.239990	148.360000
			2999.978538	106.419998			

```

66 30 57 935.239990 148.360000 2999.978538 1041.659988 148.360000
2999.978538 106.419998
67 30 57 1041.659988 148.360000 2999.978538 1148.079986 148.360000
2999.978538 106.419998
68 30 57 1148.079986 148.360000 2999.978538 1254.499985 148.360000
2999.978538 106.419998
69 30 57 1254.499985 148.360000 2999.978538 1360.919983 148.360000
2999.978538 106.419998
70 30 57 1360.919983 148.360000 2999.978538 1467.339981 148.360000
2999.978538 106.419998
71 30 57 1467.339981 148.360000 2999.978538 1467.839981 148.360000
2999.978538 0.500000

```

REPORTING-GROUP 'FlexWell: FlexWell-1'

'FlexWell-1'

1.0

BHPDEPTH 'FlexWell-1' 3000.0

FLX.WELLBORE 'FlexWell-1' ATTACHTO 'FlexWell-1'

SOLID_BLOCK OFF

SEGREGATION ON

ANNULUS ATTACHTO 'FlexWell-1'

TUBULARS CONSTANT

ID 0.1524

OD 0.1683

WALLCP 3.63e+06

WALLHCN 3.888e+06

CEMENT_HEAT_PROP 1.848e+06 118400

RELROUGH 0.0001

MAX_NUSSELT 10000

**

WELL 'FlexWell-2'

PRODUCER 'FlexWell-2'

OPERATE MAX STW 1364 CONT

** rad geofac wfrac skin

GEOMETRY K 0.0762 0.249 1.0 0.0

PERF_FLX GEOA 'FlexWell-2'

** UBA ff Status Connection

U	B	A	ff	Status	Connection
109	30	1	1.0	CLOSED	'SURFACE' REFLAYER
109	30	2	1.0	CLOSED	FLOW-TO 1
109	30	3	1.0	CLOSED	FLOW-TO 2
109	30	4	1.0	CLOSED	FLOW-TO 3
109	30	5	1.0	CLOSED	FLOW-TO 4
109	30	6	1.0	CLOSED	FLOW-TO 5
109	30	7	1.0	CLOSED	FLOW-TO 6
109	30	8	1.0	CLOSED	FLOW-TO 7
109	30	9	1.0	CLOSED	FLOW-TO 8
109	30	10	1.0	CLOSED	FLOW-TO 9
109	30	11	1.0	CLOSED	FLOW-TO 10
109	30	12	1.0	CLOSED	FLOW-TO 11
109	30	13	1.0	CLOSED	FLOW-TO 12
109	30	14	1.0	CLOSED	FLOW-TO 13
109	30	15	1.0	CLOSED	FLOW-TO 14

109 30 16	1.0	CLOSED	FLOW-TO	15
109 30 17	1.0	CLOSED	FLOW-TO	16
109 30 18	1.0	CLOSED	FLOW-TO	17
109 30 19	1.0	CLOSED	FLOW-TO	18
109 30 20	1.0	CLOSED	FLOW-TO	19
109 30 21	1.0	CLOSED	FLOW-TO	20
109 30 22	1.0	CLOSED	FLOW-TO	21
109 30 23	1.0	CLOSED	FLOW-TO	22
109 30 24	1.0	CLOSED	FLOW-TO	23
109 30 25	1.0	CLOSED	FLOW-TO	24
109 30 26	1.0	CLOSED	FLOW-TO	25
109 30 27	1.0	CLOSED	FLOW-TO	26
109 30 28	1.0	CLOSED	FLOW-TO	27
109 30 29	1.0	CLOSED	FLOW-TO	28
109 30 30	1.0	CLOSED	FLOW-TO	29
109 30 31	1.0	CLOSED	FLOW-TO	30
109 30 32	1.0	CLOSED	FLOW-TO	31
109 30 33	1.0	CLOSED	FLOW-TO	32
109 30 34	1.0	CLOSED	FLOW-TO	33
109 30 35	1.0	CLOSED	FLOW-TO	34
109 30 36	1.0	CLOSED	FLOW-TO	35
109 30 37	1.0	CLOSED	FLOW-TO	36
109 30 38	1.0	CLOSED	FLOW-TO	37
109 30 39	1.0	CLOSED	FLOW-TO	38
109 30 40	1.0	CLOSED	FLOW-TO	39
109 30 41	1.0	CLOSED	FLOW-TO	40
109 30 42	1.0	CLOSED	FLOW-TO	41
109 30 43	1.0	CLOSED	FLOW-TO	42
109 30 44	1.0	CLOSED	FLOW-TO	43
109 30 45	1.0	CLOSED	FLOW-TO	44
109 30 46	1.0	CLOSED	FLOW-TO	45
109 30 47	1.0	CLOSED	FLOW-TO	46
109 30 48	1.0	CLOSED	FLOW-TO	47
109 30 49	1.0	CLOSED	FLOW-TO	48
109 30 50	1.0	CLOSED	FLOW-TO	49
109 30 51	1.0	CLOSED	FLOW-TO	50
109 30 52	1.0	CLOSED	FLOW-TO	51
109 30 53	1.0	CLOSED	FLOW-TO	52
109 30 54	1.0	CLOSED	FLOW-TO	53
109 30 55	1.0	CLOSED	FLOW-TO	54
109 30 56	1.0	CLOSED	FLOW-TO	55
109 30 57	1.0	CLOSED	FLOW-TO	56
108 30 57	1.0	CLOSED	FLOW-TO	57
107 30 57	1.0	CLOSED	FLOW-TO	58
106 30 57	1.0	CLOSED	FLOW-TO	59
105 30 57	1.0	CLOSED	FLOW-TO	60
104 30 57	1.0	CLOSED	FLOW-TO	61
103 30 57	1.0	CLOSED	FLOW-TO	62
102 30 57	1.0	CLOSED	FLOW-TO	63
101 30 57	1.0	CLOSED	FLOW-TO	64
100 30 57	1.0	CLOSED	FLOW-TO	65
99 30 57	1.0	CLOSED	FLOW-TO	66
98 30 57	1.0	CLOSED	FLOW-TO	67
97 30 57	1.0	CLOSED	FLOW-TO	68
96 30 57	1.0	CLOSED	FLOW-TO	69

95	30	57	1.0	CLOSED	FLOW-TO	70
94	30	57	1.0	CLOSED	FLOW-TO	71
93	30	57	1.0	CLOSED	FLOW-TO	72
92	30	57	1.0	CLOSED	FLOW-TO	73
91	30	57	1.0	CLOSED	FLOW-TO	74
90	30	57	1.0	CLOSED	FLOW-TO	75
89	30	57	1.0	CLOSED	FLOW-TO	76
88	30	57	1.0	CLOSED	FLOW-TO	77
87	30	57	1.0	CLOSED	FLOW-TO	78
86	30	57	1.0	CLOSED	FLOW-TO	79
85	30	57	1.0	CLOSED	FLOW-TO	80
84	30	57	1.0	CLOSED	FLOW-TO	81
83	30	57	1.0	CLOSED	FLOW-TO	82
82	30	57	1.0	CLOSED	FLOW-TO	83
81	30	57	1.0	CLOSED	FLOW-TO	84
80	30	57	1.0	CLOSED	FLOW-TO	85
79	30	57	1.0	CLOSED	FLOW-TO	86
78	30	57	1.0	CLOSED	FLOW-TO	87
77	30	57	1.0	CLOSED	FLOW-TO	88
76	30	57	1.0	CLOSED	FLOW-TO	89
75	30	57	1.0	CLOSED	FLOW-TO	90
74	30	57	1.0	CLOSED	FLOW-TO	91
73	30	57	1.0	CLOSED	FLOW-TO	92
72	30	57	1.0	CLOSED	FLOW-TO	93
71	30	57	1.0	OPEN	FLOW-TO	94

LAYERXYZ 'FlexWell-2'

** perf geometric data: UBA, block entry(x,y,z) block exit(x,y,z), length

109	30	1	2467.559967	148.360000	0.000000	2467.559967	148.360000		
			105.615501	105.615501					
109	30	2	2467.559967	148.360000	105.615501	2467.559967	148.360000		
			211.231003	105.615501					
109	30	3	2467.559967	148.360000	211.231003	2467.559967	148.360000		
			316.846504	105.615501					
109	30	4	2467.559967	148.360000	316.846504	2467.559967	148.360000		
			422.462006	105.615501					
109	30	5	2467.559967	148.360000	422.462006	2467.559967	148.360000		
			528.077507	105.615501					
109	30	6	2467.559967	148.360000	528.077507	2467.559967	148.360000		
			633.693008	105.615501					
109	30	7	2467.559967	148.360000	633.693008	2467.559967	148.360000		
			739.308510	105.615501					
109	30	8	2467.559967	148.360000	739.308510	2467.559967	148.360000		
			844.924011	105.615501					
109	30	9	2467.559967	148.360000	844.924011	2467.559967	148.360000		
			950.539513	105.615501					
109	30	10	2467.559967	148.360000	950.539513	2467.559967	148.360000		
			1056.155014	105.615501					
109	30	11	2467.559967	148.360000	1056.155014	2467.559967	148.360000		
			1161.770515	105.615501					
109	30	12	2467.559967	148.360000	1161.770515	2467.559967	148.360000		
			1267.386017	105.615501					
109	30	13	2467.559967	148.360000	1267.386017	2467.559967	148.360000		
			1373.001518	105.615501					
109	30	14	2467.559967	148.360000	1373.001518	2467.559967	148.360000		
			1478.617020	105.615501					

109	30	15	2467.559967	148.360000	1478.617020	2467.559967	148.360000
			1584.232521	105.615501			
109	30	16	2467.559967	148.360000	1584.232521	2467.559967	148.360000
			1689.848022	105.615501			
109	30	17	2467.559967	148.360000	1689.848022	2467.559967	148.360000
			1795.463524	105.615501			
109	30	18	2467.559967	148.360000	1795.463524	2467.559967	148.360000
			1901.079025	105.615501			
109	30	19	2467.559967	148.360000	1901.079025	2467.559967	148.360000
			2006.694527	105.615501			
109	30	20	2467.559967	148.360000	2006.694527	2467.559967	148.360000
			2112.310028	105.615501			
109	30	21	2467.559967	148.360000	2112.310028	2467.559967	148.360000
			2217.925529	105.615501			
109	30	22	2467.559967	148.360000	2217.925529	2467.559967	148.360000
			2323.541031	105.615501			
109	30	23	2467.559967	148.360000	2323.541031	2467.559967	148.360000
			2429.156532	105.615501			
109	30	24	2467.559967	148.360000	2429.156532	2467.559967	148.360000
			2534.772034	105.615501			
109	30	25	2467.559967	148.360000	2534.772034	2467.559967	148.360000
			2640.387535	105.615501			
109	30	26	2467.559967	148.360000	2640.387535	2467.559967	148.360000
			2746.003036	105.615501			
109	30	27	2467.559967	148.360000	2746.003036	2467.559967	148.360000
			2851.618538	105.615501			
109	30	28	2467.559967	148.360000	2851.618538	2467.559967	148.360000
			2866.038538	14.420000			
109	30	29	2467.559967	148.360000	2866.038538	2467.559967	148.360000
			2879.148538	13.110000			
109	30	30	2467.559967	148.360000	2879.148538	2467.559967	148.360000
			2891.068538	11.920000			
109	30	31	2467.559967	148.360000	2891.068538	2467.559967	148.360000
			2901.898538	10.830000			
109	30	32	2467.559967	148.360000	2901.898538	2467.559967	148.360000
			2911.748538	9.850000			
109	30	33	2467.559967	148.360000	2911.748538	2467.559967	148.360000
			2920.698538	8.950000			
109	30	34	2467.559967	148.360000	2920.698538	2467.559967	148.360000
			2928.838538	8.140000			
109	30	35	2467.559967	148.360000	2928.838538	2467.559967	148.360000
			2936.238538	7.400000			
109	30	36	2467.559967	148.360000	2936.238538	2467.559967	148.360000
			2942.968538	6.730000			
109	30	37	2467.559967	148.360000	2942.968538	2467.559967	148.360000
			2949.088538	6.120000			
109	30	38	2467.559967	148.360000	2949.088538	2467.559967	148.360000
			2954.648538	5.560000			
109	30	39	2467.559967	148.360000	2954.648538	2467.559967	148.360000
			2959.698538	5.050000			
109	30	40	2467.559967	148.360000	2959.698538	2467.559967	148.360000
			2964.288538	4.590000			
109	30	41	2467.559967	148.360000	2964.288538	2467.559967	148.360000
			2968.468538	4.180000			

109	30	42	2467.559967	148.360000	2968.468538	2467.559967	148.360000
			2972.268538	3.800000			
109	30	43	2467.559967	148.360000	2972.268538	2467.559967	148.360000
			2975.718538	3.450000			
109	30	44	2467.559967	148.360000	2975.718538	2467.559967	148.360000
			2978.858538	3.140000			
109	30	45	2467.559967	148.360000	2978.858538	2467.559967	148.360000
			2981.708538	2.850000			
109	30	46	2467.559967	148.360000	2981.708538	2467.559967	148.360000
			2984.298538	2.590000			
109	30	47	2467.559967	148.360000	2984.298538	2467.559967	148.360000
			2986.658538	2.360000			
109	30	48	2467.559967	148.360000	2986.658538	2467.559967	148.360000
			2988.798538	2.140000			
109	30	49	2467.559967	148.360000	2988.798538	2467.559967	148.360000
			2990.748538	1.950000			
109	30	50	2467.559967	148.360000	2990.748538	2467.559967	148.360000
			2992.518538	1.770000			
109	30	51	2467.559967	148.360000	2992.518538	2467.559967	148.360000
			2994.128538	1.610000			
109	30	52	2467.559967	148.360000	2994.128538	2467.559967	148.360000
			2995.588538	1.460000			
109	30	53	2467.559967	148.360000	2995.588538	2467.559967	148.360000
			2996.918538	1.330000			
109	30	54	2467.559967	148.360000	2996.918538	2467.559967	148.360000
			2998.128538	1.210000			
109	30	55	2467.559967	148.360000	2998.128538	2467.559967	148.360000
			2999.228538	1.100000			
109	30	56	2467.559967	148.360000	2999.228538	2467.476633	148.360000
			2999.728538	0.513523			
109	30	57	2467.476633	148.360000	2999.728538	2467.309967	148.360000
			2999.895205	0.263523			
108	30	57	2467.309967	148.360000	2999.895205	2466.809967	148.360000
			2999.978538	0.513523			
107	30	57	2466.809967	148.360000	2999.978538	2465.709967	148.360000
			2999.978538	1.100000			
106	30	57	2465.709967	148.360000	2999.978538	2464.499967	148.360000
			2999.978538	1.210000			
105	30	57	2464.499967	148.360000	2999.978538	2463.169967	148.360000
			2999.978538	1.330000			
104	30	57	2463.169967	148.360000	2999.978538	2461.709967	148.360000
			2999.978538	1.460000			
103	30	57	2461.709967	148.360000	2999.978538	2460.099967	148.360000
			2999.978538	1.610000			
102	30	57	2460.099967	148.360000	2999.978538	2458.329967	148.360000
			2999.978538	1.770000			
101	30	57	2458.329967	148.360000	2999.978538	2456.379966	148.360000
			2999.978538	1.950000			
100	30	57	2456.379966	148.360000	2999.978538	2454.239966	148.360000
			2999.978538	2.140000			
99	30	57	2454.239966	148.360000	2999.978538	2451.879966	148.360000
			2999.978538	2.360000			
98	30	57	2451.879966	148.360000	2999.978538	2449.289967	148.360000
			2999.978538	2.590000			

97	30	57	2449.289967	148.360000	2999.978538	2446.439967	148.360000
			2999.978538	2.850000			
96	30	57	2446.439967	148.360000	2999.978538	2443.299967	148.360000
			2999.978538	3.140000			
95	30	57	2443.299967	148.360000	2999.978538	2439.849967	148.360000
			2999.978538	3.450000			
94	30	57	2439.849967	148.360000	2999.978538	2436.049967	148.360000
			2999.978538	3.800000			
93	30	57	2436.049967	148.360000	2999.978538	2431.869967	148.360000
			2999.978538	4.180000			
92	30	57	2431.869967	148.360000	2999.978538	2427.279967	148.360000
			2999.978538	4.590000			
91	30	57	2427.279967	148.360000	2999.978538	2422.229966	148.360000
			2999.978538	5.050000			
90	30	57	2422.229966	148.360000	2999.978538	2416.669966	148.360000
			2999.978538	5.560000			
89	30	57	2416.669966	148.360000	2999.978538	2410.549967	148.360000
			2999.978538	6.120000			
88	30	57	2410.549967	148.360000	2999.978538	2403.819967	148.360000
			2999.978538	6.730000			
87	30	57	2403.819967	148.360000	2999.978538	2396.419966	148.360000
			2999.978538	7.400000			
86	30	57	2396.419966	148.360000	2999.978538	2388.279966	148.360000
			2999.978538	8.140000			
85	30	57	2388.279966	148.360000	2999.978538	2379.329966	148.360000
			2999.978538	8.950000			
84	30	57	2379.329966	148.360000	2999.978538	2369.479966	148.360000
			2999.978538	9.850000			
83	30	57	2369.479966	148.360000	2999.978538	2358.649966	148.360000
			2999.978538	10.830000			
82	30	57	2358.649966	148.360000	2999.978538	2346.729966	148.360000
			2999.978538	11.920000			
81	30	57	2346.729966	148.360000	2999.978538	2333.619966	148.360000
			2999.978538	13.110000			
80	30	57	2333.619966	148.360000	2999.978538	2319.199966	148.360000
			2999.978538	14.420000			
79	30	57	2319.199966	148.360000	2999.978538	2212.779968	148.360000
			2999.978538	106.419998			
78	30	57	2212.779968	148.360000	2999.978538	2106.359970	148.360000
			2999.978538	106.419998			
77	30	57	2106.359970	148.360000	2999.978538	1999.939972	148.360000
			2999.978538	106.419998			
76	30	57	1999.939972	148.360000	2999.978538	1893.519974	148.360000
			2999.978538	106.419998			
75	30	57	1893.519974	148.360000	2999.978538	1787.099975	148.360000
			2999.978538	106.419998			
74	30	57	1787.099975	148.360000	2999.978538	1680.679977	148.360000
			2999.978538	106.419998			
73	30	57	1680.679977	148.360000	2999.978538	1574.259979	148.360000
			2999.978538	106.419998			
72	30	57	1574.259979	148.360000	2999.978538	1467.839981	148.360000
			2999.978538	106.419998			
71	30	57	1467.839981	148.360000	2999.978538	1467.339981	148.360000
			2999.978538	0.500000			

REPORTING-GROUP 'FlexWell: FlexWell-2'

```
'FlexWell-2'  
1.0  
BHPDEPTH 'FlexWell-2' 3000.0  
  
FLX_WELLBORE 'FlexWell-2' ATTACHTO 'FlexWell-2'  
SOLID_BLOCK OFF  
SEGREGATION ON  
ANNULUS ATTACHTO 'FlexWell-2'  
TUBULARS CONSTANT  
ID 0.1524  
OD 0.1683  
WALL_CP 3.63e+06  
WALL_HCN 3.888e+06  
CEMENT_HEAT_PROP 1.848e+06 118400  
REL_ROUGH 0.0001  
MAX_NUSSELT 10000  
  
**  
DATE 2020 1 2  
DIMAX 0.01  
**  
DATE 2020 1 3  
DIMAX 0.1  
**  
DATE 2020 1 4  
DIMAX 1.0  
**  
DATE 2020 1 5  
DIMAX 30.0  
**  
DATE 2040 1 1.00000  
STOP
```

APPENDIX D

LIST OF SUPPLEMENTAL FILES FOR COPYRIGHT PERMISSIONS

1. Reprinted permission of Koenraad Beckers for Figure 1.1 and Figure 2.2 .
2. Reuse of permission provided by Elsevier and Copyright Clearance Center for Figure 2.4.
3. Reprinted permission of Green Fire Energy Inc. for Figure 1.2.
4. Reuse permission provided by Elsevier and Copyright Clearance Center for Figure 2.1.
5. Reprinted permission of Verkis Consulting Engineers for Figure 2.3.